Florian Seeber, BSc

Finite Element Method Applied to Magnetostatics in a Toroidal Domain with Open Boundary Conditions

MASTER'S THESIS

to achieve the university degree of

Diplom-Ingenieur

Master's degree programme: Technical Physics

submitted to

Graz University of Technology

Supervisor

Ass.Prof. Dipl.-Ing. Dr.techn. Winfried Kernbichler

Co-Supervisor
Dipl.-Ing. Dr.rer.nat. Christopher Albert

Institute of Theoretical and Computational Physics

Graz, July 2018

AFFIDAVIT

I declare that I have authored this thesis independently, that I have not used other than the declared sources/resources, and that I have explicitly indicated all material which has been quoted either literally or by content from the sources used. The text document uploaded to TUGRAZonline is identical to the present master's thesis.

_____
Date

_____
Signature

iv

Kurzfassung

Bei der Kernfusion durch magnetischen Plasmaeinschluss ist es von enormer Wichtigkeit, die Plasmaströme im Fusionsreaktor in Abhängigkeit des angelegten, externen Magnetfeldes genau vorhersagen zu können. Ein wichtiger Teil dieses weitreichenderen Gesamtproblems ist die Bestimmung des Magnetfeldes, welches durch die Plasmaströme selbst im Fusionsreaktor erzeugt wird. Dieses erzeugte Magnetfeld wirkt zusätzlich zum externen Magnetfeld auf die Plasmaströme und muss berücksichtigt werden. In dieser Arbeit wurde eine Methode entwickelt, mit welcher diese Aufgabe mit einem geringst möglichen Rechenaufwand gelöst wird. Diese Methode beschränkt sich auf toroidale Maschinen, wobei die Lösung für das erzeugte Magnetfeld in einem toroidalen Gebiet bestimmt wird, welches auch die Plasmaströme eingrenzt. Um die Lösung dieses Problems zu finden muss ein entsprechendes Randwertproblem gelöst werden. Das Randwertproblem besteht aus den magnetostatischen Maxwell-Gleichungen und entsprechenden Randbedingungen am Rand des Gebiets. Die Lösung wird bestimmt durch eine Finite Elemente Methode im toroidalen Gebiet. Die a priori unbekannten Randbedingungen werden durch eine allgemeine analytische Lösung im stromfreien Außenraum bestimmt. Auf diesem Wege werden die sogenannten offenen Randbedingungen erlangt, wodurch das Problem eindeutig gelöst wird. Die Methode wurde in MATLAB implementiert. Die Ergebnisse wurden mit analytischen Lösungen und anderen FEM-Lösungen auf ihre Richtigkeit geprüft.

Abstract

In physics of magnetic confinement fusion it is essential to be able to precisely predetermine the plasma currents in a reactor, depending on the applied magnetic field. One part of this more extensive problem is to determine the magnetic field, generated by the plasma currents themselves, inside a fusion device. The generated magnetic field acts, additionally to the applied magnetic field, on the plasma currents and has to be considered. In this work a method is developed to perform this task with a minimal computational effort. The method is restricted to toroidal devices. Finding a solution for the magnetic field within the toroidal domain, confining the plasma currents, corresponds to solving a boundary value problem, consisting of the magnetostatic Maxwell equations and boundary conditions given on the boundary of the toroidal domain. The solution is obtained using a finite element method within the toroidal domain. The a priori unknown boundary values are obtained using the general analytical solution in the current free outer region. With this solution we can derive a so called open boundary condition that yields a unique solution for the magnetic field. This procedure is implemented in MATLAB. The results are compared to analytical solutions and to results obtained by a different FEM approach.

Acknowledgements

Working in the plasma physics group of Martin Heyn and Winfried Kernbichler at TU Graz was a great experience for me. In the course of this Master's thesis I had the possibility to discover yet unknown and interesting fields of research. I am especially grateful to my supervisor Christopher Albert, who patiently introduced me to the new topics and whose door was always open for questions and support. I would also like to thank Gernot Kapper with whom I shared the office and who offered his advices and support on countless occasions.

x

Contents

Chapter 1

Introduction

In the course of the last decades, humankind became more and more aware of the importance of resource-conserving power supply. A number of different technologies were developed to provide energy while leaving a minimal ecological footprint. A promising concept with an enormous potential is nuclear fusion. In the 1920s researchers first came up with the idea to use nuclear fusion to gain utilizable energy. This physical process is responsible for the extreme conditions in stars. The basic process is the fusion of two light nuclei like hydrogen isotopes to helium. The mass defect of the reactants and the products is converted to heat and radiation of different kind. The energy per mass ratio of this process exceeds any other known technology, even nuclear fission. In order to ignite fusion, certain criteria for temperature and pressure must be met (Lawson criterion, [14]). In stars, the gravitational force is responsible for the required conditions. In order to realize fusion on earth, different ways to confine and heat the nuclei are needed. At fusion temperatures, the atoms are completely ionized and create a plasma of electrons and nuclei. This plasma must be confined and heated to certain temperatures and densities for fusion. Different priciples and devices [5] have been suggested and tested, whereas the magnetic confinement in toroidal devices has been exposed to be the most convenient choice. The plasma is located in donut shaped (toroidal) reactors. Surrounding superconducting coils generate a strong magnetic field inside the reactor that guides the charged particles and confines the plasma [16]. Two reactor types, that seem to fulfil the requirements for nuclear fusion, are the stellarator [22] and the tokamak [2]. In a stellarator, the external magnetic field has a toroidal component (direction of the central circle of the torus) as well as a poloidal component (perpendicular to toroidal

component). In a tokamak, the external field is purely toroidal and axisymmetric. Based on the operation mode of the tokamak, instabilities may occur at the plasma edge, the so called edge localized modes (ELMs, see e.g. [1] for an introductionary description). They may cause deflection of the plasma onto the reactor wall which has to be avoided at any cost. Additional coils, placed periodically around the toroidal reactor, create a non-axisymmetric perturbation of the magnetic field, the so called resonant magnetic perturbations (RMPs, [1] [8]). The perturbation of the magnetic field prevents ELMs. The perturbing magnetic field can be interpreted as a toroidal harmonic field, that is superimposed to the axisymmetric main field.

In this example we get an impression of the importance of the magnetic field and its affects on the plasma. The main purpose of this work is to develop a method to determine the magnetic field, generated by the plasma currents themselves, inside the reactor. This magnetic field acts, additionally to the external magnetic field generated by the coils, on the plasma currents. It shall be noted that this method is one part of the main problem of determining the current density generated by the externally applied magnetic field. Furthermore, this method is not only restricted to tokamaks, it can be applied as well to stellarators or any situation with a current density confined to a toroidal domain.

Chapter 2

Basics

2.1 The Overall Problem

Calculating the magnetic field of a given current density is just one part of a more extensive problem. Here we will give an outline of the whole problem. The main goal is to determine the current density generated by an external magnetic field. We will keep our considerations general and only refer where necessary to the application on a fusion reactor. An external magnetic field is given and independent of any actions in the surrounding. In case of a fusion reactor, this magnetic field is generated by the surrounding coils.

$$\vec{B}^{ext} = const \tag{2.1}$$

We also define a magnetic field, created by the current density. In the beginning it is set to 0.

$$\vec{B}_0^J = \vec{0} \tag{2.2}$$

The total magnetic field is the superposition of both fields.

$$\vec{B}_0^{tot} = \vec{B}^{ext} + \vec{B}_0^J = \vec{B}^{ext} \tag{2.3}$$

This magnetic field generates a current density inside the toroidal domain, e.g. the reactor chamber. The current density may be obtained using magnetohydrodynamics

(MHD) or Monte-Carlo simulations. This procedure is denoted by an operator $\hat{M}$.

$$\vec{J}_0 = \hat{M} \left[\vec{B}_0^{tot} \right] \tag{2.4}$$

The resulting current density creates a magnetic field itself. This relation is described by Maxwell's equations (see next section). An operator $\hat{N}$ solves those equations and we obtain the magnetic field.

$$\vec{B}_1^J = \hat{N} \left[\vec{J}_0 \right] \tag{2.5}$$

The result is a new total magnetic field.

$$\vec{B}_1^{tot} = \vec{B}^{ext} + \vec{B}_1^J \tag{2.6}$$

This total magnetic field is inserted back to (2.4) and the sequence is repeated. This is an iterative process with the starting values

$$\begin{aligned} \vec{B}_0^{tot} &= \vec{B}^{ext} \\ \vec{B}_0^J &= \vec{0} \end{aligned} \tag{2.7}$$

and the iteration

$$\begin{aligned} \vec{B}_n^{tot} &= \vec{B}^{ext} + \vec{B}_n^J \\ \vec{J}_n &= \hat{M} \left[\vec{B}_n^{tot} \right] \\ \vec{B}_{n+1}^J &= \hat{N} \left[\vec{J}_n \right]. \end{aligned} \tag{2.8}$$

The iteration is stopped when the fields are self-consistent. All the fields are assumed to be stationary. The goal of this thesis is to find a numerical method that represents operator $\hat{N}$, i.e. a method to calculate the magnetic field of a given current density inside a toroidal domain (figure 2.1).

If the cross-sectional domain, confining the current density, is not circular, as will be required for our method, we can choose a toroidal domain that circumscribes this domain. This is the case for most fusion reactors, where the reactor chambers have an elliptical or triangular-like cross-section (figure 2.2).
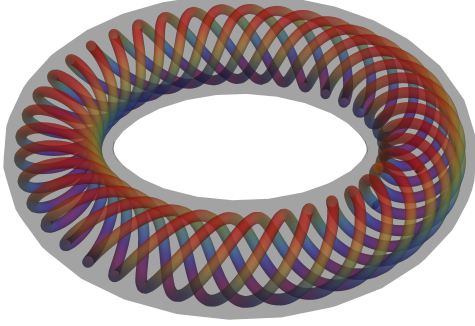
Figure 2.1: A current density, illustrated by the coloured lines, confined to a toroidal domain.
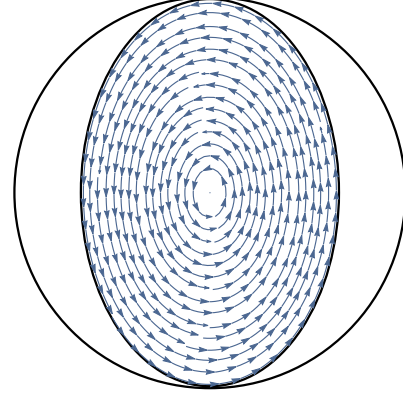
Figure 2.2: Elliptical cross-section of fusion reactor, circumscribed by a toroidal domain with a circular cross-section.

2.2 Governing Equations

The relation of a given current density and its generated magnetic field is described by Maxwell's equations. We assume the magnetostatic case, i.e. the fields are stationary. In that case, the macroscopic Maxwell equations for the magnetic field reduce to

$$\nabla \cdot \vec{B} = 0 \tag{2.9}$$
$$\nabla \times \vec{H} = \vec{J}_f. \tag{2.10}$$

Equation (2.10) is Ampere's law in differential form. $\vec{B}$ is the magnetic flux density or just magnetic field, $\vec{H}$ is the magnetic field strength and $\vec{J}_f$ the free current density. Furthermore, we only assume linear media, i.e. magnetic field and magnetic field strength are related as follows.

$$\vec{B} = \mu \vec{H} \tag{2.11}$$

μ is the magnetic permeability and independent of the magnetic field $\vec{H}$ for linear media. Nevertheless, μ can vary spatially. By introducing a vector potential

$$\vec{B} = \nabla \times \vec{A}, \tag{2.12}$$

equation (2.9) is fulfilled automatically according to vector calculus. So the two

magnetostatic Maxwell equations reduce to one equation for the vector potential $\vec{A}$.

$$\nabla \times \frac{1}{\mu} \left(\nabla \times \vec{A} \right) = \vec{J}_f \tag{2.13}$$

From now on we will denote the free current density $\vec{J}_f$ simply as $\vec{J}$. So the resulting equation

$$\nabla \times \mu^{-1} \left(\nabla \times \vec{A} \right) = \vec{J} \tag{2.14}$$

fully describes the problem. The continuity equation for the current density $\vec{J}$ in the magnetostatic case reduces to

$$\nabla \cdot \vec{J} = 0. \tag{2.15}$$

2.3   Solution Approach
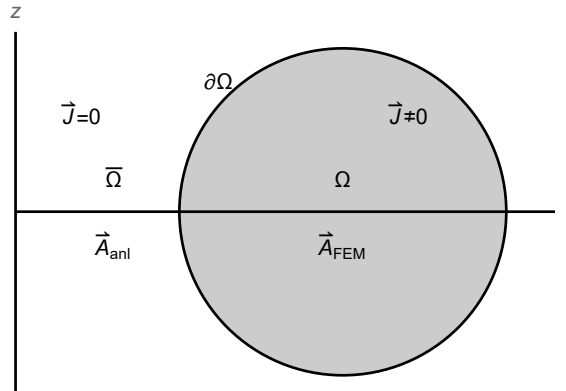
Figure 2.3: Cross-section of a toroidal domain and illustration of the applied solution approach. Inside the toroidal domain (gray) a numerical method is applied while in the outside an analytical solution is obtained.

Equation (2.14) for the vector potential $\vec{A}$ is a partial differential equation (PDE). In order to find a solution to this equation in a certain domain of interest, we have to solve a boundary value problem (BVP). The boundary value problem consists of the PDE itself and some kind of boundary conditions, imposed on the boundary of the domain. The first step in the process of solving the BVP is to determine the domain of interest, within which we want to obtain the solution, i.e. the magnetic field or

equivalent, the vector potential. In our case we choose the toroidal domain Ω (the cross-section of the toroidal domain is depicted in gray in figure 2.3), confining the current density. We are not interested of the magnetic field outside of Ω. Furthermore, we have to impose certain boundary conditions on the boundary of the domain, i.e. we have to prescribe the magnetic field on the boundary. According to [18], the boundary value problem can be formulated as follows.

$$
\begin{cases}
\nabla \times \mu^{-1} \left(\nabla \times \vec{A} \right) = \vec{J} & in \quad \Omega \\
\vec{B} \cdot \vec{n} = -b & on \quad \Gamma_B \\
\vec{H} \times \vec{n} = \vec{K} & on \quad \Gamma_H
\end{cases}
\tag{2.16}
$$

with b the magnetic surface charge density and $\vec{K}$ the surface current density [18]. The first boundary condition corresponds to the normal component of the magnetic field, the second boundary condition corresponds to the tangential component of the magnetic field strength. Γ_B and Γ_H denote parts of the boundary on which the respective boundary condition is imposed, with $\Gamma_B \cup \Gamma_H = \partial\Omega$. The obtained solution for the magnetic field is unique. It is important to note that these two boundary conditions are not the only ones that solve the problem uniquely. Different boundary conditions are possible.

This kind of BVPs are usually not solvable by analytical methods and thus, we have to solve it numerically. A well suited method is the finite element method (FEM, see chapter 5). FEM is a well studied and widely used numerical method for solving BVPs. The primary part of this work is not devoted to the FEM itself, but to the problem of obtaining the boundary values. A priori we have no knowledge about the magnetic field, neither on the boundary nor inside the domain. The only information we have is that the magnetic field at infinity must converge to 0 [11], everything else would be not physical. The asymptotic behaviour can be written like

$$
\left| \vec{B} \right| \propto \frac{1}{r^2}, \quad r \to \infty.
\tag{2.17}
$$

r denotes the distance from the origin. In the outside of the toroidal domain, $(\bar{\Omega}$, figure 2.3), the current density is $\vec{J} = 0$, i.e. equation (2.14) writes like

$$
\nabla \times \mu^{-1} \left(\nabla \times \vec{A} \right) = \vec{0}.
\tag{2.18}
$$

We can find a general analytical solution for this homogeneous problem in the outer region (see chapter 4).

Note: In order to find an analytical solution in the outer region, the magnetic permeability μ must be constant!

By construction, the analytical solution fulfils the homogeneous boundary conditions at infinity. This general analytical solution can be used to obtain the boundary values on a finite boundary, like the boundary $\partial\Omega$ of the toroidal domain Ω. The basic idea is to connect the analytical solution in the outside to a numerical solution in the inside. In other words, we transfer the boundary values from infinity, through the analytical solution, on the boundary of a finite domain. This can be done by imposing a certain kind of boundary condition for the numerical method in the inside, utilizing the general analytical solution in the outside. This boundary condition is called **open boundary condition** [20] and is similar to a homogeneous Robin boundary condition [7]. The name is reasoned by the fact, that such boundary conditions relate the computational domain with the outside of the domain. The open boundary condition maps the values of one boundary condition to the values of a second of boundary condition [10], whereas both boundary conditions solve the problem uniquely. In our case we want to find an operator $\hat{O}_{PS}$, to which the following relation applies.

$$\vec{H} \times \vec{n} = \hat{O}_{PS} \left[\vec{B} \cdot \vec{n} \right] \quad \text{on } \partial\Omega \tag{2.19}$$

Such operators are called Poincaré-Steklov operators [6] [19]. It maps the values of the normal component of the magnetic field to the values of the tangential component of the magnetic field strength. In chapter 8 we will show how to obtain the Poincaré-Steklov operators.

Chapter 3

Mathematical Formulation

In this chapter we will simplify the governing equations of the last chapter, utilizing the symmetry of the problem. By choosing an appropriate coordinate system and ansatz for the occurring fields, we can reduce the dimension of the problem. A reduction of dimensionality implies a drastically reduced computational effort for solving the problem.

3.1 Maxwell's Equations in Rotational Coordinates

In this section we will try to simplify equation (2.14) for the vector potential $\vec{A}$ by choosing an appropriate coordinate system and ansatz for the occurring fields in the PDE. Since the toroidal domain, confining the current density, has a rotational symmetry, it is reasonable to use some kind of rotational orthogonal coordinates (see Appendix A.1.2) for this application. (u, v, ϕ) denotes a general 3D rotational coordinate system, where (u, v) are general orthogonal 2D-coordinates, rotated about an axis, z usually. The azimuthal angle ϕ denotes the rotational angle around the axis of rotation. First, we expand the total current density in harmonics of the azimuthal angle ϕ.

$$\vec{J}_{tot} = \sum_{m=-\infty}^{\infty} \vec{j}^m(u, v) e^{im\phi} \tag{3.1}$$

with $m \in \mathbb{Z}$ the mode number and $\vec{j}^m$ the Fourier coefficients of the current density. Additionally, we require μ to be axisymmetric, i.e. independent of ϕ. Otherwise, modes are coupling and can not be treated independently. By treating only one mode

at a time we can write the fields as follows. From now on we omit the superscript m.

$$\vec{A}(u, v, \phi) = \vec{a}(u, v)e^{im\phi} \tag{3.2}$$

$$\vec{J}(u, v, \phi) = \vec{j}(u, v)e^{im\phi} \tag{3.3}$$

$$\vec{B}(u, v, \phi) = \vec{b}(u, v)e^{im\phi} \tag{3.4}$$

In this work, fields denoted with a lower case letter, are axisymmetric. Fields, denoted with an upper case letter, are non-axisymmetric.

Applying this ansatz to the initial equation (2.14) leads to reduced equations. For the derivation, the axisymmetric case ($m = 0$) and the non-axisymmetric cases ($m \neq 0$) have to be distinguished. Furthermore, we are going to introduce another notation, used throughout this work, namely the poloidal-toroidal decomposition of vector fields. A general vector field $\vec{E}$ can be written as a composition of a toroidal and a poloidal part. The poloidal part, denoted as $\vec{E}_p$, is the part of the vector which is projected on a $\phi = const$ plane. The toroidal part, denoted as $\vec{E}_t$, is the part of the vector perpendicular to the $\phi = const$ plane.

$$\vec{E} = \vec{E}_p + \vec{E}_t = \begin{pmatrix} E_u \\ E_v \\ E_\phi \end{pmatrix}$$

$$\vec{E}_p = \begin{pmatrix} E_u \\ E_v \\ 0 \end{pmatrix} = E_u\vec{e}_u + E_v\vec{e}_v \tag{3.5}$$

$$\vec{E}_t = \begin{pmatrix} 0 \\ 0 \\ E_\phi \end{pmatrix} = E_\phi\vec{e}_\phi$$

3.2 Axisymmetric Case

In the axisymmetric case

$$\nabla \times \mu^{-1} \left[\nabla \times \vec{a}(u,v) \right] = \vec{j}(u,v) \tag{3.6}$$

will be evaluated. To further simplify, we decompose $\vec{a}$ in a toroidal and poloidal part. Applying both parts of the vector potential to the equation above gives

$$\nabla \times \vec{a}_p = \begin{pmatrix} 0 \\ 0 \\ \frac{1}{h_u h_v} \left[\partial_u \left(h_v a_v \right) - \partial_v \left(h_u a_u \right) \right] \end{pmatrix} = \begin{pmatrix} 0 \\ 0 \\ b_\phi \end{pmatrix} = \vec{b}_t \tag{3.7}$$

$$\nabla \times \vec{a}_t = \begin{pmatrix} \frac{1}{h_v h_\phi} \partial_v \left(h_\phi a_\phi \right) \\ -\frac{1}{h_u h_\phi} \partial_u \left(h_\phi a_\phi \right) \\ 0 \end{pmatrix} = \begin{pmatrix} b_u \\ b_v \\ 0 \end{pmatrix} = \vec{b}_p. \tag{3.8}$$

A poloidal vector potential creates a toroidal magnetic field and vice versa. Applying these results to Ampere's law (2.10) leads to

$$\nabla \times \mu^{-1} \vec{b}_t = \begin{pmatrix} \frac{1}{h_v h_\phi} \partial_v \left(h_\phi \mu^{-1} b_\phi \right) \\ -\frac{1}{h_u h_\phi} \partial_u \left(h_\phi \mu^{-1} b_\phi \right) \\ 0 \end{pmatrix} = \begin{pmatrix} j_u \\ j_v \\ 0 \end{pmatrix} = \vec{j}_p \tag{3.9}$$

$$\nabla \times \mu^{-1} \vec{b}_p = \begin{pmatrix} 0 \\ 0 \\ \frac{1}{h_u h_v} \left[\partial_u \left(h_v \mu^{-1} b_v \right) - \partial_v \left(h_u \mu^{-1} b_u \right) \right] \end{pmatrix} = \begin{pmatrix} 0 \\ 0 \\ j_\phi \end{pmatrix} = \vec{j}_t. \tag{3.10}$$

A poloidal current density creates a toroidal magnetic field and vice versa. Combining equations (3.7) and (3.8) with equations (3.9) and (3.10) gives the equations

$$\nabla \times \mu^{-1} \left(\nabla \times \vec{a}_p \right) = \vec{j}_p \tag{3.11}$$

$$\nabla \times \mu^{-1} \left(\nabla \times \vec{a}_t \right) = \vec{j}_t. \tag{3.12}$$

As we can see, a poloidal current density $\vec{j}_p$ generates a poloidal vector potential $\vec{a}_p$.

The same is true for a toroidal current density $\vec{j}_t$ which generates a toroidal vector potential $\vec{a}_t$. Hence, the initial equation decouples in two independent equations for the poloidal and toroidal parts of the fields.

Expressing the toroidal vectors by the corresponding ϕ-components of the vectors leads to a different form of equation (3.12).

$$-h_\phi \nabla \frac{\mu^{-1}}{h_\phi^2} \nabla \left(h_\phi a_\phi \right) = j_\phi \tag{3.13}$$

This equation will be denoted as **modified Poisson's equation**. Evaluating the continuity equation for the current density (2.15), considering equation (A.8) for the divergence in curvilinear coordinates, gives the following result.

$$\nabla \cdot \vec{j} = \frac{1}{h_u h_v h_\phi} \begin{pmatrix} \partial_u h_v h_\phi \\ \partial_v h_u h_\phi \\ \partial_\phi h_u h_v \end{pmatrix} \cdot \vec{j} = \frac{1}{h_u h_v h_\phi} \begin{pmatrix} \partial_u h_v h_\phi j_u \\ \partial_v h_u h_\phi j_v \\ 0 \end{pmatrix} = \nabla \cdot \vec{j}_p = 0 \tag{3.14}$$

The same is valid for the magnetic field.

$$\nabla \cdot \vec{b} = \nabla \cdot \vec{b}_p = 0 \tag{3.15}$$

3.3   Non-Axisymmetric Case

In the non-axisymmetric case

$$\nabla \times \mu^{-1} \left[\nabla \times \vec{a}(u,v) e^{im\phi} \right] = \vec{j}(u,v) e^{im\phi} \tag{3.16}$$

will be evaluated. To further simplify, the vector potential will be gauged, which leaves the magnetic field unchanged.

$$\vec{A} = \vec{a} e^{im\phi} = \vec{A}' + \nabla \chi = \vec{a}' e^{im\phi} + \nabla \chi \tag{3.17}$$

The idea is to find a function χ, so that the ϕ-component of $\vec{a}$ vanishes [27]. According

to (A.7), the gradient can be written

$$\nabla\chi(u,v,\phi) = \begin{pmatrix} \frac{1}{h_u}\partial_u \\ \frac{1}{h_v}\partial_v \\ \frac{1}{h_\phi}\partial_\phi \end{pmatrix} \chi(u,v,\phi). \tag{3.18}$$

Without further considerations, we indicate the result for the function χ. By evaluating the gradient of χ and replacing it in equation (3.17), the correctness of χ is proven.

$$\chi(u,v,\phi) = -\frac{h_\phi}{im}a'_\phi e^{im\phi} \tag{3.19}$$

$$\nabla\chi(u,v,\phi) = -e^{im\phi}\begin{pmatrix} \frac{1}{h_u}\partial_u\left(\frac{h_\phi}{im}a'_\phi\right) \\ \frac{1}{h_v}\partial_v\left(\frac{h_\phi}{im}a'_\phi\right) \\ a'_\phi \end{pmatrix} \tag{3.20}$$

$$\vec{A} = \vec{a}'e^{im\phi} + \nabla\chi = e^{im\phi}\begin{pmatrix} a'_u \\ a'_v \\ a'_\phi \end{pmatrix} - e^{im\phi}\begin{pmatrix} \frac{1}{h_u}\partial_u\left(\frac{h_\phi}{im}a'_\phi\right) \\ \frac{1}{h_v}\partial_v\left(\frac{h_\phi}{im}a'_\phi\right) \\ a'_\phi \end{pmatrix} = e^{im\phi}\begin{pmatrix} a_u \\ a_v \\ 0 \end{pmatrix} = e^{im\phi}\vec{a}_p \tag{3.21}$$

As we can see in the equation above, with the gauge transformation it is possible to eliminate the toroidal part of the vector potential $\vec{A}$ without any restrictions. Therefore, the vector potential only consists of a poloidal part. It is also obvious, why we had to separate the cases $m = 0$ and $m \neq 0$. In the equation above, m appears in the denominator and thus, is not defined for $m = 0$. With this result, we can derive an expression for the magnetic field.

$$\vec{B} = \vec{b}e^{im\phi} = \nabla \times \vec{a}_p e^{im\phi} \tag{3.22}$$

Applying the vector calculus identity (A.16) gives

$$\vec{b}e^{im\phi} = e^{im\phi}\nabla \times \vec{a}_p + \nabla e^{im\phi} \times \vec{a}_p =$$
$$= e^{im\phi}\nabla \times \vec{a}_p + e^{im\phi}\frac{im}{h_\phi}\vec{e}_\phi \times \vec{a}_p. \tag{3.23}$$

By reducing the phase factor we obtain

$$\vec{b} = \nabla \times \vec{a}_p + \frac{im}{h_\phi}\vec{e}_\phi \times \vec{a}_p \tag{3.24}$$

where we can easily identify the toroidal and poloidal part.

$$\vec{b}_p = \frac{im}{h_\phi}\vec{e}_\phi \times \vec{a}_p \tag{3.25}$$

$$\vec{b}_t = \nabla \times \vec{a}_p \tag{3.26}$$

Substituting these result to Ampere's law (2.10) and applying the identity (A.16) again leads to

$$e^{im\phi}\nabla \times \left(\mu^{-1}\nabla \times \vec{a}_p\right) + ime^{im\phi}\nabla \times \left(\frac{\mu^{-1}}{h_\phi}\vec{e}_\phi \times \vec{a}_p\right) + e^{im\phi}\frac{m^2}{h_\phi^2}\mu^{-1}\vec{a}_p = \vec{j}e^{im\phi}. \tag{3.27}$$

The vector calculus identities (A.17) and (A.18) applied to the second term on the left hand side and dividing by $e^{im\phi}$ gives

$$\nabla \times \left(\mu^{-1}\nabla \times \vec{a}_p\right) + \vec{e}_\phi imh_\phi\left[\nabla \cdot \left(\frac{\mu^{-1}}{h_\phi}\vec{a}_p\right)\right] + \mu^{-1}\frac{m^2}{h_\phi^2}\vec{a}_p = \vec{j}. \tag{3.28}$$

The first term on the left hand side is a poloidal vector (compare to axisymmetric case, section 3.2), as well as the third term. The second term is only toroidal. Therefore, we can separate the equation into two independent equations.

$$\nabla \times \left(\mu^{-1}\nabla \times \vec{a}_p\right) + \mu^{-1}\frac{m^2}{h_\phi^2}\vec{a}_p = \vec{j}_p \tag{3.29}$$

$$imh_\phi\left[\nabla \cdot \left(\frac{\mu^{-1}}{h_\phi}\vec{a}_p\right)\right] = j_\phi \tag{3.30}$$

In the system of equations above, we have 3 equations and 2 unknowns, namely a_u and a_v. The first equation is a vector equation with 2 non-zero components and is therefore sufficient to determine $\vec{a}_p$. The second equation results of the continuity equation and is no longer considered. Evaluating the continuity equation for the current density and the divergence freeness of the magnetic field gives the following

results.

$$\nabla \cdot \vec{J} = \nabla \cdot e^{im\phi} \left(\vec{j}_p + \vec{j}_t \right) = e^{im\phi} \left(\nabla \cdot \vec{j}_p + \frac{im}{h_\phi} j_\phi \right) = 0 \qquad (3.31)$$

$$\nabla \cdot \vec{j}_p + \frac{im}{h_\phi} j_\phi = 0 \qquad (3.32)$$

$$\nabla \cdot \vec{b}_p + \frac{im}{h_\phi} b_\phi = 0 \qquad (3.33)$$

With these equations we can calculate the toroidal part of the current density j_ϕ or the magnetic field b_ϕ for a given poloidal current density $\vec{j}_p$ or magnetic field $\vec{b}_p$, respectively.

3.4   Summary

We can combine and generalise the governing equations for the axisymmetric case ($m = 0$) and the non-axisymmetric case ($m \neq 0$). The poloidal part of the vector potential $\vec{a}_p$ can be calculated for any given $m \in \mathbb{Z}$ by the following equation.

$$\boxed{\nabla \times \left(\mu^{-1}\nabla \times \vec{a}_p\right) + \mu^{-1}\frac{m^2}{h_\phi^2}\vec{a}_p = \vec{j}_p} \tag{3.34}$$

The toroidal part of the vector potential $\vec{a}_t$, or equivalent the component a_ϕ, can be calculated with the following equations.

$$\boxed{\begin{cases} a_\phi = 0 & m = 0 \\ -h_\phi\nabla\frac{\mu^{-1}}{h_\phi^2}\nabla\left(h_\phi a_\phi\right) = j_\phi & m \neq 0 \end{cases}} \tag{3.35}$$

As we can see, the equations are now independent of the azimuthal angle ϕ, i.e. by just treating one single toroidal mode we could reduce the 3D problem to a 2D problem. Furthermore, the vector potential has only a poloidal component in the non-axisymmetric case. The resulting magnetic field is calculated using equation (2.12). The decoupled equations are written

$$\boxed{\begin{aligned} \vec{b}_t &= \nabla \times \vec{a}_p \\ \vec{b}_p &= \begin{cases} \nabla \times \vec{a}_t & m = 0 \\ \frac{im}{h_\phi}\vec{e}_\phi \times \vec{a}_p & m \neq 0 \end{cases} \end{aligned}} \tag{3.36}$$

For any m, the continuity equation for the current density and the divergence of the magnetic field can be written as follows.

$$\boxed{\begin{aligned} \nabla \cdot \vec{j}_p + \frac{im}{h_\phi}j_\phi &= 0 \\ \nabla \cdot \vec{b}_p + \frac{im}{h_\phi}b_\phi &= 0 \end{aligned}} \tag{3.37}$$

Note: In the non-axisymmetric case, the vector potential is gauged and therefore unique. In the axisymmetric case, we did not gauge the field. The vector potential is not unique. This fact has to be considered in the process of solving the equation.

Chapter 4

Analytical Solution in Outer Region

In the outer region $\bar{\Omega}$ of the toroidal domain, the current density is equal to 0. So we have to find a solution to the homogeneous Maxwell equations. They can be solved analytically. The magnetic permeability μ has to be constant in the outer region, e.g. $\mu = \mu_0$. μ_0 is the magnetic permeability of vacuum. This assumption is reasonable if no magnetic materials (or at least strong magnetic materials, i.e. high μ/μ_0) are present in the outer region. In that case, Ampere's law is written

$$\mu_0(\nabla \times \vec{B}) = 0 \qquad in \quad \bar{\Omega}. \tag{4.1}$$

Because of the above equation we can introduce a scalar potential Φ [11], with

$$\vec{B} = -\nabla\Phi \qquad in \quad \bar{\Omega}. \tag{4.2}$$

The magnetic flux is divergence free and thus, we get the Laplace equation for the scalar potential Φ.

$$\nabla \cdot \vec{B} = \nabla \cdot (-\nabla\Phi) = -\Delta\Phi = 0 \tag{4.3}$$

As we will see in the later sections, the analytical solution for the ϕ-component of the vector potential a_ϕ (3.35) in the axisymmetric case (m=0) is needed as well in the current free outer region. The equation is similar to Laplace's equation and will be denoted as **modified Laplace's equation**.

$$-h_\phi \nabla \frac{\mu^{-1}}{h_\phi^2} \nabla (h_\phi a_\phi) = 0 \tag{4.4}$$

17

4.1 Topology Considerations

The sometimes casually supposed definition of the scalar potential (4.2) requires a more precise consideration. Locally equation (4.1) is always valid, but globally problems may occur. The requirement for this relation is that the domain, in which the magnetic field is curl-free and therefore, we can define a scalar potential, must be simply connected. A domain is simply connected if any closed path inside the domain can be reduced to a point. This is obviously not the case for a toroidal domain. The problem, that can occur in this context, is illustrated in the following.
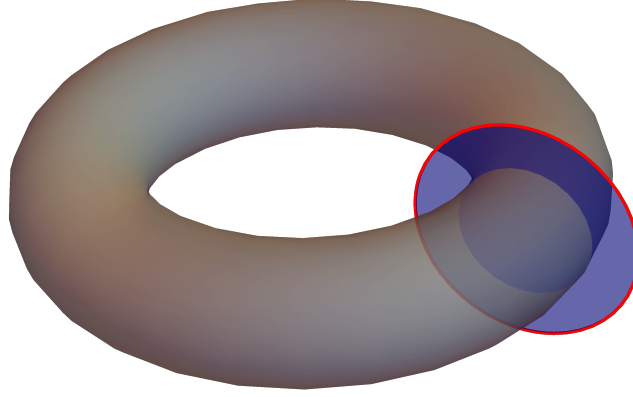
Figure 4.1: The integration path around the toroidal domain is depicted in red.

We consider Ampere's law for magnetostatics (2.10) with a current density confined to a toroidal domain Ω (see figure 4.1). We integrate Ampere's law over the cross-sectional area A_t (depicted in blue in figure 4.1) and apply Stokes' integral theorem [15].

$$\nabla \times \mu^{-1}\vec{B} = \vec{J} \qquad \left| \int_{A_t} d\vec{A} \right.$$

$$\int_{A_t} \nabla \times \mu^{-1}\vec{B} \cdot d\vec{A} = \int_{A_t} \vec{J} \cdot d\vec{A} = I_t \tag{4.5}$$

$$\mu^{-1} \oint_{\partial A_t} \vec{B} \cdot d\vec{s} = \int_{A_t} \vec{J} \cdot d\vec{A} = I_t$$

I_t denotes the toroidal current through the cross-section A_t. The integration path ∂A_t is depicted in red in figure 4.1. This integration path is outside the toroidal domain Ω and therefore, the scalar potential is defined and μ is constant. Replacing

the magnetic field by the scalar potential gives

$$-\mu^{-1} \oint_{\partial A_t} \nabla \Phi \cdot d\vec{s} = I_t = 0. \tag{4.6}$$

According to the gradient theorem [15], the integral of a gradient along a closed integration path is 0. Thus, the toroidal current through the cross-section of the torus must be $I_t = 0$. But when is this circumstance really causing problems?
In the following, we calculate the toroidal current I_t of a single toroidal mode.

$$\vec{J}(u,v,\phi) = \vec{j}(u,v)e^{im\phi} \qquad \left| \int_{A_t} d\vec{A} \right.$$

$$I_t = \int_{A_t} \vec{j}(u,v)e^{im\phi} \cdot d\vec{A} = e^{im\phi} \int_{A_t} \vec{j}(u,v) \cdot \vec{n} dA = e^{im\phi} \int_{A_t} j_\phi(u,v) dA \tag{4.7}$$

j_ϕ can be replaced using equation (3.37) for the divergence of the current density. We obtain

$$I_t = -e^{im\phi} \int_{A_t} \frac{h_\phi}{im} \nabla \cdot \vec{j}_p dA = -\frac{e^{im\phi}}{im} \int_{A_t} \nabla_\perp \cdot \left(h_\phi \vec{j}_p \right) dA. \tag{4.8}$$

$\nabla_\perp$ denotes the 2D divergence operator in the cross-sectional plane. Applying Gauss's integral theorem in 2D [15] gives

$$I_t = -\frac{e^{im\phi}}{im} \oint_{\partial A_t} h_\phi \vec{j}_p \cdot \vec{n} ds. \tag{4.9}$$

The term $\vec{j}_p \cdot \vec{n}$ is 0 in the entire outer region. Hence, the toroidal current I_t is 0 in the non-axisymmetric case and fulfils the requirement. However, in the axisymmetric case, this relation is not valid due to the mode number $m = 0$ in the denominator and we are not allowed to define a scalar potential Φ in that case.

4.2   Toroidal Coordinates

This section is based on [13] and [21]. Before solving the equations, we have to choose appropriate coordinates, such that we obtain a general, regular solution in the outer region. Coordinate surfaces should match the toroidal domain confining the current density. This simplifies the process of determining the constants, occurring in the obtained general solution. Toroidal coordinates $\{\eta, \theta, \phi\}$ fulfil these requirements. In the following, a short introduction to toroidal coordinates is given. The transformation to Cartesian coordinates can be written as

$$
\begin{aligned}
x &= a\frac{\sinh\eta}{\cosh\eta - \cos\theta}\cos\phi \\
y &= a\frac{\sinh\eta}{\cosh\eta - \cos\theta}\sin\phi \\
z &= a\frac{\sin\theta}{\cosh\eta - \cos\theta}
\end{aligned}
\tag{4.10}
$$

with

$$
\eta \geq 0, \quad -\pi < \theta \leq \pi, \quad 0 \leq \phi < 2\pi.
\tag{4.11}
$$

The inverse transformation is

$$
\begin{aligned}
\eta &= 2\,\mathrm{Re}\left[\mathrm{acoth}\left(\frac{\sqrt{x^2 + y^2} + iz}{a}\right)\right] \\
\theta &= -2\,\mathrm{Im}\left[\mathrm{acoth}\left(\frac{\sqrt{x^2 + y^2} + iz}{a}\right)\right] \\
\phi &= \mathrm{atan}\left(\frac{y}{x}\right).
\end{aligned}
\tag{4.12}
$$

The coordinate surfaces of toroidal coordinates are shown in figure 4.2. For a constant η a torus, depicted in red in the figure 4.2, is obtained. By increasing η, the radius of the torus gets smaller. When $\eta \to \infty$, the torus intersects with the so called focal ring of radius a. The radius of the central circle of a torus decreases with increasing η. The radius of a torus η_0 is r_0 and the radius of the central circle is R_0, with

$$
\begin{aligned}
R_0 &= \coth\left(\eta_0\right) \\
r_0 &= \frac{a}{\sinh\eta_0}.
\end{aligned}
\tag{4.13}
$$

For a constant, positive θ we obtain a spherical cap in positive z-direction (upper, in blue depicted spherical cap in figure 4.2), intersecting with the focal ring at z=0. A negative θ results in a spherical cap in the negative z-direction. A constant ϕ yields a half plane (depicted in green in figure 4.2), intersecting with the z axis. In figure 4.3 coordinate lines for different values of η and θ are drawn for a plane intersecting with the z axis.
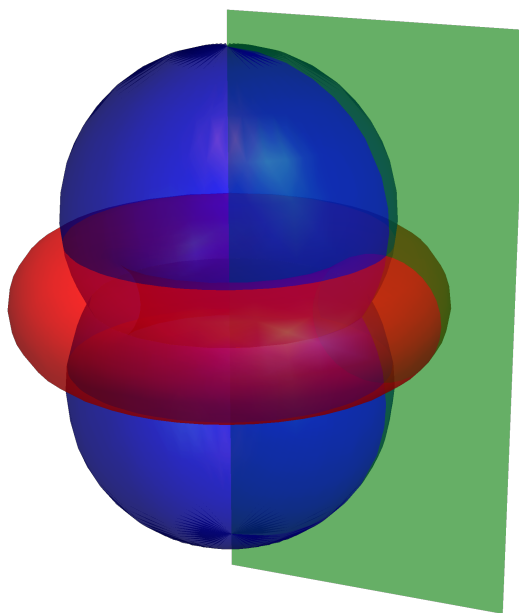
Figure 4.2: Coordinate surfaces of toroidal coordinates.

Toroidal coordinates are orthogonal. Thus, the metric tensor of the toroidal coordinate system $\{\eta, \theta, \phi\}$ is diagonal with the metric coefficients

$$
\begin{aligned}
g_{\eta\eta} = g_{\theta\theta} &= \frac{a^2}{(\cosh\eta - \cos\theta)^2} \\
g_{\phi\phi} &= \frac{a^2 \sinh^2 \eta}{(\cosh\eta - \cos\theta)^2} \\
g^{1/2} &= \frac{a^3 \sinh\eta}{(\cosh\eta - \cos\theta)^3}.
\end{aligned}
\tag{4.14}
$$
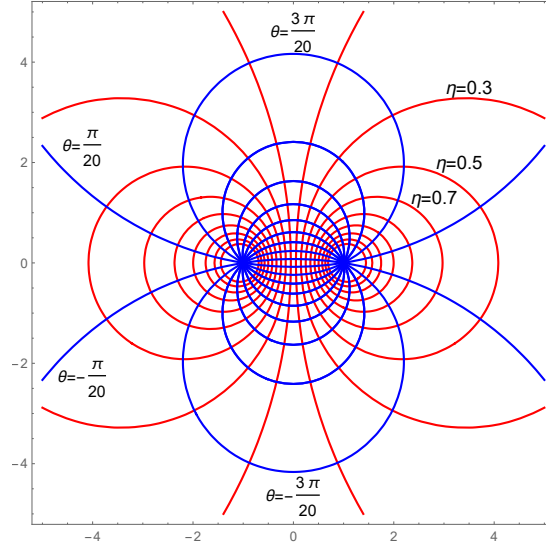
Figure 4.3: Coordinate lines of toroidal coordinates on a $\phi = $ const-plane.

For orthogonal coordinates and diagonal metric tensor we can define the scale factors.

$$
\begin{aligned}
h_i &:= \sqrt{g_{ii}} = |\vec{e}_i| \\
h_\eta &= h_\theta = \frac{a}{\cosh\eta - \cos\theta} \\
h_\phi &= \frac{a\sinh\eta}{\cosh\eta - \cos\theta}
\end{aligned}
\tag{4.15}
$$

The function $(\cosh\eta - \cos\theta)$ will appear rather frequently and thus, will be assigned to the symbol $\mathfrak{R}$.

$$
\mathfrak{R} := \cosh\eta - \cos\theta
\tag{4.16}
$$

4.3 Laplace's Equation in Toroidal Coordinates

According to [21], Laplace's equation in toroidal coordinates is

$$\Delta\Phi = \frac{\mathfrak{R}^3}{a^2\sinh\eta}\left[\frac{\partial}{\partial\eta}\left(\frac{\sinh\eta}{\mathfrak{R}}\frac{\partial\Phi}{\partial\eta}\right) + \sinh\eta\frac{\partial}{\partial\theta}\left(\frac{1}{\mathfrak{R}}\frac{\partial\Phi}{\partial\theta}\right)\right] + \frac{\mathfrak{R}^2}{a^2\sinh^2\eta}\frac{\partial^2\Phi}{\partial\phi^2}. \quad (4.17)$$

The Laplace equation in toroidal coordinates is not separable with a conventional product ansatz, but by R-separation. The ansatz is

$$\Phi_p = \sqrt{\mathfrak{R}}H(\eta)\Theta(\theta)\Psi(\phi). \quad (4.18)$$

After applying the ansatz to the Laplace's equation, the following particular solutions are obtained [21].

$$H(\eta) = A_{mn}P^m_{n-\frac{1}{2}}(\cosh\eta) + B_{mn}Q^m_{n-\frac{1}{2}}(\cosh\eta)$$
$$\Theta(\theta) = e^{in\theta} \quad (4.19)$$
$$\Psi(\phi) = e^{im\phi}$$

with the separation constants $\{n, m\} \in \mathbb{Z}$, $P^\mu_\nu(z)$ the associated Legendre function of the first kind and $Q^\mu_\nu(z)$ of the second kind (see Appendix B). The general solution is a linear combination of all the particular solutions.

$$\Phi(\eta,\theta,\phi) = \sqrt{\mathfrak{R}}\sum_{m=-\infty}^{\infty}\sum_{n=-\infty}^{\infty}\left[A_{mn}P^m_{n-\frac{1}{2}}(\cosh\eta) + B_{mn}Q^m_{n-\frac{1}{2}}(\cosh\eta)\right]e^{i(m\phi+n\theta)}$$
$$(4.20)$$

The argument of the toroidal functions $P^m_{n-\frac{1}{2}}$ and $Q^m_{n-\frac{1}{2}}$ in the solution above is $z = \cosh\eta$. In the outer region $\eta \to 0$, which corresponds to $z \to 1$. The toroidal functions of the second kind $Q^m_{n-\frac{1}{2}}(\cosh\eta)$ are therefore singular in the outer region (see Appendix B) and can be neglected by setting the constants $B_{mn} = 0$ [26]. The general solutions to Laplace's equation for the scalar potential Φ in the outer region is

$$\boxed{\Phi(\eta,\theta,\phi) = \sqrt{\mathfrak{R}}\sum_{m=-\infty}^{\infty}\sum_{n=-\infty}^{\infty}A_{mn}P^m_{n-\frac{1}{2}}(\cosh\eta)e^{i(m\phi+n\theta)}}. \quad (4.21)$$

4.4   Modified Laplace's Equation in Toroidal Coordinates

The modified Laplace's equation (4.4) in toroidal coordinates can be evaluated with the gradient and divergence in toroidal coordinates [21].

$$\nabla \Phi = \frac{\mathfrak{R}}{a} \begin{pmatrix} \frac{\partial \Phi}{\partial \eta} \\ \frac{\partial \Phi}{\partial \theta} \\ \frac{1}{\sinh \eta} \frac{\partial \Phi}{\partial \phi} \end{pmatrix} \tag{4.22}$$

$$\nabla \cdot \vec{E} = \frac{\mathfrak{R}^3}{a \sinh \eta} \left[\frac{\partial}{\partial \eta} \left(\frac{\sinh \eta}{\mathfrak{R}^2} E_\eta \right) + \sinh \eta \frac{\partial}{\partial \theta} \left(\frac{1}{\mathfrak{R}^2} E_\theta \right) \right] + \frac{\mathfrak{R}}{a \sinh \eta} \frac{\partial E_\phi}{\partial \phi} \tag{4.23}$$

Now we can evaluate equation (4.4) to

$$-h_\phi \nabla \frac{1}{h_\phi^2} \nabla \left[h_\phi a_\phi(\eta, \theta) \right] =$$

$$-\mathfrak{R}^2 \left\{ \frac{\partial}{\partial \eta} \left[\frac{\mathfrak{R}}{a^2 \sinh \eta} \frac{\partial}{\partial \eta} \left(\frac{\sinh \eta}{\mathfrak{R}} a_\phi \right) \right] + \frac{\partial}{\partial \theta} \left[\frac{\mathfrak{R}}{a^2 \sinh \eta} \frac{\partial}{\partial \theta} \left(\frac{\sinh \eta}{\mathfrak{R}} a_\phi \right) \right] \right\} = 0. \tag{4.24}$$

Multiplying with $-a^2/\mathfrak{R}^2$ gives

$$\frac{\partial}{\partial \eta} \left[\frac{\mathfrak{R}}{\sinh \eta} \frac{\partial}{\partial \eta} \left(\frac{\sinh \eta}{\mathfrak{R}} a_\phi \right) \right] + \frac{\partial}{\partial \theta} \left[\frac{\mathfrak{R}}{\sinh \eta} \frac{\partial}{\partial \theta} \left(\frac{\sinh \eta}{\mathfrak{R}} a_\phi \right) \right] = 0. \tag{4.25}$$

Also this modified Laplace equation is not separable with a conventional product ansatz, but with the ansatz

$$a_\phi^p = \sqrt{\frac{\mathfrak{R}}{\sinh \eta}} H(\eta) \Theta(\theta). \tag{4.26}$$

Applying the ansatz to the modified Laplace equation, the following particular solutions are obtained.

$$H(\eta) = A_n Q_{\frac{1}{2}}^n (\coth \eta) + B_n P_{\frac{1}{2}}^n (\coth \eta)$$

$$\Theta(\theta) = e^{in\theta} \tag{4.27}$$

with the separation constant $n \in \mathbb{Z}$, and again the associated Legendre functions

of the first and second kind, $P_\nu^\mu(z)$ and $Q_\nu^\mu(z)$. The general solution is a linear combination of all the particular solutions.

$$a_\phi(\eta, \theta) = \sqrt{\frac{\Re}{\sinh \eta}} \sum_{n=-\infty}^{\infty} \left[A_n Q_{\frac{1}{2}}^n(\coth \eta) + B_n P_{\frac{1}{2}}^n(\coth \eta) \right] e^{in\theta} \tag{4.28}$$

In the solution above, the argument of the toroidal functions $P_\nu^\mu(z)$ and $Q_\nu^\mu(z)$ is $z = \coth \eta$. $\eta \to 0$ corresponds to $z \to \infty$, so the toroidal functions of the first kind $P_{1/2}^n(\coth \eta)$ are singular in the outer region (see Appendix B) and can be neglected by setting the constants $B_n = 0$. The general solutions to the modified Laplace equation for the ϕ-component of the vector potential a_ϕ in the axisymmetric case in the outer region is

$$\boxed{a_\phi(\eta, \theta) = \sqrt{\frac{\Re}{\sinh \eta}} \sum_{n=-\infty}^{\infty} A_n Q_{\frac{1}{2}}^n(\coth \eta) e^{in\theta}}. \tag{4.29}$$

Chapter 5

Formulation of the Finite Element Method

This and the following sections are based on [12] and [17]. Problems of mathematical physics are in most applied cases hard to solve or even unsolvable with analytical methods. One kind of mathematical problems are boundary value problems (BVPs), like the Maxwell equations of chapter 3. Due to complex or non-analytical inhomogeneities or boundary conditions, complex computational domains or the complexity (e.g. non-linearity) of the equations themselves, other methods are sought. In that case, a variety of numerical methods are available to obtain an approximate solution, like the Finite-Difference-Method, Numerical-Integration and the Finite-Element-Method. For our problem of finding solutions to the equations derived in chapter 3, we will use the Finite-Element-Method (FEM). The method is well studied and very flexible in terms of the considered domain, the variation of the discretization of the domain, variation of the boundary conditions, the material properties, etc. The FEM is basically a method to find an approximate solution to a BVP by transforming the BVP to an algebraic system of equations. In the following sections we will elaborate the essential steps of the FEM. We will start with the introduction of two different approaches: The variational approach and the weighted residual approach.

5.1 Variational Approach: Ritz's Method

The idea of the variational approach is to transform the BVP to an equivalent variational form. This form can be used to formulate a minimization problem. Given is a boundary value problem, governed by differential equation

$$\mathcal{L}\Phi = f \qquad \text{in} \quad \Omega. \tag{5.1}$$

$\mathcal{L}$ is a general differential operator and $\Omega \subset \mathbb{R}^d$ the domain, in which the solution Φ is sought. It is further assumed that $\mathcal{L}$ is self-adjoint and positive definite.

$$\langle \mathcal{L}\Phi, \Psi \rangle = \langle \Phi, \mathcal{L}\Psi \rangle \tag{5.2}$$

$$\langle \mathcal{L}\Phi, \Phi \rangle \to \begin{cases} > 0 & \Phi \neq 0 \\ = 0 & \Phi = 0 \end{cases} \tag{5.3}$$

Ψ is an arbitrary function, fulfilling the same boundary conditions as Φ. Then the solution can be computed by minimizing the functional [12]

$$F(\Phi) = \frac{1}{2}\langle \mathcal{L}\phi, \phi \rangle - \frac{1}{2}\langle \Phi, f \rangle - \frac{1}{2}\langle f, \Phi \rangle. \tag{5.4}$$

The angular brackets symbolise the inner product of two functions,

$$\langle \Phi, \Psi \rangle = \int_{\Omega} \Phi \Psi^* d\Omega. \tag{5.5}$$

By showing that the variation of $F(\Phi)$ is stationary ($\delta F = 0$) and the stationary point is a minimum ($\delta(\delta F) > 0$), it can be proven that minimizing the functional is equivalent to solving the corresponding BVP (see [12] for details).

5.1.1 Discretization

The next step after obtaining the variational form is to discretize the problem. That means that we project the solution onto a finite dimensional subspace of the complete solution space of the equation. The projection is an approximation of the exact solution. The subspace is spanned by a finite number of linear independent basis functions. In the following section we will show how to obtain the approximate

solution to a minimization problem, such as the variational form of the boundary value problem of the section before. In general, a minimisation problem is written

$$F(\Phi) \stackrel{!}{=} \min \tag{5.6}$$

with a functional F and the unknown function Φ. The approximate solution $\tilde{\Phi}$ within the finite dimensional subspace is

$$\tilde{\Phi} = \sum_{j=1}^{N} c_j \Phi_j. \tag{5.7}$$

Applying this approximation to the functional leaves a residuum r, i.e.

$$F(\tilde{\Phi}) = r. \tag{5.8}$$

The goal is to minimize the residuum r. The approximation $\tilde{\Phi}$ depends on the expansion coefficients c_j. In order to minimize the residuum, we differentiate the functional with respect to c_i.

$$\frac{\partial}{\partial c_i} F(\tilde{\Phi}) \stackrel{!}{=} 0 \tag{5.9}$$

This is a system of equations for the expansion coefficients which yields the best solution, i.e. the solution with the smallest residuum, within the subspace spanned by the basis functions Φ_j. Though, it is not a solutions to the original operator problem, i.e. not the global minimum.

5.1.2   Example: Electrostatic Problem

This example is taken from [12]. Let's consider an electrostatic boundary value problem governed by the PDE

$$-\nabla \cdot (\epsilon \nabla \Phi) = \rho \qquad \text{in} \quad \Omega. \tag{5.10}$$

The differential operator $\mathcal{L}$ of equation (5.1) can be identified as

$$\mathcal{L} = -\nabla \cdot \epsilon \nabla. \tag{5.11}$$

In [12] it is proven that $\mathcal{L}$ is self-adjoint and positive definite if Φ satisfies the

boundary condition

$$\Phi = 0 \qquad \text{on} \quad S1 \tag{5.12}$$

and

$$\epsilon \frac{\partial \Phi}{\partial \vec{n}} + \gamma \Phi = 0 \qquad \text{on} \quad S2, \tag{5.13}$$

with $S1 \cup S2 = \partial\Omega$ the boundary of the domain. Furthermore, ϵ and γ must be positive and nonzero real numbers or functions. Equation (5.12) represents a **homogeneous Dirichlet boundary condition**, whereas equation (5.13) represents a **homogeneous Robin boundary condition** [7]. With these restrictions, the functional F can be calculated according to equation (5.4). We evaluate the first term of equation (5.4) by applying the divergence theorem [15]. We obtain

$$\langle \mathcal{L}\Phi, \Phi \rangle = \int_{S2} \Phi^* \left(-\epsilon \frac{\partial \Phi}{\partial \vec{n}} \right) dS - \int_{\Omega} (-\epsilon \nabla \Phi) \cdot \nabla \phi^* d\Omega. \tag{5.14}$$

Inserting the homogeneous Robin boundary condition (5.13) to the boundary integral yields

$$\langle \mathcal{L}\Phi, \Phi \rangle = \int_{S2} \gamma \left| \Phi \right|^2 dS + \int_{\Omega} \epsilon \left| \nabla \Phi \right|^2 d\Omega. \tag{5.15}$$

Hence, the functional F is written

$$F(\Phi) = \frac{1}{2} \int_{\Omega} \epsilon \left| \nabla \Phi \right|^2 d\Omega + \frac{1}{2} \int_{S2} \gamma \left| \Phi \right|^2 dS - \frac{1}{2} \int_{\Omega} (\Phi \rho^* + \rho \Phi^*) \, d\Omega \stackrel{!}{=} \min. \tag{5.16}$$

For different boundary conditions, like inhomogeneous Dirichlet boundary conditions, this method of finding the functional F is not valid. In such cases, finding the functional F is not straightforward and is strongly dependent on the individual problem. But in general it can be shown that every boundary value problem can be transformed to a variational problem. The variational form of the problem and the original problem are equivalent.

Considering this example, the solution obtained by minimizing the functional F, automatically fulfils the homogeneous Robin boundary condition (5.13) on S2. Thus, it is called the **natural boundary condition**. On the contrary, the homogeneous

Dirichlet boundary condition has to be enforced on the solution by explicitly setting the function (on the part of the boundary with homogeneous Dirichlet condition, S1) to 0. Therefore, it is called the **essential boundary condition**. After obtaining the variational form, we perform the discretization as describe in the previous section. The approximation (5.7) is applied to the functional (5.16) and differentiated with respect to the expansion coefficients c_i. $\tilde{\Phi}$ and ρ are assumed to be real.

$$\frac{\partial}{\partial c_i} F(\tilde{\Phi}) = \int_\Omega \epsilon \nabla \tilde{\Phi} \nabla \Phi_i d\Omega + \int_{S2} \gamma \tilde{\Phi} \Phi_i dS - \int_\Omega \rho \Phi_i d\Omega \overset{!}{=} 0 \qquad (5.17)$$

By rearranging and inserting the expansion (5.7) we obtain a system of linear equations for the expansion coefficients.

$$\sum_{j=1}^{N} c_j \left[\int_\Omega \epsilon \nabla \Phi_j \nabla \Phi_i d\Omega + \int_{S2} \gamma \Phi_j \Phi_i dS \right] = \int_\Omega \rho \Phi_i d\Omega \qquad (5.18)$$

In matrix form it is written

$$\mathbf{A} \cdot \mathbf{c} = \mathbf{b}$$
$$A_{ij} = \int_\Omega \epsilon \nabla \Phi_j \nabla \Phi_i d\Omega + \int_{S2} \gamma \Phi_j \Phi_i dS \qquad (5.19)$$
$$b_i = \int_\Omega \rho \Phi_i d\Omega.$$

This system of linear equations can be solved numerically.

5.2 Weighted Residual Approach: Galerkin's Method

As mentioned before, obtaining the variational form of a BVP may be rather
inconvenient. The weighted residual approach is a more general way to transform a
BVP to an algebraic system of equations. With this method, there is no need for a
corresponding functional F which is then minimized.

A general BVP, governed by a PDE, can be written as an operator problem like

$$T(\Phi) = 0 \tag{5.20}$$

with a general operator T and the solution Φ. In the case of the electrostatic problem
(see section 5.1.2), the operator would look like

$$T(\Phi) = -\nabla(\epsilon\nabla\Phi) - \rho. \tag{5.21}$$

Hence, the scalar product, defined in equation (5.5), of $T(\Phi)$ with any arbitrary
weighting function w would give 0.

$$\langle w, T(\Phi) \rangle = 0 \tag{5.22}$$

Applying an approximate solution $\tilde{\Phi}$ to the operator leaves a residuum

$$\left\langle w, T(\tilde{\Phi}) \right\rangle = r. \tag{5.23}$$

In the next section we will show how to compute $\tilde{\Phi}$ by applying Galerkin's method.

5.2.1 Discretization

As in the previous section, we try to find an approximate solution within a finite
dimensional subspace of the complete solution space of the equation.

$$\tilde{\Phi} = \sum_{j=1}^{N} c_j \Phi_j \tag{5.24}$$

This approximation, applied to equation (5.23), leaves a non-zero residuum for
arbitrary weighting functions. Choosing a specific set of weighting functions would
leave the scalar product zero by determining the expansion coefficients c_j accordingly.
In that case $\tilde{\Phi}$ is not an exact solution but a **weak solution**. Galerkin's method

uses the basis functions of the subspace as weighting functions, i.e.

$$w = \phi_i. \tag{5.25}$$

This results in a system of algebraic equations for the expansion coefficients c_j.

$$\left\langle \Phi_i, T(\tilde{\Phi}) \right\rangle = 0 \tag{5.26}$$

This is called the **weak form** of the operator equation and the corresponding **weak solution**. The method will be displayed on an example of the electrostatic problem.

5.2.2 Example: Electrostatic Problem

The governing equations are given in section 5.1.2. In this example we consider functions and constants to be real. In addition we impose the general boundary conditions

$$\Phi = f \qquad \text{on} \quad S1 \tag{5.27}$$

and

$$\epsilon \frac{\partial \Phi}{\partial \vec{n}} + \gamma \Phi = g \qquad \text{on} \quad S2. \tag{5.28}$$

ϵ, γ, g and f are constants or functions and $S1 \cup S2 = \partial\Omega$ the boundary of the domain. Equation (5.27) represents a **inhomogeneous Dirichlet boundary condition**, whereas equation (5.28) represents a **Robin boundary condition**. **Neumann conditions** are a special case of the Robin boundary conditions with $\gamma = 0$. Evaluating equation (5.22) for the electrostatic problem gives

$$\langle w, T(\Phi) \rangle = \int_\Omega w \left[-\nabla \cdot (\epsilon \nabla \Phi) \right] d\Omega - \int_\Omega w \rho d\Omega = 0. \tag{5.29}$$

The weighting function w must be zero on the part of the boundary, where Dirichlet values are imposed, i.e. S1. Hence, applying the divergence theorem to the first integral yields

$$\langle w, r \rangle = \langle w, T(\Phi) \rangle = \int_\Omega \nabla w \cdot (\epsilon \nabla \Phi) d\Omega - \int_{S2} w \left(\epsilon \frac{\partial \Phi}{\partial \vec{n}} \right) - \int_\Omega w \rho d\Omega = 0. \tag{5.30}$$

The Neumann boundary condition in the second integral can be substituted with the Robin boundary condition (5.28).

$$\langle w, T(\Phi) \rangle = \int_\Omega \nabla w \cdot (\epsilon \nabla \Phi) d\Omega - \int_{S2} w \left(g - \gamma \Phi \right) - \int_\Omega w \rho d\Omega = 0 \qquad (5.31)$$

The solution Φ, satisfying the above equation, automatically fulfils the Robin boundary condition (5.28). Thus, it is the **natural boundary condition**. The Dirichlet boundary condition has to be enforced on the solution by explicitly setting the function (on S1) to f. It is the **essential boundary condition**. It is obvious that with the weighted residual approach we can impose more general boundary conditions. With the variational approach the boundary conditions may be limited.

Applying the approximate solution and weighting function (according to Galerkin's method) yields

$$\langle \phi_i, T(\tilde{\Phi}) \rangle = \int_\Omega \nabla \phi_i \cdot (\epsilon \nabla \tilde{\Phi}) d\Omega - \int_{S2} \phi_i \left(g - \gamma \tilde{\Phi} \right) - \int_\Omega \phi_i \rho d\Omega = 0. \qquad (5.32)$$

By rearranging and inserting the expansion (5.24) we obtain a system of linear equations for the expansion coefficients.

$$\sum_{j=1}^{N} c_j \left[\int_\Omega \epsilon \nabla \Phi_j \nabla \Phi_i d\Omega + \int_{S2} \gamma \Phi_j \Phi_i dS \right] = \int_\Omega \rho \Phi_i d\Omega + \int_{S2} \Phi_i g dS \qquad (5.33)$$

For $g = 0$, Galerkin's method results in the equivalent system of equations as Ritz's method. In matrix form it is written

$$\mathbf{A} \cdot \mathbf{c} = \mathbf{b}$$
$$A_{ij} = \int_\Omega \epsilon \nabla \Phi_j \nabla \Phi_i d\Omega + \int_{S2} \gamma \Phi_j \Phi_i dS \qquad (5.34)$$
$$b_i = \int_\Omega \rho \Phi_i d\Omega + \int_{S2} \Phi_i g dS.$$

This system of linear equations can be solved numerically.

5.3 Order of Derivatives

The PDE of the electrostatic problem is of second order, which implies that the second derivative of the approximate function $\tilde{\Phi}$ should be defined. However, the resulting algebraic systems of equations, equation (5.17) for the Ritz method and equation (5.32) for the Galerkin method, only contain first order derivatives of the basis functions Φ_i.

In general we can say that by applying these methods, the order of occurring derivatives of the unknown function decreases by 1. This fact is helpful when looking for basis functions that span the subspace of the solution. For the electrostatic problem, only the first derivative of the basis functions must be defined. So piecewise linear functions would be sufficient for this problem. An introduction to the basis functions is given in section 5.4. In chapter 6 they are treated in greater detail.

5.4 Domain Discretization and Interpolating Functions
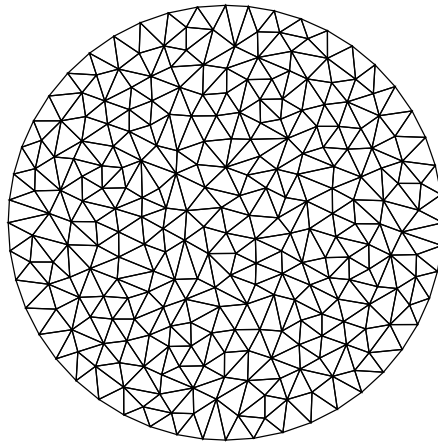
Figure 5.1: Example of the discretization of a circular domain.

In the previous sections we were talking about approximating the unknown function within a finite dimensional function space, spanned by a set of basis functions. However, we did not specify these basis functions. In this section we will give an introduction to basis functions used in FEM, whereas in the next chapter we will treat them in greater detail. An important step before defining the basis functions is

the domain discretization. That means that we divide the domain of interest, within which we want to obtain the solution, into a number of smaller subdomains, the finite elements. These subdomains do not overlap and are connected to adjacent elements. In 1D they are lines, in 2D they can be triangles and in 3D they can be tetrahedrons. The collection of finite elements is called **mesh**. In figure 5.1 we can see a 2D mesh with triangular elements of a circular domain. Such a 2D mesh is defined by the coordinates of the nodes and a list of the nodes, confining each element. To all the nodes, edges and triangles an index is assigned.

These elements are used to define the basis functions. The goal is to interpolate a function within the elements. In other words, the function is supported on the boundary of the elements (e.g. nodes, edges or faces) and interpolated within the elements. For that reason, basis functions, related to FEM, are also called **interpolating functions** or **shape functions**. We will demonstrate this concept on an example. Let's consider the electrostatic example of the previous sections in 2D. The domain of interest is discretized by a triangular mesh. We are looking for a scalar function Φ that approximates the solution. We want the function to be linear within each element (see figure 5.2), i.e.
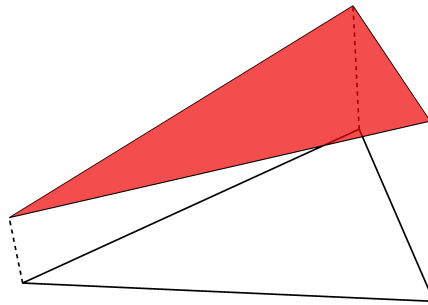
$$\Phi^K(x, y) = a^K + b^K x + c^K y. \tag{5.35}$$

Figure 5.2: A scalar function can be approximated by linear functions within each triangle of a 2D mesh.

K denotes the element index or triangle index. Enforcing the coordinates x, y of the nodes 1, 2 and 3 and the corresponding values of the potential Φ to equation (5.35),

we obtain the following system of equations.

$$\Phi_1^K = a^K + b^K x_1 + c^K y_1$$
$$\Phi_2^K = a^K + b^K x_2 + c^K y_2 \quad\quad\quad (5.36)$$
$$\Phi_3^K = a^K + b^K x_3 + c^K y_3$$

Solving for the constants a^K, b^K, c^K and expressing them in terms of Φ_j^K gives

$$\Phi^K = \sum_{j=1}^{3} \Phi_j^K \eta_j^K(x, y). \quad\quad\quad (5.37)$$

with $\eta_j^K(x, y)$ the basis functions within the element with index K, corresponding to node j. They have value 1 at the corresponding node and linearly decrease to 0 at the two adjacent nodes (see figure 5.3).
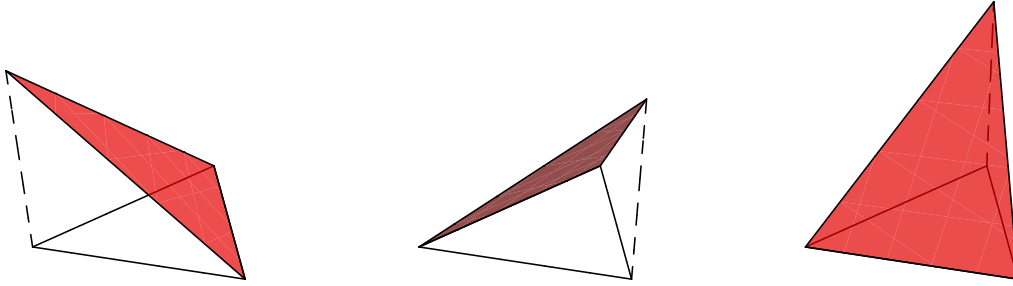
Figure 5.3: Linear shape functions within a triangle. A shape function is assigned to every node of the triangle.

Summing up all the basis functions of all elements and combining the functions related to the same node of adjacent triangles yields the following expression for the scalar function Φ.

$$\Phi(x, y) = \sum_{i=1}^{N_n} \sum_{j=1}^{3} \Phi_j^K \eta_j^K(x, y) = \sum_{i=1}^{N_n} \Phi_i \eta_i^{\mathcal{P}^1}(x, y) \quad\quad\quad (5.38)$$

with Φ_i the value of the potential at node i, N_n the number of nodes and $\eta_i^{\mathcal{P}^1}(x, y)$ the shape function corresponding to node i, which has value 1 at node i and value 0 at every adjacent node (see figure 5.4). A function, assembled by these so called **Lagrange shape functions of 1st order** (see chapter 6), are continuous in the

whole domain and additionally, the first order derivative is defined and finite in the domain, but it is not continuous.
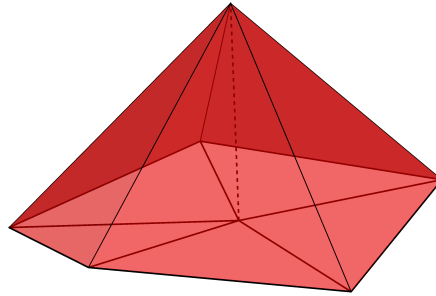

Figure 5.4: Lagrange shape function of 1st order on a 2D triangular mesh.

Depending on the demanded properties of the function, scalar valued or vector valued, continuous normal or tangential component for vector valued functions etc., a set of different shape functions is available (see chapter 6).

Chapter 6

Shape Functions for the Finite Element Method

In this section we will give an introduction to various types of shape functions used in FEM. The main goal is to demonstrate the basic concepts of finding such shape functions rather than taking a thorough mathematical approach.

Performing a FEM calculation, the unknown function and inhomogeneities (if not given in analytical form) have to be represented by approximations. The approximation is done by projecting the functions onto a finite dimensional function space which is spanned by the shape functions. Hence, the shape functions have to conserve the mathematical properties of the individual function. We will display this concept in the following sections, considering Maxwell's equations. The mathematical properties of the electromagnetic fields are given by the interface conditions of electrodynamics which we will recap shortly.

Note: If not mentioned otherwise, we will restrict ourselves to 2D shape functions.

6.1 Interface Conditions for Electrodynamics

The interface conditions for electromagnetic fields are well known [11]. In the following, we will recap the methodology to obtain the interface conditions and generalize it.
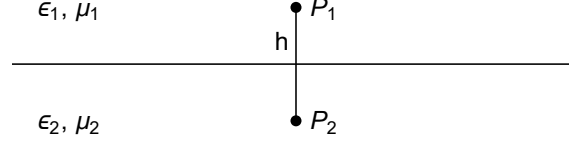
6.1.1 Gradient of Scalar Fields

Figure 6.1: Integration path on interface between two different materials.

First, we consider the behaviour of scalar fields on interfaces, which occur as gradients in the governing equations. Examples would be the electrostatic potential and the magnetostatic potential in a current-free region. We can write them in a general form

$$\nabla \Psi = \vec{U} \tag{6.1}$$

with a general scalar field Ψ and a inhomogeneity $\vec{U}$. An interface between two different materials is defined by different material parameters μ and ϵ. In FEM those interfaces can occur on element boundaries, e.g. if two adjacent elements have different material parameters. Now we integrate equation (6.1) along a path from P_1 to P_2, cutting the interface (depicted in figure 6.1).

$$\int_{P_1}^{P_2} \nabla \Psi \cdot \vec{t} d\Gamma = \int_{P_1}^{P_2} \vec{U} \cdot \vec{t} d\Gamma \tag{6.2}$$

Applying the gradient theorem to the integral on the left hand side and performing the $\lim_{h \to 0}$ leads to

$$\Psi(P_2) - \Psi(P_1) = \lim_{h \to 0} \int_{P_1}^{P_2} \vec{U} \cdot \vec{t} d\Gamma. \tag{6.3}$$

The general inhomogeneity $\vec{U}$ (could be magnetic field $\vec{B}$ or electric field $\vec{E}$) is finite. Therefore, the right hand side goes to 0 if the length of integration path goes to 0. Ψ_1 denotes the field in region 1 and Ψ_2 in region 2.

$$\Psi_1 - \Psi_2 = 0 \tag{6.4}$$

The scalar fields, which occur as gradients in the governing equations, have to be continuous on interfaces.
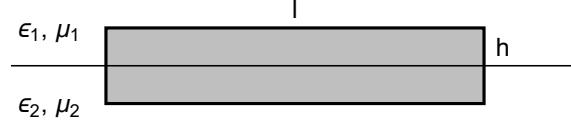
6.1.2 Curl of Vector Fields

Figure 6.2: Integration area on interface between two different materials.

In this section we investigate the behaviour of vector fields on interfaces which occur as curl in the governing equations. Examples would be Ampere's law, Faraday's law and the definition of the vector potential. We can write them in a general form.

$$\nabla \times \vec{T} = \vec{U} \tag{6.5}$$

With a general vector field $\vec{T}$ and an inhomogeneity $\vec{U}$. We integrate equation (6.5) over a rectangular surface cutting the interface (depicted in gray in figure 6.2).

$$\int_S \left(\nabla \times \vec{T} \right) \cdot \vec{n} dS = \int_S \vec{U} \cdot \vec{n} dS \tag{6.6}$$

Applying Stokes' integral theorem [15] to the integral on the left hand side and performing the $\lim_{h \to 0}$ leads to

$$\lim_{h \to 0} \int_{\partial S} \vec{T} \cdot \vec{t} d\Gamma = \lim_{h \to 0} \int_S \vec{U} \cdot \vec{n} dS. \tag{6.7}$$

We assume the inhomogeneity $\vec{U}$ to be finite, i.e. no surface effects like surface charge or surface currents are considered. Therefore, the right hand side goes to 0 if the area of the surface S goes to 0. On the left hand side, due to the $\lim_{h \to 0}$, the sides of the rectangle can be neglected and only the longer upper and lower sides contribute to the integral. $\vec{T}^1$ denotes the field in region 1 and $\vec{T}^2$ in region 2. Furthermore, we assume that the sides are short enough so the field is constant along the integration path and thus

$$\int_l \vec{T}^1 \cdot \vec{t} d\Gamma + \int_l \vec{T}^2 \cdot \vec{t} d\Gamma = 0$$
$$\left(\vec{T}^1 - \vec{T}^2 \right) \cdot \vec{t} = 0. \tag{6.8}$$

The tangential component of vector fields $\vec{T}$, which occur as curl in the governing equations, have to be continuous on interfaces. However, not the normal component.
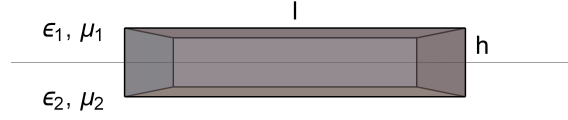
6.1.3   Divergence of Vector Fields

Figure 6.3: Integration volume on interface between two different materials.

A similar approach is chosen for vector fields that occur as divergence in the governing equations, like the Gauss's law, Gauss's law for magnetism and the continuity equation. Such equations can be written generally like

$$\nabla \cdot \vec{T} = \Psi. \tag{6.9}$$

Integrating equation (6.9) over a cuboid, centred around the interface (depicted in gray in figure 6.3), gives

$$\int_V \nabla \cdot \vec{T} dV = \int_V \Psi dV. \tag{6.10}$$

Applying Gauss's integral theorem to the integral on the left hand side and performing the $\lim_{h \to 0}$ leads to

$$\lim_{h \to 0} \int_{\partial V} \vec{T} \cdot \vec{n} dS = \lim_{h \to 0} \int_V \Psi dV. \tag{6.11}$$

As before, we assume the inhomogeneity Ψ to be finite, i.e. no surface effects like surface charge or surface currents are considered. Thus, the right hand side goes to 0 if the volume goes to 0. On the left hand side we can neglect the sides of the cuboid and only the upper and lower rectangle contribute to the integral. Furthermore, we assume that the surfaces are small enough so the field is constant on the surface.

$$\int_l \vec{T}^1 \cdot \vec{n} dS + \int_l \vec{T}^2 \cdot \vec{n} dS = 0$$
$$\left(\vec{T}^1 - \vec{T}^2 \right) \cdot \vec{n} = 0 \tag{6.12}$$

The normal component of vector fields $\vec{T}$, which occur as divergence in the governing equations, have to be continuous on interfaces. However, not the tangential component.

Note: If each component of a vector field was represented by continuous functions (like 1st order Lagrange elements, see section 5.4), the fields would not exhibit any jumps, even across interfaces. That fact would cause spurious, non physical solutions [12]. Thus, we need other sets of basis functions, preserving these mathematical properties of the fields.

6.2 Function Spaces

This section is based on [9]. In the previous section we learned that the electromagnetic fields have to satisfy certain continuity conditions. In this section we will introduce function spaces, more precisely Sobolev spaces, that preserve these mathematical properties. A Sobolev space is a complete normed vector space of weak differentiable functions. These complete function spaces contain the exact fields. In order to define such spaces, we need an additional space, the $L^2(\Omega)$-space with the L^2-norm. Ω denotes an open subset of $\mathbb{R}^n$ with sufficiently smooth boundary.

$L^2(\Omega)$-space

$$\|f\|_2 := \sqrt{\int_\Omega |f|^2 \, d\Omega} \tag{6.13}$$

$$L^2(\Omega) := \{f : \Omega \to \mathbb{C}, \|f\|_2 < \infty\} \tag{6.14}$$

Equation (6.13) denotes the L2-norm. This space contains all square integrable functions on Ω, i.e. functions that may exhibit jumps but the L2-norm is finite. With the help of $L^2(\Omega)$ we can now define some Sobolev spaces.

$H^1(\Omega)$-space

The Sobolev space $H^1(\Omega)$ is defined as follows.

$$H^1(\Omega) := \left\{ f \in L^2(\Omega), D^1 f \in L^2(\Omega) \right\} \tag{6.15}$$

D^1 denotes a differential operator of first order. $H^1(\Omega)$ contains all scalar functions, where the functions themselves and the first order derivatives of the functions are

square integrable. Functions of $H^1(\Omega)$ are continuous and therefore, all functions appearing as gradient in the governing equations belong to this function space.

$H(curl, \Omega)$-space

The Sobolev space $H(curl, \Omega)$ is defined as follows.

$$H(curl, \Omega) := \left\{ \left(\vec{f} \right)^i \in L^2(\Omega), \left(\nabla \times \vec{f} \right)^i \in L^2(\Omega) \right\} \tag{6.16}$$

This space contains all vector functions, where the components of the function and its curl are square integrable. Functions of $H(curl, \Omega)$ are tangentially continuous, but the normal component may exhibit jumps. Therefore, all functions appearing as curl in the governing equations belong to this function space.

$H(div, \Omega)$-space

The last Sobolev space that we consider is the $H(div, \Omega)$.

$$H(div, \Omega) := \left\{ \left(\vec{f} \right)^i \in L^2(\Omega), \nabla \cdot \vec{f} \in L^2(\Omega) \right\} \tag{6.17}$$

It contains all vector functions for which each component is square integrable. Also the divergence of the function is square integrable. Functions of $H(div, \Omega)$ are normally continuous, but the tangential component may exhibit jumps. Therefore, all functions appearing as divergence in the governing equations belong to this function space.

6.3   Discretization of Function Spaces

The function spaces of the section before are complete function spaces. We want to find finite dimensional subspaces within which we can approximate the exact function, i.e. we look for a finite set of basis functions or shape functions that span the subspace. As we have already seen in the section 5.4, in FEM a given domain Ω is divided into finite elements, which approximate the domain. The approximated domain is denoted as Ω_h, where h is a measure for the element size of the mesh. We will now introduce some finite dimensional or discrete subspaces

with their shape functions, that approximate the complete spaces of the section before.

Note: In this work, we will only consider lowest order shape functions within 2D triangular elements.

$\mathcal{P}^0(\Omega_h)$-**Space**

The $\mathcal{P}^0(\Omega_h)$-space is an approximation of the $L^2(\Omega)$-space. The shape functions, that span this subspace, are piecewise constant within each element and are $L^2(\Omega)$ conforming. They are called Lagrange shape functions of 0th order and are further described in section 6.5.1.

$\mathcal{P}^1(\Omega_h)$-**Space**

The $\mathcal{P}^1(\Omega_h)$-space is an approximation of the $H^1(\Omega)$-space. The shape functions, that span this subspace, are the already introduced Lagrange shape functions of 1st order (see section 5.4). They are continuous and thus, $H^1(\Omega)$ conforming.

$\mathcal{N}(\Omega_h)$-**Space**

The $\mathcal{N}(\Omega_h)$-space is an approximation of the $H(curl, \Omega)$-space. The shape functions, that span this subspace, are called Nédélec shape functions. They are $H(curl, \Omega)$ conforming and thus, preserve the tangential continuity of vector fields. A mathematical description and the shape of such functions are given in section 6.5.3.

$\mathcal{RT}(\Omega_h)$-**Space**

The $\mathcal{RT}(\Omega_h)$-space is an approximation of the $H(div, \Omega)$-space. The shape functions, that span this subspace, are called Raviart-Thomas shape functions. They are $H(div, \Omega)$ conforming and thus, preserve the normal continuity of vector fields. A mathematical description and the shape of such functions are given in section 6.5.4.

6.4 De-Rham Diagram

The de-Rham diagram links the spaces, considered in the previous sections, by differential operators in the following exact sequence in 3D.

$$
\begin{array}{ccccccc}
H^1_{3D}(\Omega) & \xrightarrow{\ \nabla\ } & H_{3D}(curl,\Omega) & \xrightarrow{\ \nabla\times\ } & H_{3D}(div,\Omega) & \xrightarrow{\ \nabla\cdot\ } & L^2_{3D}(\Omega) \\
\pi_n \downarrow & & \pi_e \downarrow & & \pi_f \downarrow & & \pi_v \downarrow \\
\mathcal{P}^1_{3D}(\Omega_h) & \xrightarrow{\ \nabla\ } & \mathcal{N}_{3D}(\Omega_h) & \xrightarrow{\ \nabla\times\ } & \mathcal{RT}_{3D}(\Omega_h) & \xrightarrow{\ \nabla\cdot\ } & \mathcal{P}^0_{3D}(\Omega_h)
\end{array}
$$

Figure 6.4: 3D de-Rham diagram: Connection of the function spaces and their discrete subspaces in 3D.

In 2D, the curl operator is not defined. Therefore, the diagram looks slightly different.

$$
\begin{array}{ccccccc}
H^1_{2D}(\Omega) & \xrightarrow{\ \nabla\ } & H_{2D}(curl,\Omega) & \xleftarrow{\ \hat{R}_{\pm\pi/2}\ } & H_{2D}(div,\Omega) & \xrightarrow{\ \nabla\cdot\ } & L^2_{2D}(\Omega) \\
\pi_n \downarrow & & \pi_e \downarrow & & \pi_f \downarrow & & \pi_v \downarrow \\
\mathcal{P}^1_{2D}(\Omega_h) & \xrightarrow{\ \nabla\ } & \mathcal{N}_{2D}(\Omega_h) & \xleftarrow{\ \hat{R}_{\pm\pi/2}\ } & \mathcal{RT}_{2D}(\Omega_h) & \xrightarrow{\ \nabla\cdot\ } & \mathcal{P}^0_{2D}(\Omega_h)
\end{array}
$$

Figure 6.5: 2D de-Rham diagram: Connection of the function spaces and their discrete subspaces in 2D.

π_i denotes a projection operator that projects from the complete space to the corresponding subspace. A projection to a subspace is independent of the point, at which the projection was performed. $\hat{R}_{\pm\pi/2}$ denotes a rotation matrix that rotates a vector by $\pm\pi/2$ (see Appendix A.2).

6.5 Conforming Shape Functions

In this section we will give a mathematical description of the shape functions that span the subspaces introduced in section 6.3.

6.5.1 0th Order Lagrange Shape Functions

Figure 6.6: Shape of 0th order Lagrange function.

These shape functions are $L^2(\Omega)$ conforming and span the $\mathcal{P}^0(\Omega_h)$-subspace. A shape function is assigned to every element of the mesh. The shape function has value 1 inside the corresponding element and 0 outside of it. In figure 6.6 we can see the shape function of a triangular element. A function, approximated in $\mathcal{P}^0(\Omega_h)$, can be written

$$f = \sum_{i=1}^{N_t} f_i \eta_i^{\mathcal{P}^0}. \tag{6.18}$$

N_t denotes the total number of triangles, f_i the expansion coefficients or DoFs and $\eta_i^{\mathcal{P}^0}$ the shape functions. For a given function f, the DoFs are calculated as follows.

$$f_i = \frac{1}{A_i} \int_{A_i} f \, dA \tag{6.19}$$

A_i denotes the area of triangle i.

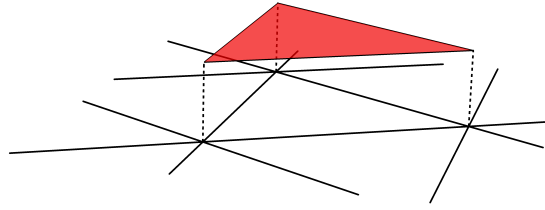## 6.5.2 1st Order Lagrange Shape Functions

These shape functions are $H^1(\Omega)$ conforming and span the $\mathcal{P}^1(\Omega_h)$-subspace. If in the weak form of a problem, the function itself and first order derivatives (e.g. gradient) appear, then the function can be approximated using such shape functions. The 1st order Lagrange elements were already introduced in section 5.4.

6.5.3   Nédélec Shape Functions

Nédélec shape functions are $H(curl, \Omega)$ conforming and span the $\mathcal{N}(\Omega_h)$-subspace. If in the weak form of a problem, the function itself and the curl of it appear, then the function can be approximated using such shape functions. For a thorough mathematical insight on the construction of these shape functions see [12]. To meet the continuity condition of the tangential component, shape functions are constructed around edges, in contrary to nodes for $H^1(\Omega)$ conforming and elements for $L^2(\Omega)$ conforming shape functions. A shape function is assigned to every edge of the mesh. By construction, the shape functions are only non-zero in the two adjacent triangles. Furthermore, every edge has an orientation. A common rule is to set the orientation from the node with the lower index to the node with the higher index. The orientation can be denoted by a normalized tangent vector $\vec{t}_i$, pointing from the first node of the edge to the second (figure 6.7).
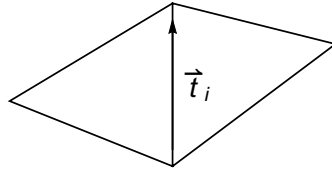
Figure 6.7: Tangent vector of edge i from the node with lower index to the node with higher index.

The tangential component on all edges, besides edge i, has to be zero to preserve tangential continuity. For a mathematical description of such functions, we consider a general triangle as shown in figure 6.8, denoted with the letter K, with the nodes n_i, the edges e_i, the tangent vectors $\vec{t}_{e_i}^K$ and the corresponding normal vectors $\vec{n}_{e_i}^K$. The tangential vectors are oriented counter-clockwise and the normal vectors are pointing outwards. It shall be noted that $\vec{t}_i^K$ is different from $\vec{t}_i$. $\vec{t}_i$ is normalized and the direction is independent of the considered triangle.

In order to mathematically express the 2D Nédélec shape function within the triangle K, assigned to edge e_1, we use barycentric coordinates $\{\lambda_2, \lambda_3\}$. The transformation from Cartesian to barycentric coordinates is

$$\vec{r} = \vec{r}_{n_1} - \lambda_2 \vec{t}_{e_2}^K + \lambda_3 \vec{t}_{e_3}^K. \tag{6.20}$$

$\vec{r}_{n_i}$ denotes the position of node n_i and the tangent and normal vectors are defined

Figure 6.8: A general triangle of a 2D triangular mesh.

as follows.

$$
\begin{aligned}
\vec{t}_{e_1}^K &= \vec{r}_{n_3} - \vec{r}_{n_2} \\
\vec{t}_{e_2}^K &= \vec{r}_{n_1} - \vec{r}_{n_3} \\
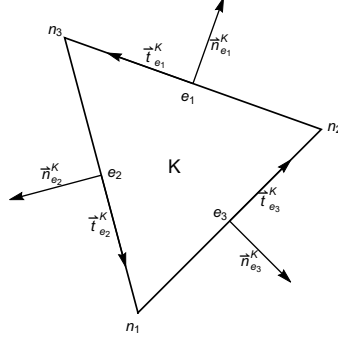\vec{t}_{e_3}^K &= \vec{r}_{n_2} - \vec{r}_{n_1} \\
\vec{n}_{e_i}^K &= \hat{R}_{-\pi/2} \cdot \vec{t}_{e_i}^K
\end{aligned}
\tag{6.21}
$$

$\hat{R}_\alpha$ is a rotation matrix (see Appendix A.2). With these tools we can find the general mathematical expression for the Nédélec shape function.

$$
\vec{\eta}_{e_1,K}^{\mathcal{N}}(\lambda_2, \lambda_3) = \frac{1}{n}\left(\lambda_2 \vec{n}_{e_2}^K - \lambda_3 \vec{n}_{e_3}^K\right)
\tag{6.22}
$$

The index (e_1, K) denotes the shape function related to edge e_1 within the adjacent triangle K. n is a normalisation factor. If $\lambda_2 = 0$, according to the transformation formula (6.20), we are moving along edge e_3. In this case, there is only a normal component and the tangential component is 0. The same is valid for edge e_2, but not for edge e_1. By setting $\lambda_2 = 1 - \lambda_3$, we are moving along edge e_1. Equation (6.22) then reads

$$
\vec{\eta}_{e_1,K}^{\mathcal{N}}(\lambda_3) = \frac{1}{n}\left(\vec{n}_{e_2}^K + \lambda_3 \vec{n}_{e_3}^K\right).
\tag{6.23}
$$

We can calculate the tangential component by multiplying with the tangential vector of edge e_1.

$$
\vec{t}_{e_1}^K \cdot \vec{\eta}_{e_1,K}^{\mathcal{N}}(\lambda_3) = \frac{1}{n}\vec{t}_{e_1}^K \cdot \vec{n}_{e_2}^K
\tag{6.24}
$$

The tangential component is constant along edge e_1. The normalisation factor is

chosen that the following requirement is fulfilled.

$$\int_{e_1} \vec{\eta}^{\mathcal{N}}_{e_1,K} \cdot \vec{t}_{e_1} ds = 1 \tag{6.25}$$

The reason for this requirement will be obvious later. Without executing the calculation, the result is

$$\vec{\eta}^{\mathcal{N}}_{e_1,K} (\lambda_2, \lambda_3) = \sigma \frac{1}{2A_K} \left(\lambda_2 \vec{n}^K_{e_2} - \lambda_3 \vec{n}^K_{e_3} \right). \tag{6.26}$$

A_K denotes the area of the triangle K. σ denotes the sign of the Nédélec shape function. Is the tangential vector $\vec{t}_{e_1}$ of edge e_1 pointing in the same direction as the tangential vector $\vec{t}^K_{e_1}$ of the reference triangle, i.e. counter-clockwise, then $\sigma = +1$. Are they pointing in the opposite direction, then $\sigma = -1$. By transforming it back to Cartesian coordinates, we obtain

$$\boxed{\vec{\eta}^{\mathcal{N}}_{e_1,K} = \sigma \frac{1}{2A_K} \hat{R}_{\pi/2} (\vec{r} - \vec{r}_{n_1})}. \tag{6.27}$$

A function, approximated in $\mathcal{N}(\Omega_h)$, can be written

$$\vec{f} = \sum_{i=1}^{N_e} f_i \vec{\eta}^{\mathcal{N}}_i. \tag{6.28}$$

N_e denotes the total number of edges, f_i the expansion coefficients or DoFs and $\vec{\eta}^{\mathcal{N}}_i$ the shape functions. For a given function f, the DoFs are calculated as follows.

$$\vec{f} = \sum_{i=1}^{N_e} f_i \vec{\eta}^{\mathcal{N}}_i \qquad\qquad \left| \int_{e_j} ... \cdot \vec{t}_j ds \right.$$

$$\int_{e_j} \vec{f} \cdot \vec{t}_j ds = \sum_{i=1}^{N_e} f_i \int_{e_j} \vec{\eta}^{\mathcal{N}}_i \cdot \vec{t}_j ds = f_i \delta_{ij} = f_j \tag{6.29}$$

$$f_j = \int_{e_j} \vec{f} \cdot \vec{t}_j ds$$

e_j denotes edge j and $\vec{t}_j$ the normalized tangential vector. Obviously the DoFs correspond to the tangential component of the function on the edges. Now we can also see the reason for the demanded requirement in equation (6.25), namely to meet the orthogonality relation in (6.29). In figure 6.9, the Nédélec shape function, assigned to edge i, is drawn within the two adjacent triangles. The tangential

component is continuous on edge i and zero on all the other edges. The normal component exhibits jumps on all edges.
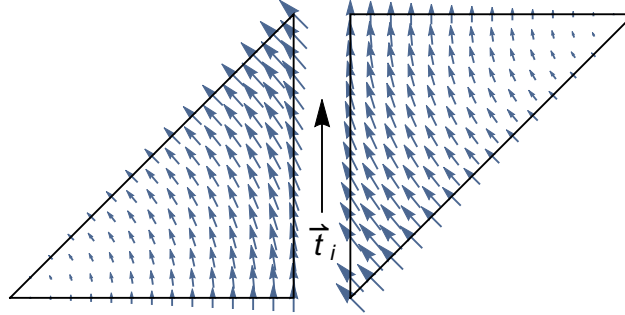
Figure 6.9: Nédélec shape function assigned to edge i of a 2D triangular mesh.

6.5.4 Raviart-Thomas Shape Functions

Raviart-Thomas shape functions are $H(div, \Omega)$ conforming and span the $\mathcal{RT}(\Omega_h)$-subspace. If in the weak form of a problem, the function itself and the divergence of it appear, then the function can be approximated using such shape functions. For a thorough mathematical insight on the construction of these shape functions see [12]. To meet the continuity condition of the normal component, shape functions are constructed around edges, like the Nédélec shape functions. In addition to the tangent vector, a normal vector is assigned to every edge (see figure 6.10).
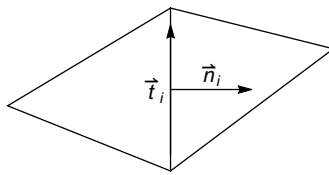
Figure 6.10: Tangent vector and normal vector of edge i.

By rotating the tangent vector $\vec{t}_i$ by $-\pi/2$, we obtain the normal vector.

$$\vec{n}_i = \hat{R}_{-\pi/2} \cdot \vec{t}_i \tag{6.30}$$

The normal component on all edges, besides edge i, has to be zero to preserve normal continuity. Considering the general triangle (figure 6.8), we can use the already introduced barycentric coordinates to express the Raviart-Thomas shape

function, assigned to edge e_1. The derivation is similar to the Nédélec shape function. Therefore, we do not execute all the steps again. In barycentric coordinates the Raviart-Thomas shape functions can be written like

$$\vec{\eta}_{e_1,K}^{\mathcal{RT}}(\lambda_2, \lambda_3) = \sigma \frac{1}{2A_K} \left(-\lambda_2 \vec{t}_{e_2}^{K} + \lambda_3 \vec{t}_{e_3}^{K} \right). \tag{6.31}$$

The index (e_1, K) denotes the shape function related to edge e_1 within the adjacent triangle K. A_K denotes the area of the triangle K. Is the tangential vector $\vec{t}_{e_1}$ of edge e_1 pointing in the same direction as the tangential vector $\vec{t}_{e_1}^{K}$ of the reference triangle, i.e. counter-clockwise, then $\sigma = +1$. Are they pointing in the opposite direction, then $\sigma = -1$.

If $\lambda_2 = 0$, according to the transformation formula (6.20), we are moving along edge e_3. In this case, there is only a tangential component and the normal component is 0. The same is valid for edge e_2, but not for edge e_1. By setting $\lambda_2 = 1 - \lambda_3$, we are moving along edge e_1. Equation (6.31) then reads

$$\vec{\eta}_{e_1,K}^{\mathcal{RT}}(\lambda_3) = \sigma \frac{1}{2A_K} \left(-\vec{t}_{e_2}^{K} - \lambda_3 \vec{t}_{e_1}^{K} \right). \tag{6.32}$$

We can calculate the normal component by multiplying with the normal vector of edge e_1.

$$\vec{n}_{e_1}^{K} \cdot \vec{\eta}_{e_1,K}^{\mathcal{RT}}(\lambda_3) = -\sigma \frac{1}{2A_K} \vec{n}_{e_1}^{K} \cdot \vec{t}_{e_2}^{K} = \sigma \tag{6.33}$$

The normal component is constant along edge e_1 and the following relation holds.

$$\int_{e_1} \vec{\eta}_{e_1,K}^{\mathcal{RT}} \cdot \vec{n}_{e_1} ds = 1 \tag{6.34}$$

By transforming it back to Cartesian coordinates, we obtain

$$\boxed{\vec{\eta}_{e_1,K}^{\mathcal{RT}} = \sigma \frac{1}{2A_K} \left(\vec{r} - \vec{r}_{n_1} \right)}. \tag{6.35}$$

A function, approximated in $\mathcal{RT}(\Omega_h)$, can be written

$$\vec{f} = \sum_{i=1}^{N_e} f_i \vec{\eta}_i^{\mathcal{RT}}. \tag{6.36}$$

N_e denotes the total number of edges, f_i the expansion coefficients or DoFs and $\vec{\eta}_i^{\mathcal{RT}}$

the shape functions. For a given function f, the DoFs are calculated as follows.

$$\vec{f} = \sum_{i=1}^{N_e} f_i \vec{\eta}_i^{RT} \qquad\qquad \left| \int_{e_j} \dots \cdot \vec{n}_j ds \right.$$

$$\int_{e_j} \vec{f} \cdot \vec{n}_j ds = \sum_{i=1}^{N_e} f_i \int_{e_j} \vec{\eta}_i^{RT} \cdot \vec{n}_j ds = f_i \delta_{ij} = f_j \qquad (6.37)$$

$$f_j = \int_{e_j} \vec{f} \cdot \vec{n}_j ds$$

e_j denotes edge j and $\vec{n}_j$ the normalized normal vector. Obviously the DoFs correspond to the normal component of the function on the edges. In figure 6.11, the Raviart-Thomas shape function, assigned to edge i, is drawn within the two adjacent triangles. The normal component is continuous on edge i and zero on all the other edges. The tangential component exhibits jumps on all edges.
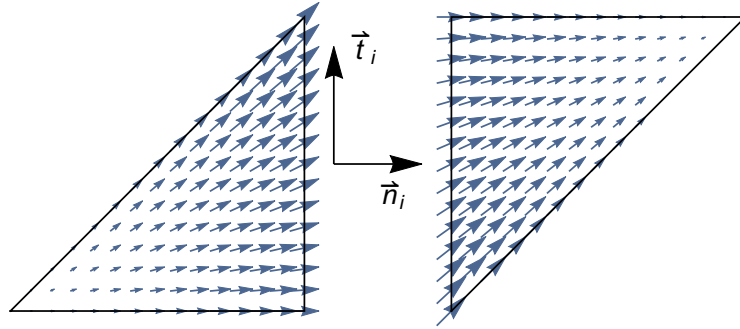
Figure 6.11: Raviart-Thomas shape function assigned to edge i of a 2D triangular mesh.

Chapter 7

Weak Formulation of Governing Equations

Now we have finally introduced all the basics and we can start applying them to our problem. The first step, performing a FEM calculation, is to transform the governing equations to a weak form, applying Galerkin's method (see section 5.2). In the following, we will derive the weak forms of the poloidal equation (3.34) and the toroidal equation (3.35).

7.1 Weak Formulation of Poloidal Equation

We take equation (3.34) for the poloidal part of the vector potential $\vec{a}_p$, multiply it with a weighting function $\vec{w}$ and integrate over the toroidal domain Ω.

$$\int_\Omega \mu^{-1} \frac{m^2}{h_\phi^2} \vec{w} \cdot \vec{a}_p d\Omega + \int_\Omega \vec{w} \cdot \left[\nabla \times \mu^{-1} \left(\nabla \times \vec{a}_p \right) \right] d\Omega = \int_\Omega \vec{w} \cdot \vec{j}_p d\Omega \qquad (7.1)$$

The following identity, obtained by integration by parts, can be applied to the second integral.

$$\int_\Omega \vec{\Psi} \cdot \left(\nabla \times \vec{\Phi} \right) d\Omega = \int_\Omega \vec{\Phi} \cdot \left(\nabla \times \vec{\Psi} \right) d\Omega - \int_{\partial\Omega} \left(\vec{\Psi} \times \vec{\Phi} \right) \cdot \vec{n} dS \qquad (7.2)$$

with $\vec{n}dS$ the vectorial surface element, which gives

$$
\begin{aligned}
&\int_\Omega \mu^{-1} \left(\nabla \times \vec{a}_p\right) \cdot \left(\nabla \times \vec{w}\right) d\Omega + \int_\Omega \mu^{-1} \frac{m^2}{h_\phi^2} \vec{w} \cdot \vec{a}_p d\Omega - \\
&- \int_{\partial\Omega} \left[\mu^{-1} \left(\nabla \times \vec{a}_p\right) \times \vec{n}\right] \cdot \vec{w} dS = \int_\Omega \vec{w} \cdot \vec{j}_p d\Omega
\end{aligned}
\tag{7.3}
$$

The boundary condition, appearing in the boundary integral, corresponds to the toroidal component of the magnetic field strength $\mathfrak{h}$.

$$
\mu^{-1} \left(\nabla \times \vec{a}_p\right) \times \vec{n} = \mu^{-1} \vec{b}_t \times \vec{n} = \mu^{-1} b_\phi \left(\vec{e}_\phi \times \vec{n}\right) = \mathfrak{h}_\phi \left(\vec{e}_\phi \times \vec{n}\right) \tag{7.4}
$$

Note: In the axisymmetric case $(m = 0)$ the boundary integral vanishes, because $\mathfrak{h}_\phi = 0$ in the outer region and on the boundary. If that was not the case, according to Ampere's circuit law, we would have a current density in the outer region.

7.2   Weak Formulation of Toroidal Equation

We follow the same procedure as in the section before. We take equation (3.35) for the toroidal part of the vector potential a_ϕ, multiply it with a weighting function w and integrate over the toroidal domain Ω.

$$
-\int_\Omega h_\phi \nabla \frac{\mu^{-1}}{h_\phi^2} \nabla \left(h_\phi a_\phi\right) w d\Omega = \int_\Omega j_\phi w d\Omega \tag{7.5}
$$

To the integral on the left hand side the Gauss's theorem

$$
\int_\Omega g \left(\nabla \cdot \vec{F}\right) d\Omega = \int_{\partial\Omega} g \vec{F} \cdot \vec{n} dS - \int_\Omega \vec{F} \cdot \nabla g d\Omega \tag{7.6}
$$

can be applied, which leads to the following result.

$$
-\int_{\partial\Omega} h_\phi w \frac{\mu^{-1}}{h_\phi^2} \nabla \left(h_\phi a_\phi\right) \cdot \vec{n} dS + \int_\Omega \frac{\mu^{-1}}{h_\phi^2} \nabla \left(h_\phi a_\phi\right) \cdot \nabla (h_\phi w) d\Omega = \int_\Omega j_\phi w d\Omega \tag{7.7}
$$

With the following definitions

$$\boxed{\begin{aligned} a_\phi^r &:= h_\phi a_\phi \\ w^r &:= h_\phi w \end{aligned}} \tag{7.8}$$

we can rewrite equation (7.7) and we obtain

$$\boxed{\int_\Omega \frac{\mu^{-1}}{h_\phi^2} \nabla a_\phi^r \cdot \nabla w^r d\Omega - \int_{\partial\Omega} w^r \frac{\mu^{-1}}{h_\phi^2} \frac{\partial a_\phi^r}{\partial \vec{n}} dS = \int_\Omega \frac{1}{h_\phi} j_\phi w^r d\Omega} . \tag{7.9}$$

The boundary condition, appearing in the boundary integral, is a Neumann boundary condition for a_ϕ^r. Taking into account equation (3.25) and applying some vector calculus, it can be shown that the Neumann boundary condition for a_ϕ^r corresponds to the tangential component of the poloidal magnetic field strength.

$$\frac{\mu^{-1}}{h_\phi} \frac{\partial a_\phi^r}{\partial \vec{n}} = \mu^{-1} \vec{b}_p \cdot (\vec{e}_\phi \times \vec{n}) = \vec{h}_p \cdot (\vec{e}_\phi \times \vec{n}) \tag{7.10}$$

Chapter 8

Boundary Conditions

In the weak form of the Maxwell equations for the poloidal part of the vector potential (7.3) and the toroidal part of it (7.9), the boundary values appear in the occurring boundary integral and are imposed on the boundary of the domain Ω. As we have already discussed in section 2.3, those values are a priori unknown and we need the so called open boundary conditions, i.e. we need a Poincaré-Steklov operator which maps the boundary values of one kind to the boundary values of another kind [10]. Both boundary values have to solve the problem uniquely.

Note: Since we demanded a constant magnetic permeability μ in the outer region, it follows that μ is also constant on the boundary. So within this chapter, μ is treated as constant parameter.

We already introduced two boundary conditions in section 2.3 that solve our problem uniquely, namely

$$\vec{B} \cdot \vec{n} = -b \qquad\qquad on \quad \partial\Omega \qquad\qquad (8.1)$$

$$\vec{H} \times \vec{n} = \vec{K} \qquad\qquad on \quad \partial\Omega. \qquad\qquad (8.2)$$

Considering the identities (7.4) and (7.10) for the occurring boundary conditions, we can see that they correspond to boundary condition (8.2). Thus we need an operator

$\hat{O}_{PS}$ which maps the boundary values as follows.

$$\vec{H} \times \vec{n} = \hat{O}_{PS} \left[\vec{B} \cdot \vec{n}\right] \quad \text{on } \partial\Omega \tag{8.3}$$

This expression is then substituted to the boundary integrals in the weak forms. Furthermore, the boundary values have to be expressed in terms of the vector potential. The derivation is different for the toroidal and poloidal equation, so we will treat them separately.

In the following sections, certain expressions appear more frequently, so we introduce some definitions.

$$\vec{t} := \vec{n} \times \vec{e}_\phi \tag{8.4}$$

$$\hat{f}_n\left[g(\theta)\right] := \frac{1}{2\pi} \int_{-\pi}^{\pi} g(\theta)e^{-in\theta}d\theta \tag{8.5}$$

$$\left(\hat{\mathbf{f}}\left[g(\theta)\right]\right)_k := \hat{f}_k\left[g(\theta)\right] \tag{8.6}$$

$\vec{t}$ denotes the poloidal tangential vector on the toroidal surface. $\hat{f}_n[g(\theta)]$ denotes a functional, giving the n-th Fourier coefficient of function g. $\hat{\mathbf{f}}\left[g(\theta)\right]$ denotes a vector of all the Fourier coefficients.

8.1   Boundary Condition for Poloidal Equation

The boundary integral in the weak form of the poloidal equation (7.3) is

$$\int_{\partial\Omega} \left[\mu^{-1}\left(\nabla \times \vec{a}_p\right) \times \vec{n}\right] \cdot \vec{w}dS. \tag{8.7}$$

According to identity (7.4), the boundary values in the square brackets correspond to the toroidal component of the magnetic field strength.

$$\mu^{-1}\left(\nabla \times \vec{a}_p\right) \times \vec{n} = \vec{h}_t \times \vec{n} \tag{8.8}$$

For the poloidal vector potential, the general boundary conditions (8.1) and (8.2) transform to

$$\vec{H} \times \vec{n} \rightarrow \vec{h}_t \times \vec{n} \tag{8.9}$$

$$\vec{B} \cdot \vec{n} \rightarrow \vec{b}_p \cdot \vec{n}. \tag{8.10}$$

So we need an operator $\hat{O}_p$ that maps the boundary conditions as follows.

$$\vec{h}_t \times \vec{n} = \hat{O}_p \left[\vec{b}_p \cdot \vec{n} \right] \quad \text{on } \partial\Omega \tag{8.11}$$

We can write the boundary values (8.9) in therms of the scalar potential Φ, introduced in chapter 4.

$$\begin{aligned} \vec{h}_t \times \vec{n} &= \mu^{-1} b_\phi \left(\vec{e}_\phi \times \vec{n} \right) \\ &= \mu^{-1} \left(-\nabla\Phi \right)_\phi \left(\vec{e}_\phi \times \vec{n} \right) \\ &= \mu^{-1} \frac{im}{h_\phi} \Phi \, \vec{t} \end{aligned} \tag{8.12}$$

In the last step we used the definition (8.4) of the tangential vector $\vec{t}$. The boundary values (8.10) are also expressed in terms of Φ.

$$\vec{b}_p \cdot \vec{n} = \vec{n} \cdot \left(-\nabla\Phi \right) = -\frac{\partial\Phi}{\partial\vec{n}} \tag{8.13}$$

So the two boundary conditions can be related using the scalar potential Φ. The connection is obtained by finding a so-called **Neumann-to-Dirichlet operator** $\hat{O}_{NtD}$ with

$$\Phi = \hat{O}_{NtD} \left[\frac{\partial\Phi}{\partial\vec{n}} \right]. \tag{8.14}$$

By substituting this expression together with (8.13) to equation (8.12) we get

$$\vec{h}_t \times \vec{n} = -\mu^{-1} \frac{im}{h_\phi} \vec{t} \hat{O}_{NtD} \left[\vec{b}_p \cdot \vec{n} \right]. \tag{8.15}$$

We express the boundary condition in the square brackets in terms of the vector potential, considering equation (3.25) for the poloidal magnetic field.

$$\vec{b}_p \cdot \vec{n} = \frac{im}{h_\phi} \vec{a}_p \cdot \vec{t} \tag{8.16}$$

With this result we can write equation (8.15) in terms of the poloidal vector potential.

$$\mu^{-1}\left(\nabla \times \vec{a}_p\right) \times \vec{n} = \mu^{-1}\frac{m^2}{h_\phi}\vec{t}\,\hat{O}_{NtD}\left[\frac{1}{h_\phi}\vec{a}_p \cdot \vec{t}\right] \tag{8.17}$$

Now we consider the Dirichlet-to-Neumann operator, starting with the analytical solution for Φ, equation (4.21). We only consider one toroidal mode m at the time. Additionally, we introduce a normalization constant to the solution by dividing with the Legendre function $P^m_{n-1/2}(\cosh \eta_0)$ at the reference torus η_0 (representing the boundary of Ω).

$$\Phi(\eta, \theta, \phi) = \sqrt{\Re(\eta, \theta)} \sum_{n=-\infty}^{\infty} A_n \frac{P^m_{n-1/2}(\cosh \eta)}{P^m_{n-1/2}(\cosh \eta_0)} e^{i(m\phi+n\theta)} \tag{8.18}$$

First we want to obtain the normal derivative of Φ, i.e. the Neumann values. In order to obtain the Neumann values, we calculate the directional derivative along the unit vector normal to the toroidal surface (pointing outwards by definition). In toroidal coordinates, that vector is equal to the basis vector $-\vec{e}_\eta$. The minus is needed due to the inverse behaviour of the coordinate η. Thus, the Neumann boundary values are

$$\frac{\partial \Phi}{\partial \vec{n}} = -\vec{e}_\eta \cdot \nabla \Phi = -\frac{\Re}{a}\frac{\partial \Phi}{\partial \eta} =$$
$$= -\frac{\Re}{a} \sum_{n=-\infty}^{\infty} A_n e^{i(m\phi+n\theta)} \frac{\partial_\eta\left[\sqrt{\Re}P^m_{n-1/2}\right]}{P^m_{n-1/2}}. \tag{8.19}$$

For the sake of clarity, the function arguments are dropped from now on. Considering equation (B.11) for the derivative of the Legendre functions we obtain

$$-\frac{a}{\sqrt{\Re}}\left.\frac{\partial \Phi}{\partial \vec{n}}\right|_{\eta=\eta_0} = \sum_{n=-\infty}^{\infty} A_n e^{i(m\phi+n\theta)}\left[\frac{\sinh \eta_0}{2} + \Re m \coth \eta_0 + \Re \frac{P^{m+1}_{n-1/2}}{P^m_{n-1/2}}\right]. \tag{8.20}$$

Assuming that we know the Neumann values on the reference torus η_0, we can determine the Fourier coefficients A_n by multiplying with a phase factor $e^{-ik\theta}$ and integrating over the interval $\theta \in [-\pi, \pi]$.

$$-a \int_{-\pi}^{\pi} \left[\frac{1}{\sqrt{\mathfrak{R}}} \frac{\partial \Phi}{\partial \vec{n}} \right]_{\eta=\eta_0} e^{-ik\theta} d\theta = \tag{8.21}$$

$$= \sum_{n=-\infty}^{\infty} A_n e^{im\phi} \left[\frac{\sinh \eta_0}{2} \int_{-\pi}^{\pi} e^{i(n-k)\theta} d\theta + \left(m \coth \eta_0 + \frac{P_{n-1/2}^{m+1}}{P_{n-1/2}^m} \right) \int_{-\pi}^{\pi} \mathfrak{R} e^{i(n-k)\theta} d\theta \right]$$

This equation describes a system of equations for the Fourier coefficients A_n. In practice, the index of summation n has an upper and lower limit so that the system is finite. The occurring Fourier integrals on the right hand side of the equation can be expressed using Kronecker's delta.

$$\int_{-\pi}^{\pi} e^{i(n-k)\theta} d\theta = 2\pi \delta_{kn} \tag{8.22}$$

$$\int_{-\pi}^{\pi} \mathfrak{R} e^{i(n-k)\theta} d\theta = \cosh \eta_0 2\pi \delta_{kn} - \pi \delta_{|k-n|,1} \tag{8.23}$$

With these results we can rewrite the expression in square brackets on the right hand side of equation (8.21). For the sake of clarity, we introduce a variable representing the expression.

$$(\chi_m)_{kn} := \left(\frac{\sinh \eta_0}{2} + m \cosh \eta_0 \coth \eta_0 + \cosh \eta_0 \frac{P_{n-1/2}^{m+1}}{P_{n-1/2}^m} \right) \delta_{kn} - $$
$$- \frac{1}{2} \left(m \coth \eta_0 + \frac{P_{n-1/2}^{m+1}}{P_{n-1/2}^m} \right) \delta_{|k-n|,1} \tag{8.24}$$

χ_m is a tridiagonal matrix. The numerical evaluation of fractions of contiguous Legendre functions, like in the above equation, is shown in Appendix B.1. With the definitions (8.6) and (8.24), equation (8.21) can be written in matrix form as follows.

$$-2\pi a \, \hat{\mathbf{f}} \left[\frac{1}{\sqrt{\mathfrak{R}}} \frac{\partial \Phi}{\partial \vec{n}} \right]_{\eta=\eta_0} = \chi_m \cdot \mathbf{A} \, e^{im\phi} \tag{8.25}$$

The Fourier coefficients A_n can the be calculated as follows.

$$\mathbf{A} = -2\pi a \, e^{-im\phi} \, \chi_m^{-1} \cdot \hat{\mathbf{f}} \left[\frac{1}{\sqrt{\mathfrak{R}}} \frac{\partial \Phi}{\partial \vec{n}} \right]_{\eta=\eta_0} \tag{8.26}$$

Equation above applied to equation (8.18) gives the Neumann-to-Dirichlet operator.

$$\Phi|_{\eta=\eta_0} = -2\pi a\sqrt{\mathfrak{R}}\left(e^{in\theta}\right)^T \cdot \chi_m^{-1} \cdot \hat{\mathbf{f}}\left[\frac{1}{\sqrt{\mathfrak{R}}}\frac{\partial\Phi}{\partial\vec{n}}\right]_{\eta=\eta_0} \tag{8.27}$$

This result applied to equation (8.17) and substituted to the boundary integral (8.7) gives the final result.

$$\boxed{\int_{\partial\Omega}\left[\mu^{-1}\left(\nabla\times\vec{a}_p\right)\times\vec{n}\right]\cdot\vec{w}dS = -\frac{8\pi^3 m^2 a}{\mu\sinh\eta_0}\hat{\mathbf{f}}^*\left[\frac{1}{\sqrt{\mathfrak{R}}}\vec{w}\cdot\vec{t}\right]^T\cdot\chi_m^{-1}\cdot\hat{\mathbf{f}}\left[\sqrt{\mathfrak{R}}\,\vec{a}_p\cdot\vec{t}\right]}$$
$$\tag{8.28}$$

χ_m is defined according to equation (8.24). $\hat{\mathbf{f}}^*$ denotes the complex conjugate of $\hat{\mathbf{f}}$.

8.2 Boundary Condition for Toroidal Equation

The boundary integral in the weak form of the toroidal equation (7.9) is

$$\int_{\partial\Omega} w^r\frac{\mu^{-1}}{h_\phi^2}\frac{\partial a_\phi^r}{\partial\vec{n}}dS. \tag{8.29}$$

In the integral we can identify a Neumann boundary condition for a_ϕ^r. According to identity (7.10) and the definition of the tangential vector, equation (8.4), the boundary values in the integral correspond to the tangential component of the poloidal magnetic field strength.

$$\frac{\mu^{-1}}{h_\phi}\frac{\partial a_\phi^r}{\partial\vec{n}} = -\vec{h}_p\cdot\vec{t} \tag{8.30}$$

For the toroidal vector potential, the general boundary conditions (8.1) and (8.2) transform to

$$\vec{H}\times\vec{n}\rightarrow\vec{h}_p\cdot\vec{t} \tag{8.31}$$

$$\vec{B}\cdot\vec{n}\rightarrow\vec{b}_p\cdot\vec{n}. \tag{8.32}$$

So we need an operator $\hat{O}_t$ that maps the boundary conditions as follows.

$$\vec{h}_p \cdot \vec{t} = \hat{O}_t \left[\vec{b}_p \cdot \vec{n} \right] \quad \text{on } \partial\Omega \tag{8.33}$$

Using equation (3.8) and the definition of the tangential vector, equation (8.4), we can write the boundary values (8.32) in therms of the toroidal vector potential a_ϕ^r.

$$\begin{aligned} \vec{b}_p \cdot \vec{n} &= \frac{1}{h_\phi} \left(\nabla a_\phi^r \times \vec{e}_\phi \right) \cdot \vec{n} \\ &= -\frac{1}{h_\phi} \vec{t} \cdot \nabla a_\phi^r \end{aligned} \tag{8.34}$$

This boundary condition corresponds to the tangential derivative of the toroidal vector potential. We can simplify the derivation by changing the boundary condition. Instead of the tangential derivative, we can simply take the Dirichlet values. They contain the same information and thus, solve the problem uniquely.

$$\vec{B} \cdot \vec{n} \to \vec{t} \cdot \nabla a_\phi^r \to a_\phi^r \tag{8.35}$$

As a result, equation (8.33) can be written in terms of a_ϕ^r as follows.

$$\frac{\mu^{-1}}{h_\phi} \frac{\partial a_\phi^r}{\partial \vec{n}} = \hat{O}_t \left[a_\phi^r \right] \quad \text{on } \partial\Omega \tag{8.36}$$

So the two boundary conditions can be related using the toroidal vector potential a_ϕ. The connection is obtained by finding a so-called **Dirichlet-to-Neumann operator** $\hat{O}_{DtN}$ with

$$\frac{\partial a_\phi^r}{\partial \vec{n}} = \hat{O}_{DtN} \left[a_\phi^r \right] \tag{8.37}$$

Using the analytical solution for a_ϕ, equation equation (4.29), and apply it to definition of a_ϕ^r, equation (7.8), gives

$$a_\phi^r(\eta, \theta) := h_\phi(\eta, \theta)\, a_\phi^r(\eta, \theta) = a\sqrt{\frac{\sinh\eta}{\Re(\eta,\theta)}} \sum_{n=-\infty}^{\infty} A_n Q_{1/2}^n(\eta \coth)\, e^{in\theta} \tag{8.38}$$

Note: This is the reason why we had to obtain an analytical solution for a_ϕ in chapter 4.

Assuming that we know the Dirichlet values on the toroidal surface $\eta = \eta_0$, we can

determine the Fourier coefficients A_n by multiplying with a phase factor $e^{-ik\theta}$ and integrating over the interval $\theta \in [-\pi, \pi]$. Considering the definition (8.5), we can write the result as follows.

$$A_n = \frac{1}{a\sqrt{\sinh\eta_0}\,Q^n_{1/2}(\coth\eta_0)}\hat{f}_n\left[\sqrt{\mathfrak{R}}\,a^r_\phi\right]_{\eta=\eta_0} \tag{8.39}$$

By substituting the Fourier coefficients back into equation (8.38), we obtain

$$a^r_\phi(\eta, \theta) = \frac{1}{\sqrt{\mathfrak{R}(\eta, \theta)}}\sqrt{\frac{\sinh\eta}{\sinh\eta_0}}\sum_{n=-\infty}^{\infty}\frac{Q^n_{1/2}(\coth\eta)}{Q^n_{1/2}(\coth\eta_0)}e^{in\theta}\hat{f}_n\left[\sqrt{\mathfrak{R}}\,a^r_\phi\right]_{\eta=\eta_0}. \tag{8.40}$$

In order to obtain the Neumann values, we calculate the directional derivative along the unit vector normal to the toroidal surface (pointing outwards by definition). In toroidal coordinates, that vector is equal to the basis vector $-\vec{e}_\eta$. The minus is needed due to the inverse behaviour of the coordinate η. Thus, the Neumann boundary values are

$$\frac{\partial a^r_\phi(\eta, \theta)}{\partial\vec{n}} = -\vec{e}_\eta \cdot \nabla a^r_\phi(\eta, \theta) = -\frac{\mathfrak{R}(\eta, \theta)}{a}\frac{\partial a^r_\phi}{\partial\eta} =$$
$$= -\frac{\mathfrak{R}(\eta, \theta)}{a}\sum_{n=-\infty}^{\infty}\frac{\partial}{\partial\eta}\left[\frac{1}{\sqrt{\mathfrak{R}(\eta, \theta)}}\sqrt{\frac{\sinh\eta}{\sinh\eta_0}}\frac{Q^n_{1/2}(\coth\eta)}{Q^n_{1/2}(\coth\eta_0)}\right]e^{in\theta}\hat{f}_n\left[\sqrt{\mathfrak{R}}a^r_\phi\right]_{\eta=\eta_0}. \tag{8.41}$$

Considering equation (B.12) for the derivative of the Legendre function and applying the chain rule, we can compute the derivative in the equation above. Evaluating at η_0 gives

$$\left.\frac{\partial a^r_\phi}{\partial\vec{n}}\right|_{\eta=\eta_0} = -\frac{\mathfrak{R}}{a}\sum_{n=-\infty}^{\infty}\left[\left(n+\frac{1}{2}\right)\frac{Q^n_{-1/2}}{Q^n_{1/2}} - \frac{1}{2}\frac{\sinh\eta_0}{\mathfrak{R}}\right]e^{in\theta}\hat{f}_n\left[\sqrt{\mathfrak{R}}\,a^r_\phi\right]_{\eta=\eta_0}. \tag{8.42}$$

For the sake of clarity, we introduce a variable, representing the expression in the square brackets on the right hand side in the equation above.

$$\chi_n := \left(n+\frac{1}{2}\right)\frac{Q^n_{-1/2}}{Q^n_{1/2}} - \frac{1}{2}\frac{\sinh\eta_0}{\mathfrak{R}} \tag{8.43}$$

The numerical evaluation of fractions of contiguous Legendre functions, like in the above equation, is shown in Appendix B.1. Equation above applied to equation (8.42) gives the Neumann-to-Dirichlet operator.

$$\left.\frac{\partial a_\phi^r}{\partial \vec{n}}\right|_{\eta=\eta_0} = -\frac{\mathfrak{R}}{a} \sum_{n=-\infty}^{\infty} e^{in\theta}\, \chi_n\, \hat{f}_n \left[\sqrt{\mathfrak{R}}\, a_\phi^r\right]_{\eta=\eta_0} \tag{8.44}$$

This result substituted to the boundary integral (8.29) gives the final result.

$$\boxed{\int_{\partial\Omega} w^r \frac{\mu^{-1}}{h_\phi^2} \frac{\partial a_\phi^r}{\partial \vec{n}} dS = -\frac{4\pi^2}{a\mu \sinh \eta_0} \sum_{n=-\infty}^{\infty} \hat{f}_n^* \left[\sqrt{\mathfrak{R}}\chi_n w^r\right] \cdot \hat{f}_n \left[\sqrt{\mathfrak{R}}a_\phi^r\right]} \tag{8.45}$$

χ_n is defined according to equation (8.43). $\hat{f}^*$ denotes the complex conjugate of $\hat{f}$.

Chapter 9

Assembly of Algebraic System of Equations

Having obtained the weak forms of the poloidal and toroidal equation and the boundary conditions, we can now discretize the equations. In the following sections we will investigate the approximation of the occurring fields according to chapter 6 and finally apply the discrete approximations to the weak forms. This will lead to a finite system of linear equations.

Note: Until now we have assumed a general magnetic permeability μ in the toroidal domain and a constant magnetic permeability $\mu = \mu_0$ in the outer region (see chapter 4). In this chapter, due to simplicity, we assume $\mu = \mu_0$ also inside the toroidal domain and we include the magnetic permeability in the current density. This assumption is reasonable for applications on fusion reactors, where the toroidal domain is placed inside the vacuum chamber of the reactor. The resulting current density must be divided by μ_0 in the end.

9.1   Discretization of Fields

The governing equations of section 3.4 are embedded in the $\mathbb{R}^3$. However, the occurring fields only depend on the general poloidal coordinates u and v, i.e. they are axisymmetric. Furthermore, the poloidal vector fields have only components in the uv-plane. Therefore, it is sufficient to describe these fields by 2D vector shape

functions, e.g. 2D Nédélec or Raviart-Thomas shape functions (see section 6.5). The toroidal components can be represented by 2D scalar shape functions in the uv-plane, e.g. Lagrange elements of 0th or 1st order.

The 2D function spaces, spanned by the named shape functions, are linked in the 2D de-Rham diagram (figure 6.5) by the corresponding 2D differential operators. Hence, we have to express the governing equations in terms of the 2D differential operators. We denote the 2D differential operators with $\nabla_\perp$. The divergence and gradient are

$$\nabla_\perp \cdot \vec{f} = \frac{1}{h_u h_v} \left[\frac{\partial (h_v f_u)}{\partial u} + \frac{\partial (h_u f_v)}{\partial v} \right] \tag{9.1}$$

$$\nabla_\perp \Psi = \frac{\vec{e}_u}{h_u} \frac{\partial \Psi}{\partial u} + \frac{\vec{e}_v}{h_v} \frac{\partial \Psi}{\partial v}. \tag{9.2}$$

We denote 2-component vectors in the uv-plane by the superscript uv, e.g.

$$\vec{a}_p^{uv} = \vec{e}_u a_u + \vec{e}_v a_v = \begin{pmatrix} a_u \\ a_v \end{pmatrix}. \tag{9.3}$$

With this notation we can rewrite the governing equations of section 3.4 in terms of the 2D differential operators. The governing equations for the vector potential are written

$$\vec{B} = \nabla \times \vec{A} \longrightarrow \quad \begin{aligned} b_\phi &= \nabla_\perp \cdot \left(\hat{R}_{-\pi/2} \cdot \vec{a}_p^{uv} \right) & (9.4) \\ \\ h_\phi \vec{b}_p &= \begin{cases} \hat{R}_{-\pi/2} \cdot \nabla_\perp a_\phi^r & m = 0 \\ im \left(\hat{R}_{\pi/2} \cdot \vec{a}_p^{uv} \right) & m \neq 0 \end{cases}. & (9.5) \end{aligned}$$

$\hat{R}_\alpha$ denotes a 2D rotation matrix (see Appendix A.2). The governing equations for the magnetic field and current density are written

$$\nabla \cdot \vec{B} = 0 \longrightarrow \quad \nabla_\perp \cdot \left(h_\phi \vec{b}_p^{uv} \right) = -im b_\phi \tag{9.6}$$

$$\nabla \cdot \vec{J} = 0 \longrightarrow \quad \nabla_\perp \cdot \left(h_\phi \vec{j}_p^{uv} \right) = -im j_\phi. \tag{9.7}$$

According to the considerations about continuity conditions and conforming function spaces in chapter 6, we are now able to expand the functions within the appropriate function spaces.

j_ϕ and b_ϕ are scalar functions to whom no differential operator is applied. Such functions need to be finite, but not continuous. They are expanded in the $\mathcal{P}^0(\Omega_h)$-space, spanned by the 0th order Lagrange shape functions.

$$j_\phi = \sum_{j=i}^{N_t} j_j \eta_j^{\mathcal{P}^0} \tag{9.8}$$

$$b_\phi = \sum_{j=i}^{N_t} b_j \eta_j^{\mathcal{P}^0} \tag{9.9}$$

a_ϕ^r is a scalar function and occurs as gradient in equation (9.5). Therefore, it must be a continuous function and is expanded in the $\mathcal{P}^1(\Omega_h)$-space, spanned by the 1st order Lagrange shape functions.

$$a_\phi^r = \sum_{j=i}^{N_n} a_j \eta_j^{\mathcal{P}^1} \tag{9.10}$$

$h_\phi \vec{b}_p^{uv}$ and $h_\phi \vec{j}_p^{uv}$ are vector functions that occur as divergence in equation (9.6) and (9.7). Therfore, they have to be normally continuous and are expanded in the $\mathcal{RT}(\Omega_h)$-space, spanned by the Raviart-Thomas shape functions.

$$h_\phi \vec{j}_p^{uv} = \sum_{j=i}^{N_e} j_j \vec{\eta}_j^{\mathcal{RT}_{2D}} \tag{9.11}$$

$$h_\phi \vec{b}_p^{uv} = \sum_{j=i}^{N_e} b_j \vec{\eta}_j^{\mathcal{RT}_{2D}} \tag{9.12}$$

$\hat{R}_{\pi/2} \cdot \vec{a}_p^{uv}$ is a vector function and occurs as divergence in equation (9.4). Therefore, it must be normally continuous. A normally continuous function, rotated by $\pm\pi/2$ must be tangentially continuous (see 2D de-Rham diagram, figure 6.5). Hence, $\vec{a}_p^{uv}$ is expanded in the $\mathcal{N}(\Omega_h)$-space, spanned by the Nédélec shape functions.

$$\vec{a}_p^{uv} = \sum_{j=i}^{N_e} a_j \vec{\eta}_j^{\mathcal{N}_{2D}} \tag{9.13}$$

9.2   Discretization of Poloidal Equation

In order to discretize the the weak form of the poloidal equation (7.3), we apply the approximations equation (9.11) and (9.13) for the current density and the vector potential to it. Since the weak form is embedded in the $\mathbb{R}^3$ we first have to expand the 2D vector fields to 3D by just adding the ϕ-component and set it to zero.

$$\vec{\eta}_j^{\mathcal{N}} = \vec{\eta}_j^{\mathcal{N}_{2D}} + 0 \cdot \vec{e}_\phi \tag{9.14}$$

$$\vec{\eta}_j^{\mathcal{RT}} = \vec{\eta}_j^{\mathcal{RT}_{2D}} + 0 \cdot \vec{e}_\phi \tag{9.15}$$

So we can write the 3D poloidal vector fields in terms of 2D vector shape functions like

$$\vec{a}_p = \sum_{j=1}^{N_e} a_j \vec{\eta}_j^{\mathcal{N}} \tag{9.16}$$

$$h_\phi \vec{j}_p = \sum_{j=1}^{N_e} j_j \vec{\eta}_j^{\mathcal{RT}} \tag{9.17}$$

$$h_\phi \vec{b}_p = \sum_{j=1}^{N_e} b_j \vec{\eta}_j^{\mathcal{RT}}. \tag{9.18}$$

We apply these discretizations to the weak form and choose the weighting function according to Galerkin's method. Furthermore we express the infinitesimal volume and surface element in general rotational coordinates.

$$d\Omega = h_\phi d\phi dA \tag{9.19}$$

$$dS = h_\phi d\phi d\Gamma \tag{9.20}$$

where dA denotes an infinitesimal area in the uv-plane and $d\Gamma$ an infinitesimal line element in the same plane. Since all integrands are independent of ϕ, the ϕ

integration only gives a factor 2π which can be reduced.

$$\sum_{j_1}^{N_e} a_j \left[\int_A \left(\nabla \times \vec{\eta}_j^{\mathcal{N}} \right) \cdot \left(\nabla \times \vec{\eta}_i^{\mathcal{N}} \right) h_\phi dA + m^2 \int_A \frac{1}{h_\phi} \vec{\eta}_i^{\mathcal{N}} \cdot \vec{\eta}_j^{\mathcal{N}} dA - \right.$$
$$\left. - \int_{\partial A} \left[\left(\nabla \times \vec{\eta}_j^{\mathcal{N}} \right) \times \vec{n} \right] \cdot \vec{\eta}_i^{\mathcal{N}} h_\phi d\Gamma \right] = \sum_{j_1}^{N_e} j_j \int_A \vec{\eta}_i^{\mathcal{N}} \cdot \vec{\eta}_j^{RT} dA \tag{9.21}$$

A denotes the cross-sectional domain of the toroidal domain Ω. We label the occurring integrals of equation (9.21) as follows.

$$A_{ij}^{(1)} := \int_A \left(\nabla \times \vec{\eta}_j^{\mathcal{N}} \right) \cdot \left(\nabla \times \vec{\eta}_i^{\mathcal{N}} \right) h_\phi dA \tag{9.22}$$

$$A_{ij}^{(2)} := \int_A \frac{1}{h_\phi} \vec{\eta}_i^{\mathcal{N}} \cdot \vec{\eta}_j^{\mathcal{N}} dA \tag{9.23}$$

$$B_{ij} := \int_{\partial A} \left[\left(\nabla \times \vec{\eta}_j^{\mathcal{N}} \right) \times \vec{n} \right] \cdot \vec{\eta}_i^{\mathcal{N}} h_\phi d\Gamma \tag{9.24}$$

$$C_{ij} := \int_A \vec{\eta}_i^{\mathcal{N}} \cdot \vec{\eta}_j^{RT} dA \tag{9.25}$$

With these definitions we can write equation (9.21) in matrix form.

$$\left[\mathbf{A}^{(1)} + m^2 \mathbf{A}^{(2)} - \mathbf{B} \right] \cdot \mathbf{a} = \mathbf{C} \cdot \mathbf{j} \tag{9.26}$$

$\mathbf{A}^{(1)}$, $\mathbf{A}^{(2)}$, $\mathbf{B}$ and $\mathbf{C}$ are sparse and square $N_e \times N_e$ matrices[1]. We can evaluate the integrals by applying the definition of the Nédélec and Raviart-Thomas shape functions (see section 6.5). The boundary matrix $\mathbf{B}$ will be treated separately in the next section.

The integrals are solved in cylindrical coordinates $\{r, \phi, z\}$. The results are given without derivation.

---

[1]N_e denotes the total number of edges in mesh.

$$A_{ij}^{(1)} = \sum_K \frac{r_M^K}{A_K} \tag{9.27}$$

$$A_{ij}^{(2)} = \int_A \frac{1}{r} \vec{\eta}_i^{\mathcal{N}} \cdot \vec{\eta}_j^{\mathcal{N}} \, dr \, dz \approx \frac{1}{r_M} \int_A \vec{\eta}_i^{\mathcal{N}} \cdot \vec{\eta}_j^{\mathcal{N}} \, dr \, dz \approx$$

$$\approx \sum_K \frac{1}{r_M^K} \frac{1}{4A_K^2} \left[A_K \vec{r}_i \cdot \vec{r}_j - A_K \vec{r}_M^K \cdot (\vec{r}_i + \vec{r}_j) + \sum_{k,l \geq k}^{3} \vec{r}_k^K \cdot \vec{r}_l^K \right] \tag{9.28}$$

$$C_{ij} = \sum_K \frac{1}{6} \mathrm{sign} \left[\left(\vec{r}_M^K - \vec{r}_j \right) \cdot \hat{R}_{\pi/2} \cdot (\vec{r}_j - \vec{r}_i) \right] \tag{9.29}$$

The sum over the index K denotes the sum over the overlapping triangles of shape function i and j. For diagonal elements i=j, the two triangles, sharing the edge i, contribute. If edge i is on the boundary, only one triangle contributes. If $i \neq j$ and edge i and j share a triangle, only the common triangle contributes. Otherwise, the sum gives 0. A_K is the area of the triangle with index K. r_m^K denotes the mean cylindrical radius r of triangle K. $\vec{r}_M^K$ denotes the mean position vector of triangle K and the position vector $\vec{r}_i$ denotes the position of the node, opposite to edge i, within the considered triangle K.

In order to find a compact expression for the second integral, we assumed that the term $1/r$ is constant within the triangle. The other two integral are solved exactly. The diagonal elements of matrix **C** are 0.

The matrices $\mathbf{A}^{(1)}$, $\mathbf{A}^{(2)}$, **B** and **C** are only dependent on the mesh and not on the mode number m. Performing a calculation for different modes on a given mesh, these matrices have to be calculated only once. The boundary matrix on the other hand is dependent on the mode number m (see next section) and therefore must be recalculated for every mode.

Once the matrices are calculated, the system of equations can be solved using exact solvers like LU decomposition or iterative solvers like GMRES. Special care has to be taken in the axisymmetric case. Recalling chapter 3, we notice that in the axisymmetric case we did not imply any gauge to the vector potential. Therefore, the system of equations will not have a unique solution, but many solutions giving the same correct magnetic field. We can either solve the system of equations using an iterative solver, which converges to a random solution or precondition the matrix and using an exact solver. Another problem, occurring in the axisymmetric case, is

the demanded divergence freeness of the poloidal current density, equation (3.37). If that condition is not exactly fulfilled, solving the linear system of equations may not be possible. In section 9.2.2 we will consider this special case and demonstrate a method to avoid this problem.

9.2.1 Discretization of Boundary Condition

In order to evaluate the boundary matrix B_{ij} equation (9.24), we apply the boundary condition equation (8.28).

$$
\begin{aligned}
B_{ij} = \int_{\partial\Omega} &\left[\left(\nabla \times \vec{\eta}_j^{\mathcal{N}} \right) \times \vec{n} \right] \cdot \vec{\eta}_i^{\mathcal{N}} h_\phi d\Gamma = \\
&- \frac{4\pi^2 m^2 a}{\sinh \eta_0} \, \hat{\mathbf{f}}^* \left[\frac{1}{\sqrt{\mathfrak{R}}} \vec{\eta}_i^{\mathcal{N}} \cdot \vec{t} \right]^T \cdot \chi_m^{-1} \cdot \hat{\mathbf{f}} \left[\sqrt{\mathfrak{R}} \, \vec{\eta}_j^{\mathcal{N}} \cdot \vec{t} \right]
\end{aligned}
\tag{9.30}
$$

The Nédélec shape function $\vec{\eta}_i^{\mathcal{N}}$, where edge i is on the boundary, is non-zero only on a small part of the boundary. In toroidal coordinates the function is non-zero in the θ-interval $\left[\theta_i^-, \theta_i^+ \right]$. Hence, the slowly varying terms of the integrand can be assumed to be constant within the integration interval. Equation (9.30) can be written in the following form.

$$
B_{ij} \approx - \frac{4\pi^2 m^2 a}{\sinh \eta_0} \sqrt{\frac{\mathfrak{R}(\eta_0, \bar{\theta}_j)}{\mathfrak{R}(\eta_0, \bar{\theta}_i)}} \, \hat{\mathbf{f}}^* \left[\vec{\eta}_i^{\mathcal{N}} \cdot \vec{t} \right]^T \cdot \chi_m^{-1} \cdot \hat{\mathbf{f}} \left[\vec{\eta}_j^{\mathcal{N}} \cdot \vec{t} \right]
\tag{9.31}
$$

$\bar{\theta}_i$ denotes the mean value of θ of edge i. η_0 denotes the boundary torus. In figure 9.1, we can see the cross section of a torus Ω, with its boundary $\partial\Omega$ depicted in blue. Ω_h denotes an approximation of Ω with a simple triangular mesh (depicted in gray), with its boundary $\partial\Omega_h$, depicted in black. The red circle is the cross section of a torus with toroidal coordinate η_0. In order to avoid systematic errors, while performing the integration along the boundary, the length of $\partial\Omega_h$ and the red circle, corresponding to η_0, must be identical.

Considering equation (8.6) for the definition of $\hat{\mathbf{f}}$, we can evaluate the Fourier integrals in equation (9.31).

$$
\left(\hat{\mathbf{f}} \left[\vec{\eta}_j^{\mathcal{N}} \cdot \vec{t} \right] \right)_n = \frac{1}{2\pi} \int_{\theta_j^-}^{\theta_j^+} \vec{\eta}_j^{\mathcal{N}} \cdot \vec{t} e^{-in\theta} d\theta
\tag{9.32}
$$

According to the considerations in section 6.5, the tangential component of the

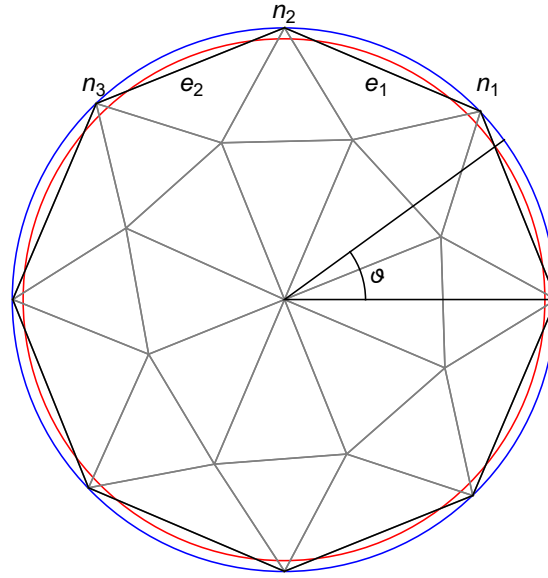Figure 9.1: Cross-section of toroidal domain.

Nédélec shape functions is constant along the edge.

$$\vec{\eta}_j^{\mathcal{N}} \cdot \vec{t}_j = \frac{1}{l_j} \tag{9.33}$$

l_j denotes the length of edge j. We can approximate the tangential vector $\vec{t}_j$ of edge j with the tangential vector of the boundary $\vec{t}$ (see figure 9.2). Depending on the orientation of $\vec{t}_j$, we might have to change its direction with a parameter $\sigma_j = \pm 1$.

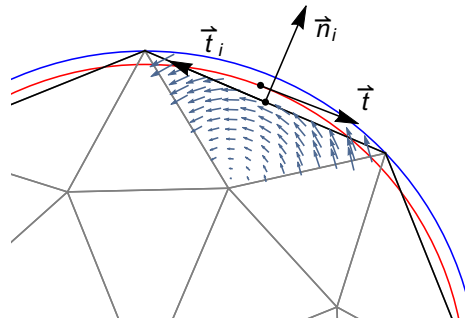$$\vec{t}_j \approx \sigma_j \vec{t} \tag{9.34}$$

Figure 9.2: Nédélec shape function assigned to a boundary edge.

Equation above applied to equation (9.33) gives

$$\vec{\eta}_j^{\mathcal{N}} \cdot \vec{t} = \frac{\sigma_j}{l_j}.$$
(9.35)

This identity inserted to integral (9.32) results in the following.

$$\left(\hat{\mathbf{f}} \left[\vec{\eta}_j^{\mathcal{N}} \cdot \vec{t} \right] \right)_n = \frac{1}{2\pi} \frac{\sigma_j}{l_j} \int_{\theta_j^-}^{\theta_j^+} e^{-in\theta} d\theta$$
(9.36)

With these results we can rewrite equation (9.31) as follows.

$$B_{ij} = \int_{\partial\Omega} \left[(\nabla \times \vec{\eta}_j^{\mathcal{N}}) \times \vec{n} \right] \cdot \vec{\eta}_i^{\mathcal{N}} dS \approx$$

$$\approx -\frac{2\pi m^2 a}{\sinh\eta_0} \sqrt{\frac{\mathfrak{R}(\eta_0, \bar{\theta}_j)}{\mathfrak{R}(\eta_0, \bar{\theta}_i)}} \frac{\sigma_i \sigma_j}{l_i l_j} \sum_{k=-N}^{N} \sum_{n=-N}^{N} \left[\int_{\theta_i^-}^{\theta_i^+} e^{-in\theta} d\theta \right]^* \left(\chi_m^{-1} \right)_{nk} \left[\int_{\theta_j^-}^{\theta_j^+} e^{-ik\theta} d\theta \right]$$
(9.37)

The infinite summations are truncated at an upper and lower limit N. N specifies the number of poloidal modes used to approximate the boundary values. The occurring Fourier integrals can be solved analytically and can be given in a closed form. The θ-values of the starting and ending point of the boundary edge can be calculated using the transformation formulas of the toroidal coordinates. Then the Fourier integrals can be written like

$$\int_{\theta_i^-}^{\theta_i^+} e^{-in\theta} d\theta = \begin{cases} \frac{i}{n} \left(e^{-in\theta_i^+} - e^{-in\theta_i^-} \right) & n \neq 0 \\ \theta_i^+ - \theta_i^- & n = 0 \end{cases}.$$
(9.38)

Special care has to be taken of jumps at the interval boundary of θ from $-\pi$ to π in case n=0. Otherwise, an extra term of 2π is incorrectly added.

9.2.2 Correction of Current Density

As mentioned in section 9.2, the demanded divergence freeness of the poloidal current density in the axisymmetric case may cause problems. The degrees of freedom for the poloidal current density are the coefficients of the Raviart-Thomas elements. They correspond to the flux of the current density through an edge of the mesh, equation (6.37). The sum of the DoFs, corresponding to the 3 edges of the triangle, gives the

total flux. In case of divergence freeness it should be 0. Depending on the quality of the given DoFs, the flux through the edges of a triangle may deviate from 0. In this case, the system of equations cannot be solved to any given precision. Thus, it might be necessary to correct the DoFs.

We consider an arbitrary triangle K of the mesh. The total flux can be calculated by summing up the degrees of freedom of the 3 edges confining the triangle, multiplied by the corresponding sign of the edge within the considered triangle. If an edge is on the boundary, the DoF is set to 0.

$$\sigma_1^K j_1^K + \sigma_2^K j_2^K + \sigma_3^K j_3^K = \delta f^K \neq 0 \tag{9.39}$$

For every triangle, we can write such an equation, i.e. N_t equations. One triangle or equation can be removed, since it results of all the other triangles or equations. Otherwise the matrix will be rank deficient. We can write this system of equations in matrix form.

$$\sigma \cdot \mathbf{j} = \delta \mathbf{f} \tag{9.40}$$

σ is a sparse, rectangular matrix containing only ± 1 and dimension $N_t \times N_e$ [2]. The goal is to find a modified current density $\tilde{\mathbf{j}}$ which is divergence free and thus, satisfies the following equation.

$$\sigma \cdot \tilde{\mathbf{j}} = 0 \tag{9.41}$$

The system of equations is under-determined. Therefore, an infinite number of solutions exist. We want to find the solution with a minimal deviation from the original current density, i.e.

$$\mathbf{j} - \tilde{\mathbf{j}} = \delta \mathbf{j} \tag{9.42}$$

$$|\delta \mathbf{j}| \overset{!}{=} \min. \tag{9.43}$$

Subtracting equation (9.41) from equation (9.40), results in the following.

$$\sigma \cdot \delta \mathbf{j} = \delta \mathbf{f} \tag{9.44}$$

---

[2]N_t denotes the total number of triangles and N_e the total number of edges.

We want to find the minimum norm solution for $\delta\mathbf{j}$. According to [23], this is done in the following way.

$$\delta\mathbf{j} = \sigma^T \cdot \left(\sigma \cdot \sigma^T\right)^{-1} \cdot \delta\mathbf{f} \tag{9.45}$$

The modified current density is then simply

$$\tilde{\mathbf{j}} = \mathbf{j} - \delta\mathbf{j}. \tag{9.46}$$

9.3 Discretization of Toroidal Equation

We follow the same steps for the toroidal equation. We apply the discrete approximations of the toroidal current density and vector potential, equations (9.8) and (9.10), to the weak form of the toroidal equation (7.9). The weighting function is chosen according to Galerkin's method. We apply the infinitesimal volume and surface element, equation (9.19) and (9.20), and execute the ϕ-integration. That gives a factor 2π which is reduced. As a result we obtain

$$\sum_{j=1}^{N_n} a_j \left[\int_A \frac{1}{h_\phi} \nabla\eta_j^{\mathcal{P}1} \cdot \nabla\eta_i^{\mathcal{P}1} dA - \int_{\partial A} \frac{1}{h_\phi} \eta_i^{\mathcal{P}1} \frac{\partial\eta_j^{\mathcal{P}1}}{\partial\vec{n}} d\Gamma \right] = \sum_{k=1}^{N_t} j_k \int_A \eta_k^{\mathcal{P}0} \eta_i^{\mathcal{P}1} dA. \tag{9.47}$$

A denotes the cross-sectional domain of the toroidal domain Ω. We label the occurring integrals of equation (9.47) as follows.

$$A_{ij} := \int_A \frac{1}{h_\phi} \nabla\eta_j^{\mathcal{P}1} \cdot \nabla\eta_i^{\mathcal{P}1} dA \tag{9.48}$$

$$B_{ij} := \int_{\partial A} \frac{1}{h_\phi} \eta_i^{\mathcal{P}1} \frac{\partial\eta_j^{\mathcal{P}1}}{\partial\vec{n}} d\Gamma \tag{9.49}$$

$$C_{ik} := \int_A \eta_k^{\mathcal{P}0} \eta_i^{\mathcal{P}1} dA \tag{9.50}$$

We can rewrite the system of equations in matrix form.

$$[\mathbf{A} - \mathbf{B}] \cdot \mathbf{a} = \mathbf{C} \cdot \mathbf{j} \tag{9.51}$$

All the matrices are sparse, whereas $\mathbf{A}$ and $\mathbf{B}$ are square $N_n \times N_n$ matrices and $\mathbf{C}$ is a rectangular $N_n \times N_t$ matrix [3]. With the definition of the Lagrange shape functions of 0th and 1st order (see section 6.5), we can evaluate the integrals. The boundary integral $\mathbf{B}$ will be treated in the next section.

The integrals are evaluated in cylindrical coordinates $\{r, \phi, z\}$. The results are given without derivation.

$$
\begin{aligned}
A_{ij} &= \int_A \frac{1}{r} \nabla \eta_j^{\mathcal{P}^1} \cdot \nabla \eta_i^{\mathcal{P}^1} \, dr \, dz \approx \frac{1}{r_M^K} \int_A \nabla \eta_j^{\mathcal{P}^1} \cdot \nabla \eta_i^{\mathcal{P}^1} \, dr \, dz \\
&\approx \sum_K \frac{1}{r_M^K} \frac{1}{4 A_K} \vec{n}_i^K \cdot \vec{n}_j^K
\end{aligned}
\tag{9.52}
$$

$$
C_{ik} = \sum_K \frac{1}{3} A_k
\tag{9.53}
$$

The sum over the index K denotes the sum of the overlapping triangles of shape function i and j or i and k, respectively. For diagonal elements i=j of matrix $\mathbf{A}$, all the triangles, sharing the considered node i, contribute. If $i \neq j$ and node i and j are the nodes of an edge, the two adjacent triangles contribute. If the edge is on the boundary, only one triangle contributes. Otherwise, the sum gives 0. For the matrix $\mathbf{C}$, we get a non-zero result if node i is contained in triangle k. Then triangle k contributes. Otherwise the sum gives 0.

A_K is the area of the triangle with index K. r_m^K denotes the mean cylindrical radius r of triangle K. $\vec{n}_i^K$ denotes the normal vector on the edge, opposite to the node i within the considered triangle K. The vector is defined in equation (6.21). It is pointing outwards and not normalized.

In order to find a compact expression for the first integral, we assumed that the term $1/r$ is constant within the triangle. The second integral is solved exactly.

Once the matrices are calculated, the system of equations can be solved using exact solvers like LU decomposition or iterative solvers like GMRES. The solution of the toroidal vector potential is unique.

---

[3] N_t denotes the total number of triangles and N_n the total number of nodes.

9.3.1 Discretization of Boundary Condition

Evaluating the boundary matrix B_{ij} (9.49), using the boundary condition (8.45), gives

$$
\begin{aligned}
B_{ij} &= \int_{\partial A} \frac{1}{h_\phi} \eta_i^{\mathcal{P}^1} \frac{\partial \eta_j^{\mathcal{P}^1}}{\partial \vec{n}} d\Gamma = \\
&= -\frac{4\pi^2}{a \sinh \eta_0} \sum_{n=-\infty}^{\infty} \hat{f}_n^* \left[\chi_n \sqrt{\mathfrak{R}} \, \eta_i^{\mathcal{P}^1} \right] \hat{f}_n \left[\sqrt{\mathfrak{R}} \, \eta_j^{\mathcal{P}^1} \right].
\end{aligned}
\tag{9.54}
$$

The Lagrange shape function of 1st order $\eta_i^{\mathcal{P}^1}$, where node i is on the boundary, is only non-zero on a small part of the boundary. $\left[\theta_i^-, \theta_i^+ \right]$ confines the interval of θ, within $\eta_i^{\mathcal{P}^1}$ is non-zero. Therefore, the slowly varying terms of the integrand can be assumed to be constant within the integration interval. Hence, equation above writes like

$$
B_{ij} \approx -\frac{4\pi^2 \sqrt{\mathfrak{R}\left(\eta_0, \bar{\theta}_i\right) \mathfrak{R}\left(\eta_0, \bar{\theta}_j\right)}}{a \sinh \eta_0} \sum_{n=-N}^{N} \chi_n \left(\eta_0, \bar{\theta}_i\right) \hat{f}_n^* \left[\eta_i^{\mathcal{P}^1} \right] \hat{f}_n \left[\eta_j^{\mathcal{P}^1} \right].
\tag{9.55}
$$

$\bar{\theta}_i$ denotes the mean value of θ of the interval $\left[\theta_i^-, \theta_i^+ \right]$. η_0 denotes the boundary torus. The same as in section 9.2.1, the boundary torus must have the same circumference than the boundary of the meshed domain Ω_h, in order to avoid systematic errors while performing the integration along the boundary. The infinite summation is truncated at an upper and lower limit N. N specifies the number of poloidal modes used to approximate the boundary values.

Considering equation (8.5) for the definition of $\hat{f}$, we evaluate the Fourier integrals.

$$
\hat{f}_n \left[\eta_i^{\mathcal{P}^1} \right] = \frac{1}{2\pi} \int_{\theta_i^-}^{\theta_i^+} \eta_i^{\mathcal{P}^1} \left(\eta_0, \theta \right) e^{-in\theta} d\theta
\tag{9.56}
$$

In order to solve this integral we have to find an expression for $\eta_i^{\mathcal{P}^1}\left(\eta_0, \theta\right)$. The shape function, belonging to node n_2 in figure 9.1, is plotted in figure 9.3 along the boundary Ω_h. In figure 9.4 we can see the same function depending on θ. The θ-values are obtained using the transformation formulas for the toroidal coordinates. The shape function depending on θ is slightly distorted (compare to straight lines depicted in gray). The extend of the distortion depends on the θ-interval as well
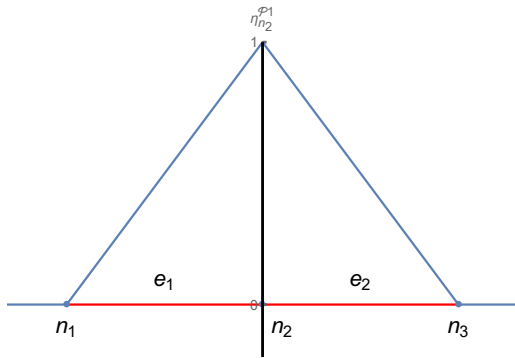
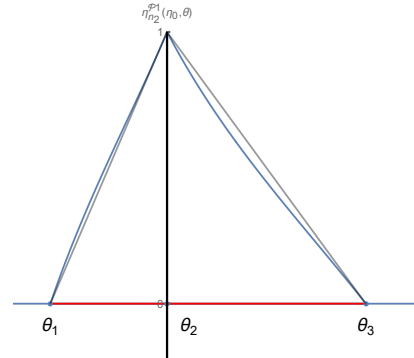Figure 9.3: The Lagrange shape function of 1st order assigned to the boundary node n_2, plotted along the boundary.

Figure 9.4: The Lagrange shape function of 1st order depending on θ, plotted along the boundary torus η_0.

as on the aspect ratio of the torus (ratio of the radius of the central circle to the radius of the torus). This is depicted in figure 9.5, where the relation of the toroidal coordinate θ and the polar angle of the circle ϑ (figure 9.1) are plotted for different aspect ratios. If the aspect ratio R/r is large, θ and ϑ are almost identical and the distortion will be insignificant. For larger aspect ratios, the distortion will be noticeable. Choosing the mesh fine enough, the shape functions are only non-zero in a very small θ interval. Thus, an approximation with a piecewise linear function in θ is reasonable.
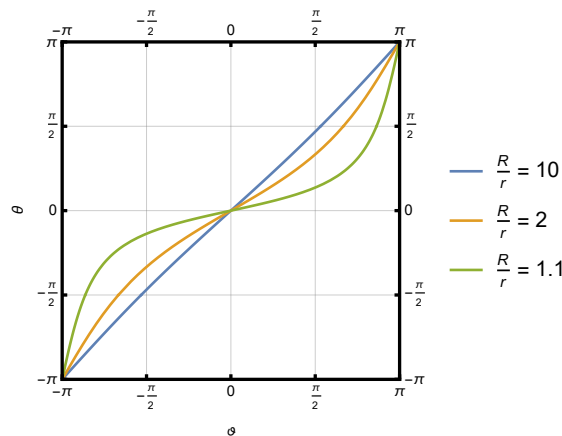

Figure 9.5: Relation of the toroidal coordinate θ and the polar angle of the circle ϑ, depending on different aspect ratios R/r.

$$\eta_i^{\mathcal{P}^1}(\eta_0, \theta) \approx \begin{cases} \frac{\theta_i^- - \theta}{\theta_i^- - \theta_i} & \theta \leq \theta_i \wedge \theta \geq \theta_i^- \\ \frac{\theta_i^+ - \theta}{\theta_i^+ - \theta_i} & \theta \leq \theta_i^+ \wedge \theta \geq \theta_i \\ 0 & \theta \leq \theta_i^- \vee \theta \geq \theta_i^+ \end{cases} \tag{9.57}$$

θ_i is the θ-value of the node i, to which the function $\eta_i^{\mathcal{P}^1}$ corresponds. θ_i^+ and θ_i^- are the θ-values of the adjacent nodes along the boundary. θ_i^+ denotes the upper θ-value and θ_i^- the lower θ-value. Now we can solve the Fourier integral (9.56) analytically and give the result in a closed form.

$$\int_{\theta_i^-}^{\theta_i^+} \eta_i^{\mathcal{P}^1}(\eta_0, \theta)\, e^{-in\theta}\, d\theta \approx \begin{cases} \frac{e^{-in\theta_i^+}\left(\theta_i^- - \theta_i\right) + e^{-in\theta_i^-}\left(\theta_i - \theta_i^+\right) + e^{-in\theta_i}\left(\theta_i^+ - \theta_i^-\right)}{n^2\left(\theta_i^- - \theta_i\right)\left(\theta_i - \theta_i^+\right)} & n \neq 0 \\ \frac{\theta_i^+ - \theta_i^-}{2} & n = 0 \end{cases} \tag{9.58}$$

Again, special care has to be taken of jumps at the interval boundary of θ from $-\pi$ to π. Otherwise, an extra term of 2π is incorrectly added.

Chapter 10

MATLAB Implementation

With the knowledge of the previous chapters, the FEM procedure was implemented in MATLAB. In this chapter, a brief introduction to the implementation is given, considering the input and output of the program, needed parameters and finally, the procedure is demonstrated on a short example.

In the following, N_t denotes the total number of triangles in the mesh, N_e the total number of edges and N_n the total number of nodes.

10.1 Input

In order to calculate the magnetic field of a given current density inside a torus, 3 essential components are needed: The mesh, the current density and the maximum number of poloidal modes.

10.1.1 Mesh

In order to perform the FEM calculation, a 2D triangulation of the cross-section of the torus is needed. Following 3 informations are necessary:

- The (r, z)-coordinates of the nodes given in an array of dimension $N_n \times 2$. Every row contains the r and z coordinate of the node with the index of the row-number.

- The 3 nodes of every triangle, orientated counter-clockwise is given in a $N_t \times 3$ array. Every row contains the indices of the contained nodes of a triangle with

the index of the row-number.

- A logical array of size $N_n \times 1$, which is true if the node with index of the row-number is on the boundary.

With these 3 arrays as input, an instance of the class `TriMesh` is created. The created object determines and stores further information about the mesh, like the connectivity, edges and their indexing etc.

```
1  Th = TriMesh(nodes,triangles,boundary_nodes);
```

For this work, the triangulation is generated with the open source FEM program *FreeFEM++* and imported it into MATLAB. The same program will be used later to validate the results (see chapter 11) and therefore, it was convenient to use its built-in mesh generator.

10.1.2   Current Density

We assume, that the current density has already been decomposed in harmonics of the azimuthal angle ϕ, as described in chapter 3. The decomposition is not treated within this work.

$$\vec{J}(r,\phi,z) = \sum_{m=-M}^{M} \vec{j}^m(r,z)\,e^{im\phi} \tag{10.1}$$

Only modes with $m \geq 0$ are considered, since the negative modes result from the corresponding positive modes (Theory of Fourier-Decomposition).

$$\vec{j}^{-m}(r,z) = \left[\vec{j}^m(r,z)\right]^* \tag{10.2}$$

The same relation is valid for the magnetic field $\vec{b}^m$ and the vector potential $\vec{a}^m$. We reintroduced the superscript m which indicates the toroidal mode number. According to the discretizations (9.8) and (9.17) of the current density, the DoFs of the 0th order Lagrange shape functions for j_ϕ^m and the Raviart-Thomas DoFs for $h_\phi \vec{j}_p^m$ have to be calculated. For every mode m, a set of DoFs for the poloidal and toroidal current density is obtained. The DoFs of the considered modes are combined to arrays and committed to the FEM procedure. In the following, an instruction on

how to obtain the DoFs and structure them into arrays is given. First, a vector m, containing the considered toroidal mode numbers, is needed.

$$m = \begin{pmatrix} m_1 & m_2 & ... & m_M \end{pmatrix} \overset{e.g.}{=} \begin{pmatrix} 0 & 1 & 2 & ... \end{pmatrix} \tag{10.3}$$

Now the DoFs for every single mode of array m can be calculated. According to considerations in section 6.5, the DoFs for the poloidal current density, corresponding to the Raviart-Thomas DoFs, are calculated as follows.

$$\left(rj_{rz}^{\mathcal{RT}}\right)_{k,q} = \int_{e_k} r\,\vec{j}_p^{\,m_q} \cdot \vec{n}_k\, ds \approx r_k\, \vec{n}_k \cdot \vec{j}_p^{\,m_q}(r_k, z_k) \tag{10.4}$$

The integration is performed along the considered edge e_k in cylindrical coordinates. Performing this integral for every edge and every mode, an array $rj_{rz}^{\mathcal{RT}}$ of size $N_e \times M$, where M denotes the number of considered modes, is obtained. The integral can be approximated by the value of the poloidal current density on the center of the edge, denoted with the cylindrical coordinates (r_k, z_k). The DoFs for the toroidal current density, corresponding to the DoFs of the 0th order Lagrange elements, are obtained as follows.

$$\left(j_\phi^{\mathcal{P}^0}\right)_{l,q} = \frac{1}{A_l} \int_{A_l} j_\phi^{m_q}\, dA \approx j_\phi^{m_q}(r_l, z_l) \tag{10.5}$$

The integration is performed over the region of the considered triangle A_l in cylindrical coordinates. Performing this integral for every triangle and every mode, an array $j_\phi^{\mathcal{P}^0}$ of size $N_t \times M$ is obtained. The integral can be approximated by the value of the toroidal current density in the middle of the triangle, denoted with the cylindrical coordinates (r_l, z_l). According to chapter 3, the toroidal current density is explicitly needed only in the axisymmetric case $(m = 0)$. In the non-axisymmetric cases $(m \neq 0)$, the toroidal current density can be simply set to 0.

10.1.3 Poloidal Modes

The only parameters needed, are the maximum numbers of poloidal harmonics n_{max}, which occur in the boundary integrals. This parameter specifies how many poloidal harmonics are used to represent the boundary values. They can be chosen to be different for every mode m_q. In that case they are represented by a vector n.

$$n = \begin{pmatrix} n_1 & n_2 & ... & n_M \end{pmatrix} \overset{e.g.}{=} \begin{pmatrix} 10 & 20 & 5 & ... \end{pmatrix} \tag{10.6}$$

If they are the same for every mode m_q, n is simply a scalar integer. An appropriate number of n_{max} is strongly dependent on the shape of the current density.

10.2   Program and Output

With the input, described in the previous section, the program can be run.

```
1  [rBrz_RT,Bphi_P0,Arz_N,rAphi_P1] = ...
      main_func(Th,rJrz_RT,Jphi_P0,m,n);
```

The input argument `Th` is an instance off the class `TriMesh` and represents the mesh, as described in the previous section. The input arguments `rJrz_RT` and `Jphi_P0` correspond to the arrays $rj_{rz}^{\mathcal{RT}}$ and $j_\phi^{\mathcal{P}^0}$ of the previous section. The vectors `m` and `n` contain the toroidal mode numbers and the maximum numbers of poloidal modes. The main function `main_func` forwards the input to the FEM solvers. The implementation consists of two FEM solvers, one for the toroidal vector potential (only in the axisymmetric case) and one for the poloidal vector potential. The implementations of the two FEM procedures are gathered to MATLAB packages, called `+FEM_Arz` and `+FEM_Aphi`. Every package contains a main function, solving the equations for the vector potential, as well as functions to transform the vector potential to the corresponding magnetic field. The structure of the implementation is shown in figure 10.1.

```
MATLAB
├─ main_func.m
├─ +FEM_Arz
│   ├─ functions
│   ├─ A2B.m
│   └─ main.m
├─ +FEM_Aphi
│   ├─ functions
│   ├─ A2B.m
│   └─ main.m
└─ general_functions
```

Figure 10.1: Structure of the MATLAB implementation

As output, the DoFs of the magnetic field and the vector potential are obtained. The DoFs correspond to the discretizations of section 9.1. So for the magnetic field the Raviart-Thomas DoFs of $r \cdot \vec{b}_p^m$ and the DoFs of the 0th order Lagrange elements for b_ϕ^m are obtained. For the vector potential the Nédélec DoFs of $\vec{a}_p^m$ and the DoFs of
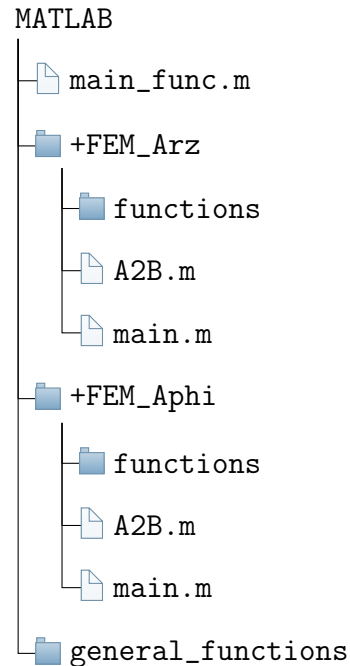
the 1st order Lagrange elements for $r \cdot a_\phi^m$ are obtained. In order to calculate, for example the magnetic field, in an arbitrary point inside the domain, the DoFs are inserted to the discretizations and the sum is evaluated, using the definitions of the shape functions.

10.3 Example

We will demonstrate the application of the MATLAB implementation on an example. Since we do not have any data for the current density, we choose an arbitrary analytical current density and calculate the generated magnetic field. First we import a triangulation of the domain from *FreeFEM++*.

```
1  filepath_mesh = '../data/Nb00050_01/mesh_file.msh';
2  filepath_meshdata = '../data/Nb00050_01/mesh.dat';
3
4  meshdata = importdata(filepath_meshdata);
5  R0 = meshdata(1);
6  r0 = meshdata(2);
7
8  [nodes,triangles,boundary_nodes] = read_FreeFEM_mesh(filepath_mesh);
9  Th = TriMesh(nodes,triangles,boundary_nodes);
```

The file *mesh_file.msh* is the output file of *FreeFEM++*. The file *mesh.dat* contains information about the computational domain, namely the radius $R0$ of the central circle of the torus and the radius $r0$ of the torus. The function `read_FreeFEM_mesh` reads the information of the triangulation, as described in section 10.1.1. With this information we create an instance of the class `TriMesh`.

Now we can prescribe the current density. For this example, we prescribe the Fourier coefficients for $m = 0$ and $m = 1$, namley $\vec{j}^0$ and $\vec{j}^1$.

```
1  m = [0 1];
2
3  f = @(r,z) (r-R0).^2 + z.^2 - r0.^2;
4
5  rj0_r    = @(r,z) z       .*f(r,z);
6  j0_phi   = @(r,z) 1./r    .*f(r,z);
```

```
7  rj0_z    = @(r,z) -(r-R0) .*f(r,z);
8
9  rj1_r  = @(r,z) 1i*r                        .*f(r,z);
10 j1_phi = @(r,z) -1-2*r.*((r-R0)-1i*z)./f(r,z).*f(r,z);
11 rj1_z  = @(r,z) 1*r                         .*f(r,z);
```

With the analytical form of the current density, we can obtain the DoFs, as described
in the previous section.

```
1  Jphi_P0 = zeros(Th.Ntriangles,2);
2  rJrz_RT = zeros(Th.Nedges,2);
3
4  rJrz_RT(:,1) = get_rt_dofs(Th,rj0_r,rj0_z);
5  rJrz_RT(:,2) = get_rt_dofs(Th,rj1_r,rj1_z);
6
7  Jphi_P0(:,1) = j0_phi(Th.xt,Th.yt);
```

The function `get_rt_dofs` calculates the Raviart-Thomas DoFs by performing
the integral (10.4). In order to perform the FEM calculations, we need one more
parameter, namely the maximum number of poloidal modes n_{max}. For this example
we simply set it to $n_{max} = 10$. Now we have all the inputs and we can perform the
actual FEM calculations, calling the `main_func` procedure.

```
1  nmax = 10;
2  [rBrz_RT,Bphi_P0,Arz_N,rAphi_P1] = ...
      main_func(Th,rJrz_RT,Jphi_P0,m,nmax);
```

Finally, the `main_func` procedure gives the DoFs of the magnetic field and the vector
potential, as described in section 10.2.

Chapter 11

Results

In order to verify the results of our MATLAB implementation, we compare them with data obtained by other methods. We are going to validate our data, i.e. magnetic field, by two different methods. One way will be to obtain an analytical form of a magnetic field and current density using the software *Mathematica* and compare it to the MATLAB results. The second way will be to use results obtained with the open source program *FreeFEM++*. In the following sections, we will describe the applied procedures more precisely.

The difference of a function $\vec{f}$ to a reference function $\vec{f}_{ref}$ is estimated using the L2-norm, equation (6.13). The relative difference is calculated like

$$\delta f_{L_2} = \frac{\|\vec{f} - \vec{f}_{ref}\|_{L_2}}{\|\vec{f}_{ref}\|_{L_2}}. \tag{11.1}$$

11.1   Verification with *FreeFEM++*

The basic idea of using *FreeFEM++* to obtain comparable results is to perform the calculation in a far bigger area than the cross-section of the torus that confines the current density. This allows us to impose homogeneous boundary conditions and we do not need to deal with the boundary conditions at all. This strategy of course goes along with far higher computational effort. In this example we chose a torus of central radius $R = 1$ and the radius of the torus $r = 0.4$. The area surrounding the torus is a square (in the rz-plane) of side length $l = 20$ (depicted in gray in figure 11.1). The weak forms of the governing equations have already been derived in chapter 7 and can be used for *FreeFEM++*.
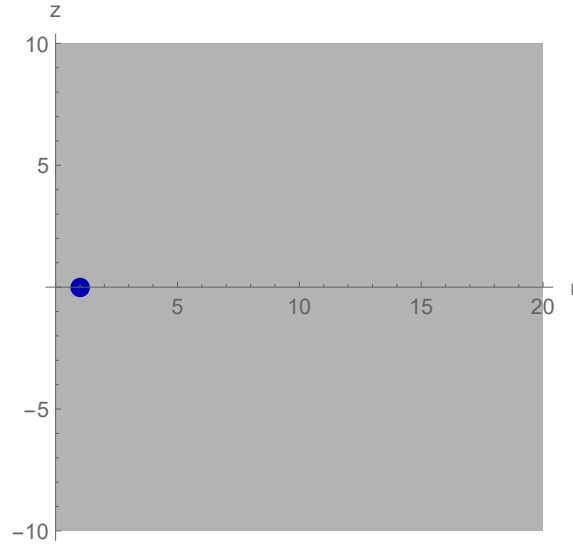
Figure 11.1: Solution approach using *FreeFEM++*. The computational domain is depicted in gray. In blue depicted is the cross-section of the toroidal domain.

11.1.1   Axisymmetric Case

In the axisymmetric case we have to solve both, the poloidal and the toroidal equation for the vector potential. The boundary values for the poloidal problem are zero in the current-free outer region (see section 7.1). Hence, the poloidal equation can be solved in the cross-section of the torus only. In the weak form of the toroidal problem (see section 7.2), the Neumann boundary condition occurs. This expression corresponds to the tangential component of the poloidal magnetic field and therefore, does not need to be zero on the z-axis. So it is convenient to imply a homogeneous Dirichlet boundary condition. a_ϕ^r must be zero at infinity, otherwise it would create a magnetic field at infinity, which would be non physical. Furthermore, it must be zero as well on the z-axis. According to equation (3.8), a gradient of a_ϕ^r along the z-axis creates a radial magnetic field, which would cause normal discontinuities on the z-axis.

For this example we chose an arbitrary analytical current density, fulfilling the continuity equation. The toroidal and poloidal part of the current density and the resulting magnetic field are depicted in figure 11.2. The plots should just give a qualitative picture of the fields, so no units are given.
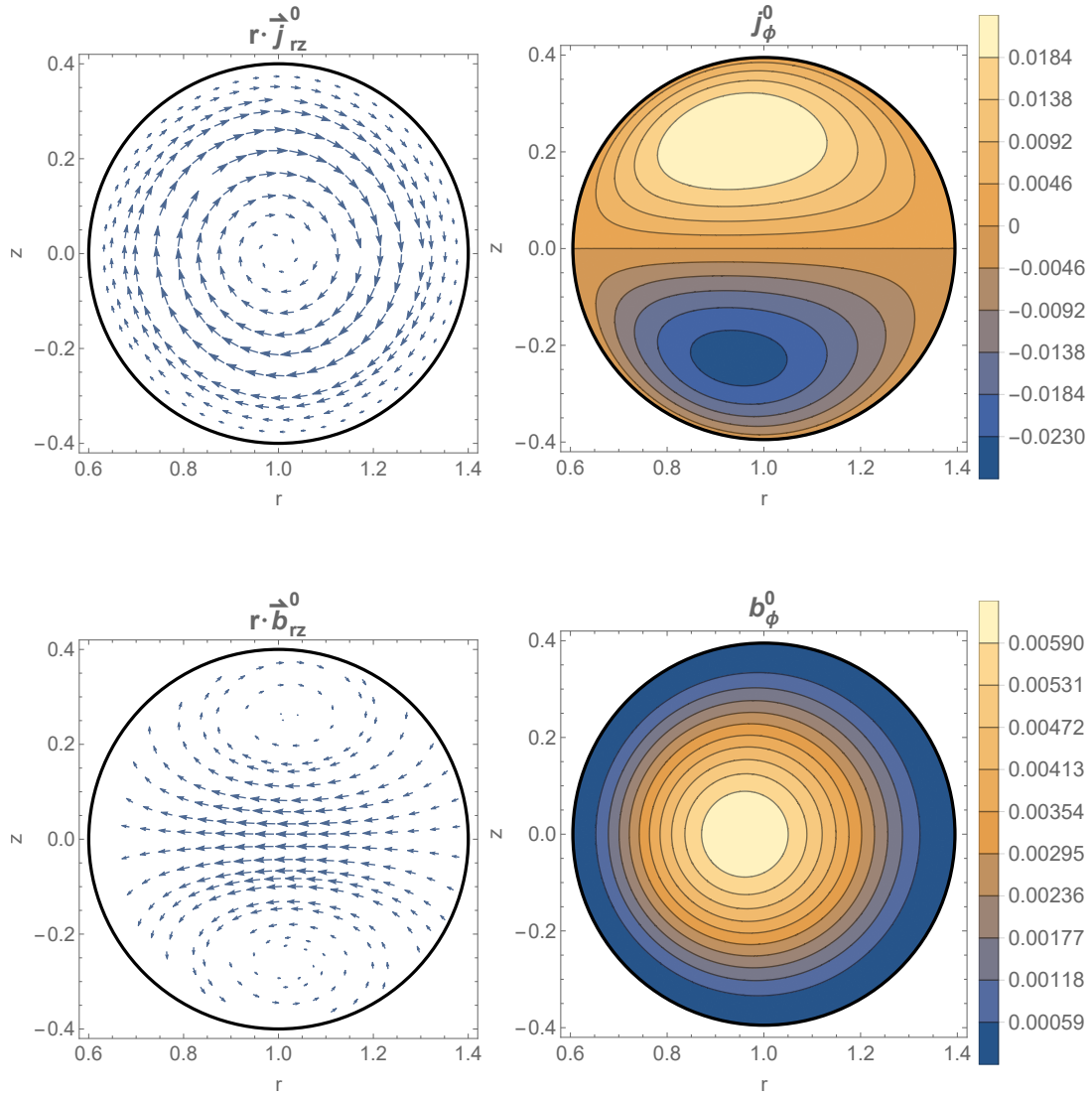
Figure 11.2: Poloidal and toroidal part of the current density (top left and right) and resulting magnetic field (bottom left and right) in the axisymmetric case.

In figure 11.3, the relative differences of the MATLAB solution and the *FreeFEM++* solution for the toroidal and poloidal magnetic field is plotted for different meshes, specified by the number of boundary nodes N_b. We can see that the difference converges to 0 for finer meshes, i.e. more boundary elements. Furthermore, we investigated the convergence of the MATLAB solution, depending on the maximum number of considered poloidal modes N_{modes} for a given mesh ($N_b = 200$, figure 11.4). The poloidal modes occur in the boundary conditions. The maximum number of

poloidal modes tells, how many harmonics are used to approximate the boundary values on the reference torus. In the axisymmetric case, homogeneous boundary conditions are imposed on b_ϕ (or equally $\vec{a}_p$) and therefore, it does not depend on the maximum number of modes. The difference for the poloidal magnetic field converges to a lower limit for a higher number of modes. The lower limit is related to the employed mesh. The finer the mesh, the lower the approached limit will be. The number of poloidal modes at which the solution has sufficiently converged is strongly dependent on the shape of the current density and the values in figure 11.4 should not be interpreted as standard values.
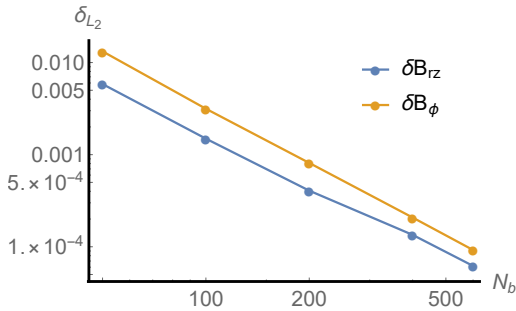
Figure 11.3: Double logarithmic plot of the relative errors of the toroidal and poloidal magnetic fields obtained with MATLAB and *FreeFEM++*, depending on the mesh.
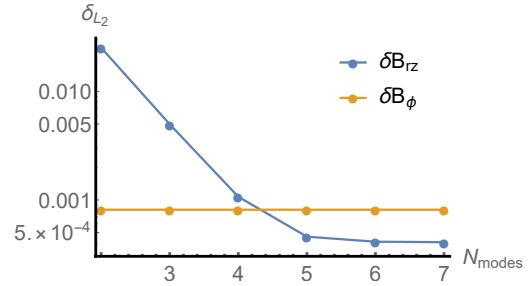

Figure 11.4: Logarithmic plot of relative errors of the two solutions depending on the number of poloidal modes for a mesh with $N_b = 200$.

11.1.2   Non-Axisymmetric Case

In the non-axisymmetric case we only have to solve the poloidal equation for the vector potential. In this case we chose $m = 2$. The occurring boundary condition in the weak form (see section 7.1) corresponds to the toroidal magnetic field strength. At infinity it must be zero as well as on the z-axis to avoid discontinuities.

Again, we chose an arbitrary analytical current density, fulfilling the continuity equation. The toroidal and poloidal part of the current density and the resulting magnetic field are depicted in figure 11.5. The plots should just give a qualitative picture of the fields, so no units are given.
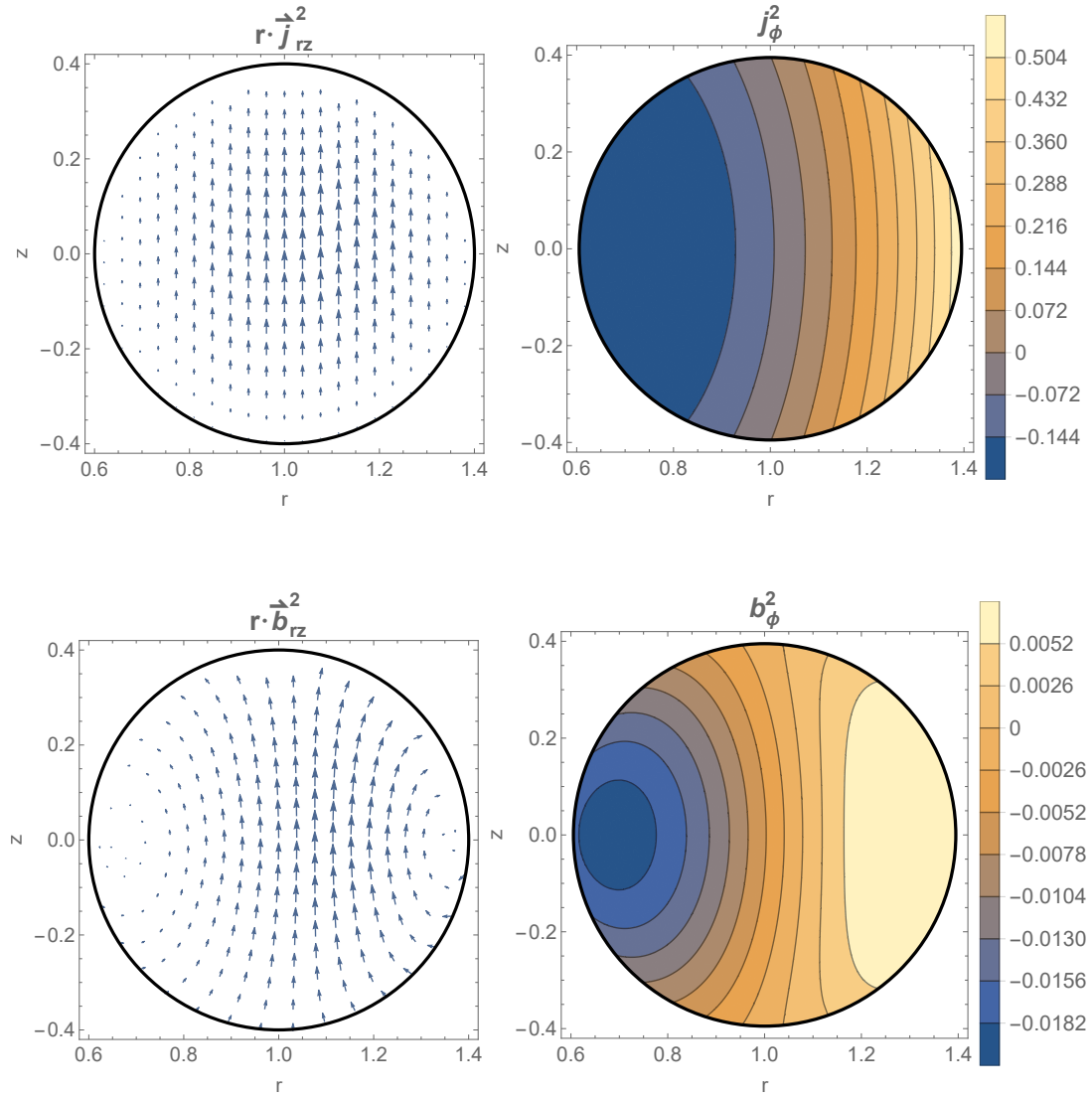
Figure 11.5: Poloidal and toroidal part of the current density (top left and right) and resulting magnetic field (bottom left and right) in the non-axisymmetric case ($m = 2$).

Like in the previous section, the relative differences of the MATLAB solution and the *FreeFEM++* solution for different meshes are plotted in figure 11.6. We can see that the difference decreases steadily for finer meshes, i.e. more boundary elements. We also investigated the convergence of the MATLAB solution, depending on the maximum number of considered poloidal modes N_{modes} for a given mesh ($N_b = 200$, figure 11.7). The errors converge to a lower limit for a higher number of modes. The lower limit is related to the employed mesh. The finer the mesh, the lower the
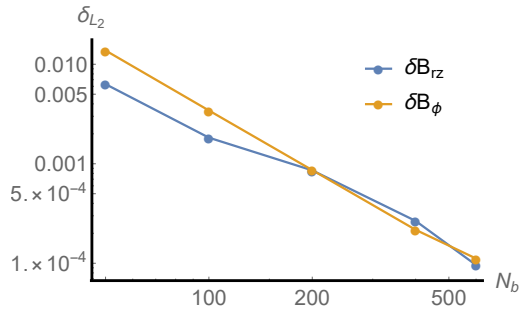
approached limit will be.

Figure 11.6: Double logarithmic plot of the relative errors of the toroidal and poloidal magnetic fields obtained with MATLAB and *FreeFEM++*, depending on the mesh.
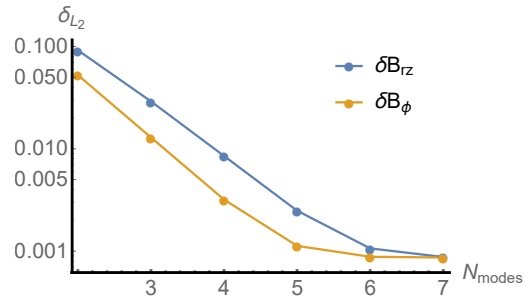

Figure 11.7: Logarithmic plot of relative errors of the two solutions depending on the number of poloidal modes for a mesh with $N_b = 200$.

11.2   Verification with *Mathematica*

In order to have a comparison of the obtained results to data, independent of any FEM approach, we compare the results to analytical solutions. The goal is to find an analytical form for the magnetic field, that generates a current density which is only non-zero in the toroidal domain. We take slightly different approaches in the axisymmetric and non-axisymmetric case.

11.2.1   Axisymmetric Case

To find an analytical form of the fields in the axisymmetric case we take the general solution for the toroidal vector potential in the outer region, equation (4.29), and choose an arbitrary particular solution, e.g.

$$a_\phi^{out}(\eta, \theta) = \sqrt{\frac{\Re}{\sinh \eta}} Q_{1/2}^1(\coth \eta) \sin \theta. \tag{11.2}$$

We connect this particular solution in the outer region, to a function in the inside, that does not fulfil the homogeneous problem and therefore, generates a current density.

$$a_\phi^{in}(\eta, \theta) = \sqrt{\frac{\Re}{\sinh \eta}} f(\eta) \sin \theta \tag{11.3}$$

$f(\eta)$ is an arbitrary, regular function in the inside. The functions itself, its first and second derivatives must be continuous on the boundary torus $\eta = \eta_0$. The generated magnetic field is written

$$\vec{b}_p = \nabla \times (a_\phi \vec{e}_\phi). \tag{11.4}$$

The toroidal part of the magnetic field is derived directly and not from the vector potential. In the axisymmetric case it has to be 0 in the outside, so it is sufficient to find a function that is zero on the boundary torus and non-zero inside.

The derived magnetic field generates a current density according to Maxwell's equation. The toroidal and poloidal part of the current density and the resulting magnetic field are depicted in figure 11.8. The plots should just give a qualitative picture of the fields, so no units are given.
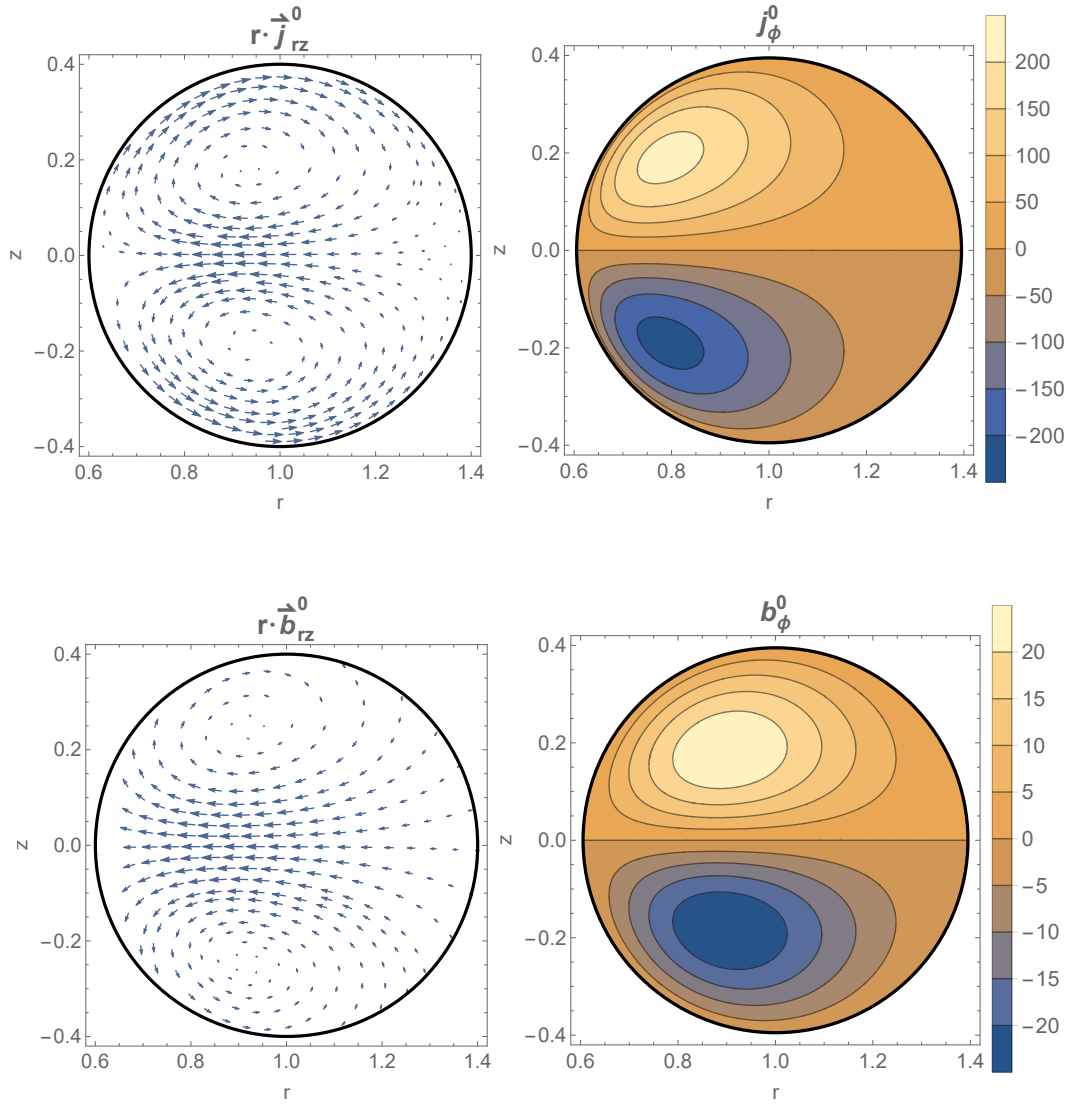
Figure 11.8: Poloidal and toroidal part of the current density (top left and right) and resulting magnetic field (bottom left and right) in the axisymmetric case.

The analytical functions for the current density and magnetic field are approximated in the appropriate function spaces (see section 9.1). The obtained DoFs for the current density can be used as input for the MATLAB implementation. The resulting magnetic field is then compared to the magnetic field obtained with *Mathematica*. In figure 11.9 we can see the relative differences of the 2 solutions, depending on the number of boundary nodes N_b of the mesh. The relative differences of the toroidal and poloidal magnetic field decrease for finer meshes, i.e. more boundary

elements, but the poloidal part seems to converge slower than the toroidal part. In the axisymmetric case, the poloidal magnetic field corresponds to the toroidal vector potential a_ϕ. So obviously the solution of the equation for the toroidal vector potential converges slower than the poloidal part. The reason for this behaviour could be the error due to the approximation and could be investigated in a future work. By construction of the analytical fields, only one poloidal mode is active and thus, an investigation of the convergence depending on the maximum number of poloidal modes is unnecessary.
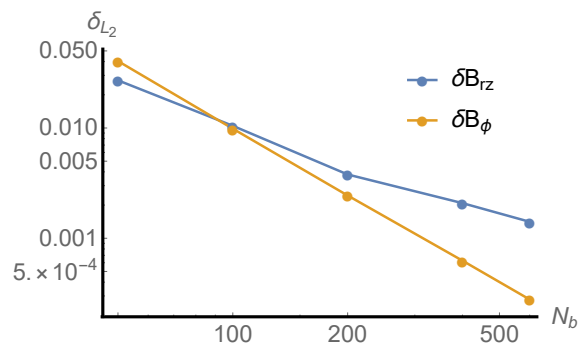

Figure 11.9: Double logarithmic plot of the relative errors of the toroidal and poloidal magnetic fields obtained with MATLAB and *Mathematica*, depending on the mesh.

11.2.2   Non-Axisymmetric Case

To find an analytical solution in the non-axisymmetric case, we take a slightly different approach. We take the general solution for the scalar potential Φ in the outer region, equation (4.21), and chose an arbitrary particular solution, e.g.

$$\Phi^{out}(\eta, \theta, \phi) = \sqrt{\Re}\, P_{1/2}^m(\cosh \eta) \sin \theta\, e^{im\phi}. \qquad (11.5)$$

Same as before, we connect this particular solution in the outer region, to a function in the inside, that does not fulfil the homogeneous problem and therefore, generates a current density.

$$\Phi^{in}(\eta, \theta, \phi) = \sqrt{\Re}\, f(\eta) \sin \theta\, e^{im\phi} \qquad (11.6)$$

$f(\eta)$ is an arbitrary, regular function in the inside. The functions itself, its first and second derivatives must be continuous on the boundary torus $\eta = \eta_0$. The generated poloidal part of the magnetic field is

$$\vec{b}_p = -\nabla \Phi^m(\eta, \theta). \qquad (11.7)$$

Φ^m denotes the potential Φ reduced by the phase factor $e^{im\phi}$. The toroidal part of the magnetic field is derived from the divergence.

$$b_\phi = -\frac{h_\phi}{im} \nabla \cdot \vec{b}_p \qquad (11.8)$$

The derived magnetic field generates a current density according to Maxwell's equation. The toroidal and poloidal part of the current density and the resulting magnetic field in the non-axisymmetric case $m = 6$ are depicted in figure 11.10. The plots should just give a qualitative picture of the fields, so no units are given.
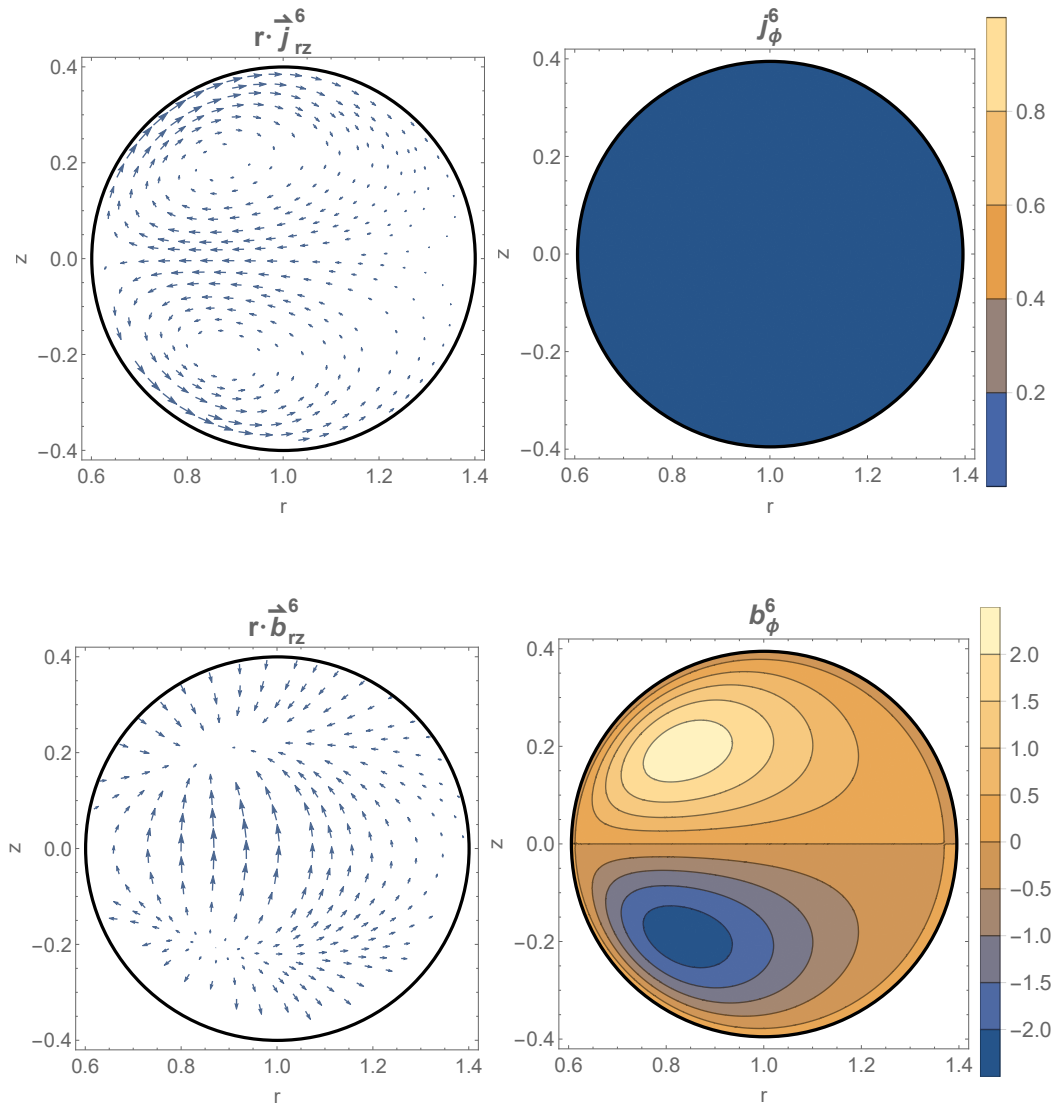
Figure 11.10: Poloidal and toroidal part of the current density (top left and right) and resulting magnetic field (bottom left and right) in the non-axisymmetric case ($m = 6$).

The same as in the axisymmetric case, the analytical functions for the current density and magnetic field are approximated in the appropriate function spaces and compared to the results of the MATLAB implementation. In figure 11.11 we can see the relative differences of the 2 solutions, depending on the number of boundary nodes N_b of the mesh. The relative differences converge similarly for finer meshes, i.e. more boundary nodes. This is reasonable, because both, the toroidal and poloidal magnetic field are generated by the same poloidal vector potential.
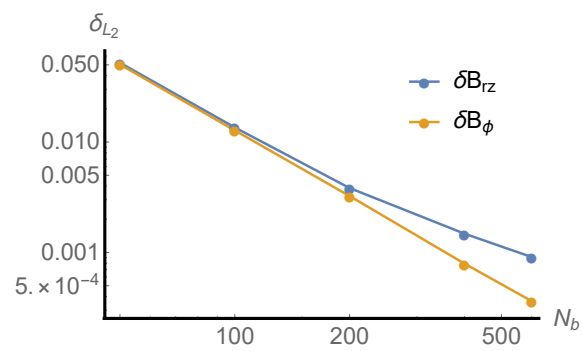
Figure 11.11: Double logarithmic plot of the relative errors of the toroidal and poloidal magnetic fields obtained with MATLAB and *Mathematica*, depending on the mesh.

Chapter 12

Conclusion and Outlook

In this work, an efficient method to calculate the magnetic field, generated by a current density that is confined to a toroidal domain, was developed and implemented in MATLAB. The solution is obtained in the same toroidal domain that confines the current density. The equations, describing the problem, are Maxwell's equations of magnetostatics. A Fourier decomposition of the occurring fields with respect to the toroidal angle yields a decoupling of the initial equations to equations for the single Fourier modes. By treating one mode at a time, a reduction of dimensionality was achieved. The governing 3D Maxwell equations reduced to 2D equations. Such 2D partial differential equations are solved by finding the solution to a corresponding boundary value problem, consisting of the equation itself and the values of the solution on the boundary of the toroidal domain. The a priori unknown boundary values are obtained by imposing a so-called open boundary condition. The open boundary condition is derived from the analytical solution in the outer region. The analytical solution was obtained by solving the homogeneous Maxwell equations in toroidal coordinates. With the open boundary condition, the boundary value problem was solved in the toroidal domain by applying a finite element method.

The implementation was validated by comparing the obtained solutions to analytical solutions and solutions, obtained with the open source program *FreeFEM++*. The relative difference of the solutions converged to 0 for finer meshes, used for the FEM calculation.

This method will be further used to compute the plasma response of resonant magnetic perturbations (RMPs, [1] [8]). For future applications it may be advantageous to implement the method in a faster programming language. Furthermore, there is no

error estimation implemented yet which is crucial for a numerical result and should be added in the future.

Appendix A

Mathematical Tools

A.1   Orthogonal Curvilinear Coordinates

An orthogonal curvilinear coordinate system (u_1, u_2, u_3) can be defined by the metric coefficients g_{11}, g_{22} and g_{33} [13]. With the metric coefficients, an infinitesimal distance can be written like

$$(ds)^2 = g_{11}(du_1)^2 + g_{22}(du_2)^2 + g_{33}(du_3)^2. \tag{A.1}$$

The metric coefficients are calculated like

$$g_{ii} = \left(\frac{\partial x_1}{\partial u_i}\right)^2 + \left(\frac{\partial x_2}{\partial u_i}\right)^2 + \left(\frac{\partial x_3}{\partial u_i}\right)^2. \tag{A.2}$$

x_i are the Cartesian coordinates. For orthogonal coordinates it is more convenient to use the scale factors instead of the metric coefficients.

$$h_i = \left|\frac{\partial \vec{r}}{\partial u_i}\right| = \sqrt{g_{ii}} \tag{A.3}$$

The infinitesimal surface and volume element are then

$$dA = h_1 h_2 \, du_1 du_2 \tag{A.4}$$

$$dV = h_1 h_2 h_3 \, du_1 du_2 du_3. \tag{A.5}$$

The unit basis vectors of this coordinate system are

$$\vec{e}_i = \frac{1}{h_i} \frac{\partial \vec{r}}{\partial u_i}. \tag{A.6}$$

A.1.1   Differential Operators

The differential operators in orthogonal curvilinear coordinates look as follows [13].

- Gradient
$$\nabla \Phi = \frac{\vec{e}_1}{h_1} \frac{\partial \Phi}{\partial u_1} + \frac{\vec{e}_2}{h_2} \frac{\partial \Phi}{\partial u_2} + \frac{\vec{e}_3}{h_3} \frac{\partial \Phi}{\partial u_3} \tag{A.7}$$

- Divergence

$$\nabla \cdot \vec{E} = \frac{1}{h_1 h_2 h_3} \left[\frac{\partial}{\partial u_1} (h_2 h_3\, E_1) + \frac{\partial}{\partial u_2} (h_1 h_3\, E_2) + \frac{\partial}{\partial u_3} (h_1 h_2\, E_3) \right] \tag{A.8}$$

- Curl

$$\nabla \times \vec{E} = \frac{1}{h_1 h_2 h_3} \begin{vmatrix} \vec{e}_1 h_1 & \vec{e}_2 h_2 & \vec{e}_3 h_3 \\ \frac{\partial}{\partial u_1} & \frac{\partial}{\partial u_2} & \frac{\partial}{\partial u_3} \\ h_1\, E_1 & h_2\, E_2 & h_3\, E_3 \end{vmatrix} \tag{A.9}$$

- Laplacian
$$\Delta \Phi = \nabla \cdot (\nabla \Phi) \tag{A.10}$$

A.1.2   Rotational Coordinates

An orthogonal rotational coordinate system (u, v, ϕ) is an orthogonal 2D coordinate system (u, v) which is rotated about an axis of rotation. The transformation of general rotational coordinates, rotated about the z-axis, to Cartesian coordinates is

$$\vec{r}(u, v, \phi) = \begin{pmatrix} x(u, v, \phi) \\ y(u, v, \phi) \\ z(u, v, \phi) \end{pmatrix} = \begin{pmatrix} f_1(u, v) \cos \phi \\ f_1(u, v) \sin \phi \\ f_2(u, v) \end{pmatrix}. \tag{A.11}$$

f_1 and f_2 are general functions. The scale factors for a rotational coordinate system are

$$h_u = \sqrt{[\partial_u f_1(u, v)]^2 + [\partial_u f_2(u, v)]^2} = h_u(u, v) \tag{A.12}$$

$$h_v = \sqrt{[\partial_v f_1(u, v)]^2 + [\partial_v f_2(u, v)]^2} = h_v(u, v) \tag{A.13}$$

$$h_\phi = \sqrt{f_1(u, v)^2} = h_\phi(u, v). \tag{A.14}$$

The scale factors are independent of the azimuthal angle ϕ, i.e. $h_i = h_i(u, v)$.

A.2 Rotation Matrix in 2D

A 2D rotation matrix $\hat{R}_\alpha$ rotates a vector in the 2D plane by an angle α [13]. The direction of rotation is counter-clockwise, i.e. a positive angle α rotates the vector by the angle α in counter-clockwise direction. In 2D Cartesian coordinates, the rotation matrix is

$$\hat{R}_\alpha = \begin{pmatrix} \cos\alpha & -\sin\alpha \\ \sin\alpha & \cos\alpha \end{pmatrix}. \tag{A.15}$$

A.3 Vector Calculus Identities

In the following, a number of useful vector calculus identities are listed [15].

$$\nabla \times \left(\psi \vec{A}\right) = \psi \left(\nabla \times \vec{A}\right) + \nabla\psi \times \vec{A} \tag{A.16}$$

$$\nabla \times \left(\vec{A} \times \vec{B}\right) = \vec{A} \left(\nabla \cdot \vec{B}\right) - \vec{B} \left(\nabla \cdot \vec{A}\right) + \left(\vec{B} \cdot \nabla\right) \vec{A} - \left(\vec{A} \cdot \nabla\right) \vec{B} \tag{A.17}$$

$$\nabla \cdot \left(\psi \vec{A}\right) = \psi \nabla \cdot \vec{A} + \vec{A} \cdot \nabla\psi \tag{A.18}$$

Appendix B

Associated Legendre Functions

This section is based on [4]. The associated Legendre functions $P_\nu^\mu(z)$ and $Q_\nu^\mu(z)$ are solutions to Legendre's differential equation of order μ and degree ν.

$$(1 - z^2)\frac{\partial^2 w}{\partial z^2} - 2z\frac{\partial w}{\partial z} + \left[\nu(\nu + 1) - \frac{\mu^2}{1 - z^2}\right] w = 0 \tag{B.1}$$

$\{z, \mu, \nu\} \in \mathbb{C}$ are unrestricted. The points $z = \infty$ and $z = \pm 1$ are singular. The equation is invariant under the following transformations: $\mu \to -\mu$, $\nu \to -\nu - 1$ and $z \to -z$. Therefore all the functions

$$P_\nu^{\pm\mu}(\pm z), \quad Q_\nu^{\pm\mu}(\pm z), \quad P_{-\nu-1}^{\pm\mu}(\pm z), \quad Q_{-\nu-1}^{\pm\mu}(\pm z) \tag{B.2}$$

fulfil Legendre's differential equation. A thorough investigation of associated Legendre functions is given in [4]. The functions $P_\nu^\mu(z)$ and $Q_\nu^\mu(z)$ are one-valued and holomorphic in the z-plane cut along the real axis from 1 to $-\infty$, where the functions have a branch cut. These functions can be expressed by integral representations, recurrence relations or hypergeometric functions $_2F_1(a_1, a_2; b_1; z)$ [4]. The hypergeometric functions are defined by the power series

$$_2F_1(a_1, a_2; b_1; z) = \sum_{n=0}^{\infty} \frac{(a_1)_n (a_2)_n}{(b_1)_n} \frac{z^n}{n!} \tag{B.3}$$

with the Pochhammer symbol

$$(a)_n = \frac{\Gamma(a + n)}{\Gamma(a)} = \begin{cases} 1 & n = 0 \\ (a + n - 1)(a + n - 2)...a & n > 0 \end{cases}. \tag{B.4}$$

This series converges within the unit circle $|z| < 1$. The associated Legendre functions can be expressed using the hypergeometric functions.

$$P_\nu^\mu(z) = \frac{1}{\Gamma(1-\mu)} \left(\frac{z+1}{z-1}\right)^{\mu/2} {}_2F_1\left(-\nu, \nu+1; 1-\mu; \frac{1-z}{2}\right), \quad |z-1| < 2 \quad \text{(B.5)}$$

$$\begin{aligned}
Q_\nu^\mu(z) = &e^{i\pi\mu} 2^{-1-\nu} \sqrt{\pi} \frac{\Gamma(\nu+\mu+1)}{\Gamma\left(\nu+\frac{3}{2}\right)} \left(z^2-1\right)^{\mu/2} z^{-\nu-\mu-1} \cdot \\
&{}_2F_1\left(\frac{\mu}{2}+\frac{\nu}{2}+1, \frac{\mu}{2}+\frac{\nu}{2}+\frac{1}{2}; \nu+\frac{3}{2}; \frac{1}{z^2}\right), \quad |z| > 1
\end{aligned} \quad \text{(B.6)}$$

If one is interested in the values of the functions for different z values, the transformation formulae of the hypergeometric functions can be applied [4]. Following useful relations between Legendre functions are valid.

$$P_\nu^\mu(z) = P_{-\nu-1}^\mu(z) \tag{B.7}$$

$$P_\nu^m(z) = \frac{\Gamma(\nu+m+1)}{\Gamma(\nu-m+1)} P_\nu^{-m}(z), \quad m \in \mathbb{Z} \tag{B.8}$$

$$Q_{n-\frac{1}{2}}^\mu(z) = Q_{-n-\frac{1}{2}}^\mu(z), \quad n \in \mathbb{Z} \tag{B.9}$$

$$Q_\nu^\mu(z) = e^{2i\pi\mu} \frac{\Gamma(\nu+\mu+1)}{\Gamma(\nu-\mu+1)} Q_\nu^{-\mu}(z) \tag{B.10}$$

The derivatives of the Legendre functions can be given in terms of contiguous Legendre functions. The given formulae are valid for both, the Legendre functions of the first and second kind.

$$\left(z^2-1\right) \frac{dP_\nu^\mu(z)}{dz} = \mu z P_\nu^\mu(z) + \sqrt{z^2-1} P_\nu^{\mu+1}(z) \tag{B.11}$$

$$\left(z^2-1\right) \frac{dP_\nu^\mu(z)}{dz} = \nu z P_\nu^\mu(z) - (\nu+\mu) P_{\nu-1}^\mu(z) \tag{B.12}$$

The different expressions for the derivatives can be obtained using the recurrence relation for the Legendre functions [4].

The Legendre functions of the first and second kind with integer order m and half integer degree $n-1/2$, $P_{n-\frac{1}{2}}^m$ and $Q_{n-\frac{1}{2}}^m$, are called ring or toroidal functions [4]. They

occur in systems with toroidal symmetry, like the Laplace equation (4.3) and the modified Laplace equation (4.4).

In order to identify regular and singular solutions within a certain domain, we give the asymptotic behaviour, i.e. the leading term of the functions at the singular points $z = 1$ and $z = \infty$ [4].

z = 1 :

$$P_\nu^\mu(z) \approx 2^{\mu/2} \frac{1}{\Gamma(1-\mu)} (z-1)^{-\frac{\mu}{2}}, \qquad \mu \neq 1, 2, 3, \ldots$$

$$Q_\nu^\mu(z) \approx e^{i\pi\mu} 2^{\frac{\mu}{2}-1} \Gamma(\mu)(z-1)^{-\frac{\mu}{2}}, \qquad \Re(\mu) > 0$$

$$(\text{B.13})$$

z = ∞ :

$$P_\nu^\mu(z) \approx \frac{2^\nu}{\sqrt{\pi}} \frac{\Gamma\left(\nu+\frac{1}{2}\right)}{\Gamma(1+\nu-\mu)} z^\nu, \qquad \Re(\nu) > 0$$

$$Q_\nu^\mu(z) \approx e^{i\pi\mu} 2^{-\nu-1} \sqrt{\pi} \frac{\Gamma\left(1+\nu+\mu\right)}{\Gamma\left(\nu+\frac{3}{2}\right)} z^{-\nu-1}$$

We can calculate the limits of the toroidal functions using the equations above for the asymptotic behaviour near the singular points.

z = 1 :

$$\lim_{z \to 1} P_{n-\frac{1}{2}}^m(z) = \begin{cases} 0 & m \neq 0 \\ 1 & m = 0 \end{cases}$$

$$\lim_{z \to 1} Q_{n-\frac{1}{2}}^m(z) = \infty$$

$$(\text{B.14})$$

z = ∞ :

$$\lim_{z \to \infty} P_{n-\frac{1}{2}}^m(z) = \begin{cases} \infty & n \neq 0 \\ 0 & n = 0 \end{cases}$$

$$\lim_{z \to \infty} Q_{n-\frac{1}{2}}^m(z) = \infty$$

B.1 Fractions of Legendre Functions

B.1.1 Fraction of Contiguous Legendre Functions of First Kind

Calculating fractions of contiguous Legendre functions of the first kind, like

$$\frac{P_\nu^{\mu+1}(z)}{P_\nu^\mu(z)} \tag{B.15}$$

may cause numerical problems since the Legendre functions tend to give very large results for large degree and order. Therefore, it would be better to find a method to calculate the ratio directly, instead of calculating both, numerator and denominator separately.

The Legendre functions can be expressed in terms of hypergeometric functions $_2F_1(a, b; c; z)$ (see chapter B). For arguments with $\Re(z) > 0$, $P_\nu^\mu(z)$ can be written

$$P_\nu^\mu(z) = 2^{-\nu}(z+1)^{\frac{\mu}{2}+\nu}(z-1)^{-\frac{\mu}{2}} \frac{_2F_1\left(-\mu-\nu, -\nu; 1-\mu; \frac{z-1}{z+1}\right)}{\Gamma(1-\mu)}. \tag{B.16}$$

This expression is derived from (B.5) by applying the transformation formulae of the hypergeometric functions [4]. In this form $1 - \mu = b_1 \notin \mathbb{Z}_0^-$ has to be valid. By defining the regularized hypergeometric functions

$$_2F_1^{reg}(a_1, a_2; b_1; z) := \frac{_2F_1(a_1, a_2; b_1; z)}{b_1} \tag{B.17}$$

we can rewrite equation (B.16) with no restrictions to b_1 in the following form.

$$P_\nu^\mu(z) = 2^{-\nu}(z+1)^{\frac{\mu}{2}+\nu}(z-1)^{-\frac{\mu}{2}} {}_2F_1^{reg}\left(-\mu-\nu, -\nu; 1-\mu; \frac{z-1}{z+1}\right) \tag{B.18}$$

With this equation we can rewrite the fraction (B.15) as follows.

$$\frac{P_\nu^{\mu+1}(z)}{P_\nu^\mu(z)} = \sqrt{\frac{z+1}{z-1}} \frac{_2F_1^{reg}\left(-\mu-\nu-1, -\nu; -\mu; \frac{z-1}{z+1}\right)}{_2F_1^{reg}\left(-\mu-\nu, -\nu; 1-\mu; \frac{z-1}{z+1}\right)} \tag{B.19}$$

Calculating the fraction of two contiguous Legendre functions comes down to calculating the fraction of two hypergeometric functions. A method to calculate such fractions are Gauss's continued fractions [25]. According to Gauss, a fraction of contiguous hypergeometric functions can be calculated by a continued fraction. This method is known to converge rather quickly, compared to a series. In the following,

the calculations of such a fraction is shown.

$$\frac{{}_2F_1^{reg}\left(a,b;c;x\right)}{{}_2F_1^{reg}\left(a+1,b;c+1;x\right)} = c + \cfrac{(a-c)bx}{(c+1)+\cfrac{\frac{(b-c-1)(a+1)x}{(c+2)+\frac{(a-c-1)(b+1)x}{(c+3)+\frac{(b-c-2)(a+2)x}{(c+4)+\dots}}}}{}} \tag{B.20}$$

With $a = -\mu - \nu$, $b = -\nu$, $c = 1 - \mu$ and $x = \frac{z-1}{z+1}$ this expression corresponds to the inverse ratio of hypergeometric functions in equation (B.19).

By applying equation (B.19) to the toroidal functions with half integer degree, integer order and $z = \cosh \eta$ as argument, we obtain

$$\frac{P_{n-1/2}^{m+1}(\cosh \eta)}{P_{n-1/2}^{m}(\cosh \eta)} = \frac{1}{\tanh\left(\frac{\eta}{2}\right)} \frac{{}_2F_1^{reg}\left(-m-n-\frac{1}{2}, -n+\frac{1}{2}; -m; \tanh\left(\frac{\eta}{2}\right)^2\right)}{{}_2F_1^{reg}\left(-m-n+\frac{1}{2}, -n+\frac{1}{2}; 1-m; \tanh\left(\frac{\eta}{2}\right)^2\right)} \tag{B.21}$$

B.1.2 Fraction of Contiguous Legendre Functions of Second Kind

Calculating fractions of contiguous Legendre functions of the second kind, like

$$(1 + \mu + \nu) \frac{Q_\nu^\mu(z)}{Q_{\nu+1}^\mu(z)} \tag{B.22}$$

may cause numerical problems for the same reason as for the Legendre functions of the first kind in the previous section, namely that these functions tend to give very large results for large degree and order. Therefore, we want to evaluate the fraction directly.

The Legendre functions of the second kind $Q_\nu^\mu(z)$ (B.6) can be rewritten for arguments with $\Re(z) > 1$ using the transformation formulae for the hypergeometric functions in the following form [4].

$$Q_\nu^\mu(z) = e^{i\pi\mu}\sqrt{\pi}2^\mu\Gamma(1+\mu+\nu)\left(z^2-1\right)^{\mu/2}\left(z+\sqrt{z^2-1}\right)^{-1-\mu-\nu}\cdot$$
$$\qquad {}_2F_1^{reg}\left(1+\mu+\nu, \mu+\frac{1}{2}; \nu+\frac{3}{2}; \frac{z-\sqrt{z^2-1}}{z+\sqrt{z^2-1}}\right) \tag{B.23}$$

In this expression we have used the regularized hypergeometric functions, defined in

equation (B.17). This expression applied to the fraction (B.22) gives

$$(1 + \mu + \nu) \, \frac{Q_\nu^\mu(z)}{Q_{\nu+1}^\mu(z)} = \left(z + \sqrt{z^2 - 1}\right) \frac{{}_2F_1^{reg}\left(1 + \mu + \nu, \mu + \frac{1}{2}; \nu + \frac{3}{2}; \frac{z - \sqrt{z^2 - 1}}{z + \sqrt{z^2 - 1}}\right)}{{}_2F_1^{reg}\left(2 + \mu + \nu, \mu + \frac{1}{2}; \nu + \frac{5}{2}; \frac{z - \sqrt{z^2 - 1}}{z + \sqrt{z^2 - 1}}\right)}$$

$$(B.24)$$

Similarly to the previous section, the fraction of hypergeometric functions in the equation above can be calculated using Gauss's continued fractions. With $a = 1 + \mu + \nu$, $b = \mu + \frac{1}{2}$, $c = \nu + \frac{3}{2}$ and $x = \frac{z - \sqrt{z^2 - 1}}{z + \sqrt{z^2 - 1}}$, equation (B.20) corresponds to the ratio of hypergeometric functions in the equation above.

By applying equation above to the toroidal functions with half integer degree $\nu = -1/2$, integer order $\mu = n$ and $z = \coth \eta$ as argument we obtain

$$\left(n + \frac{1}{2}\right) \frac{Q_{-\frac{1}{2}}^n(\coth \eta)}{Q_{\frac{1}{2}}^n(\coth \eta)} = (\coth \eta + \operatorname{csch} \eta) \frac{{}_2F_1^{reg}\left(n + \frac{1}{2}, n + \frac{1}{2}; 1; \tanh\left(\frac{\eta}{2}\right)^2\right)}{{}_2F_1^{reg}\left(n + \frac{3}{2}, n + \frac{1}{2}; 2; \tanh\left(\frac{\eta}{2}\right)^2\right)}.$$

$$(B.25)$$

B.1.3   Numerical Evaluation of Continued Fractions

$$f = b_0 + \cfrac{a_1}{b_1 + \cfrac{a_2}{b_2 + \cfrac{a_3}{b_3 + \cfrac{a_4}{b_4 + \ldots}}}} \qquad (B.26)$$

The problem evaluating continued fractions conventionally is, that one has to guess a reasonable breaking point of the continued fraction. From this last fraction the result can be calculated by evaluating the continued fraction from the end to the beginning. With this method it's hard to implement a proper convergence condition. A more suitable way to calculate continued fractions is by recurrence relations. In the modified Lentz's algorithm, recurrence relations are used for evaluation [24]. With this method, convergence conditions are easily implemented. Thompson and Barnett introduced in [3] a slight modification to the algorithm. This algorithm, additionally to the basic modified Lentz's algorithm avoids problems with possibly occurring recurrence results approaching zero. [24] gives an example to implement the algorithm. a_j and b_j are the values according to equation (B.26) for a general continued fraction.

Algorithm 1 Modified Lentz's algorithm

1: $f_0 = b_0$
2: **if** $f_0 = 0$ **then** $f_0 = 10^{-30}$;
3: $C_0 = f_0$
4: $D_0 = 0$
5: **for** $j = 1 : n_{max}$ **do**
6:     $D_j = b_j + a_j D_{j-1}$
7:     **if** $D_j = 0$ **then** $D_j = 10^{-30}$;
8:     $C_j = b_j + a_j/C_{j-1}$
9:     **if** $C_j = 0$ **then** $C_j = 10^{-30}$;
10:     $D_j = 1/D_j$
11:     $\Delta_j = C_j D_j$
12:     $f_j = f_{j-1}\Delta_j$
13:     **if** $|\Delta_j - 1| < eps$ **then** $break$;
14: **end for**

Bibliography

[1] CG Albert. *Hamiltonian Approach to Resonant Transport Regimes due to Non-Axisymmetric Magnetic Perturbations in Tokamak Plasmas.* PhD thesis, TU Graz, 2016.

[2] LA Artsimovich. Tokamak devices. *Nuclear Fusion*, 12(2):215, 1972.

[3] IJ Thompson, AR Barnett. Coulomb and bessel functions of complex arguments and order. *Journal of Computational Physics*, 64:490–509, 1986.

[4] H Bateman. *Higher Transcendental Functions*, volume 1. McGraw-Hill Book Company, 1953.

[5] JL Bobin. *Controlled Thermonuclear Fusion.* World Scientific Publishing Co. PTE. Ltd., 2014.

[6] M Menad, C Daveau. Comparison of several discretization methods of the steklov-poincaré operator. *International Journal of Numerical Modelling: Electronic Networks, Devices and Fields*, 19:271–287, 2006.

[7] AJ Davies. *The Finite Element Method: An Introduction with Partial Differential Equations.* Oxford University Press, 2 edition, 2011.

[8] TE Evans, et al. Edge stability and transport control with resonant magnetic perturbations in collisionless tokamak plasmas. *Nature Physics*, 2, 2006.

[9] D Boffi, F Brezzi, M Fortin. *Mixed Finite Element Methods and Applications.* Springer, 2013.

[10] JB Keller, D Givoli. Exact non-reflecting boundary conditions. *Journal of Computational Physics*, 82:172–192, 1989.

[11] JD Jackson. *Classical Electrodynamics*. John Wiley & Sons, INC., 2 edition, 1975.

[12] JM Jin. *The finite element method in electromagnetics*. John Wiley & Sons, INC., 2 edition, 2002.

[13] GA Korn, TM Korn. *Mathematical Handbook for Scientists and Engineers: Definitions, Theorems, and Formulas for Reference and Review*. Dover Publications Inc., 2003.

[14] JD Lawson. Some criteria for a power producing thermonuclear reactor. *Proc. Phys. Society*, Section B, 70(1):6, 1957.

[15] PC Matthews. *Vector Calculus*. Springer, 2000.

[16] DR Nicholson. *Introduction to Plasma Theory*. John Wiley & Sons, INC., 1983.

[17] AC Polycarpou. *Introduction to the Finite Element Method in Electromagnetics*. Morgan & Claypool, 2006.

[18] O Biro, KR Richter. Cad in electromagnetism. In *Advances in Electronics and Electron Physics*, volume 82. Academic Press, Inc., 1991.

[19] P Demarcke, H Rogier. The poincaré–steklov operator in hybrid finite element-boundary integral equation formulations. *IEEE Antennas and Wireless Propagation Letters*, 10:503–506, 2011.

[20] MVK Chari, SJ Salon. *Numerical Methods in Electromagnetism*. Academic Press, 2000.

[21] P Moon, DE Spencer. *Field Theory Handbook*. Springer, 1971.

[22] L Spitzer. The stellarator concept. *Phys. Fluids*, 1(4):253–264, 1958.

[23] JQ Sun. *Stochastic Dynamics and Control*, volume 4. Elsevier, 2006.

[24] WH Press, BP Flannery, SA Teukolsky, WT Vetterling. *Numerical Recipes in Fortran 77*, volume 1. Cambridge University Press, 1986.

[25] HS Wall. *Analytic Theory of Continued Fractions*. New York: Chelsea, 1948.

[26] L Brouwer, S Caspi, D Robin, W Wan. 3d toroidal multipoles for curved accelerator magnets. In *Proceedings of PAC2013, Pasadena, CA USA*, pages 907–909, September 2013.

[27] F Weißenbacher. Numerical solution of magnetostatic problems. Bachelor's thesis, TU Graz, 2018.